REACTION OF IRON-TITANIUM OXIDE MINERALS WITH KIMBERLITE MAGMA:

A CASE STUDY FOR ORAPA KIMBERLITE CLUSTER

Rachel S. Milligan

Submitted in Partial Fulfilment of the Requirements

For the Degree of Bachelor of Sciences, Honours

Department of Earth Sciences

Dalhousie University, Halifax, Nova Scotia

March, 2014

Distribution License

DalSpace requires agreement to this non-exclusive distribution license before your item can appear on DalSpace.

NON-EXCLUSIVE DISTRIBUTION LICENSE

You (the author(s) or copyright owner) grant to Dalhousie University the non-exclusive right to reproduce and distribute your submission worldwide in any medium.

You agree that Dalhousie University may, without changing the content, reformat the submission for the purpose of preservation.

You also agree that Dalhousie University may keep more than one copy of this submission for purposes of security, back-up and preservation.

You agree that the submission is your original work, and that you have the right to grant the rights contained in this license. You also agree that your submission does not, to the best of your knowledge, infringe upon anyone's copyright.

If the submission contains material for which you do not hold copyright, you agree that you have obtained the unrestricted permission of the copyright owner to grant Dalhousie University the rights required by this license, and that such third-party owned material is clearly identified and acknowledged within the text or content of the submission.

If the submission is based upon work that has been sponsored or supported by an agency or organization other than Dalhousie University, you assert that you have fulfilled any right of review or other obligations required by such contract or agreement.

Dalhousie University will clearly identify your name(s) as the author(s) or owner(s) of the submission, and will not make any alteration to the content of the files that you have submitted.

If you have questions regarding this license please contact the repository manager at dalspace@dal.ca.

Grant the distribution license by signing and dating below.

_____ _____

Name of signatory Date

DALHOUSIE UNIVERSITY
Inspiring Minds

Department of Earth Sciences
Halifax, Nova Scotia
Canada B3H 4R2
(902) 494-2358
FAX (902) 494-6889

DATE: April 17/14

AUTHOR: Rachel Milligan

TITLE: Reaction of Iron-Titanium oxide minerals with Kimberlite magma: a case study for Orapa Kimberlite cluster

Degree: B.Sc. Honours Convocation: May Year: 2014

ABSTRACT

Fe-Ti oxides, chromite and ilmenite, are common minerals in kimberlite diamond-bearing kimberlites. They are brought to the surface during the eruption of kimberlitic magmas that are derived from the upper mantle. Previous studies have shown that, similar to diamonds, partial dissolution and interaction of Fe-Ti oxides with the kimberlite magma results in complex reaction rims and dissolution patterns. The nature of this interaction reflects both the chemical composition of the magma and fluid phases present. The goal of this study is to investigate the reactions that occur between chromite and ilmenite grains and the kimberlite melt, their implications for diamond preservation. The possible connections between resorption features and chemical composition are also investigated.

Chromite and ilmenite grains from two kimberlites in the Orapa cluster, Botswana, with different geological features were examined. Kimberlite A is a small pipe, filled with coherent kimberlite facies. Kimberlite B is larger and has two lobes filled with two different types of coherent kimberlite facies; the pipe also contains massive volcaniclastic and resedimented volcaniclastic facies. 75 grains were selected for examination of dissolution features under Scanning Electron Microscope: 20 chromites and 21 ilmenites from Kimberlite A and 10 chromites and 24 ilmenites from Kimberlite B. After the grains were imaged, they were mounted and polished to investigate reaction textures, zoning and reaction phases using Back Scatter Electron imaging, X-ray mapping and Wavelength Dispersive Spectroscopic analysis methods. Most of the chromite samples displayed rounded ovoid morphologies with oriented, euhedral, octahedral nodules. Very few of the imaged ilmenite grains display dissolution features, and most were surrounded with reaction phases such as perovskite and titanite. The results of the WDS analysis, BSE images and X-ray maps show that ilmenites from Kimberlite A show visible diffusive zonation and trending compositions. The grains have Mg-enriched, Fe-depleted rims indicative of a reduced kimberlite melt, with some reaction products (mostly perovskite) on the grain surface. Kimberlite B ilmenite grains have restricted compositions and are not visibly zoned. However, WDS analyses show a trend towards titanium-magnetite (depletion in Ti) around the rims of the ilmenite grains, as well as decreases of MgO and Cr_2O_3. This trend is more indicative of an oxidizing environment. Kimberlite B ilmenites also have large volumes of reaction products on the surface of the grains, both perovskite and titanite. In Kimberlite A, based on the volume of reaction products, ilmenite was likely closer to the liquidus composition than in Kimberlite B. Based on comparisons with experimentally produced surface features, Kimberlite A had a free fluid H_2O phase, while Kimberlite B had less H_2O, in a dissolved phase. Both kimberlites had low proportions of CO_2 in a dissolved state. In both kimberlites there does not seem to be a correlation between the nature of dissolution features and the composition of the grains. The resorption features seen in Fe-Ti oxides are likely influenced by some other condition within the kimberlite, such as pressure, or temperature. It was determined that Kimberlite A, the simple kimberlite with free-fluid H_2O and a reducing redox state, has a higher potential for diamond preservation than Kimberlite B.

Keywords: kimberlite, chromite, ilmenite, resorption, surface features

TABLE OF CONTENTS

TABLE OF FIGURES

TABLE OF TABLES

ACKNOWLEDGEMENTS

Many thanks to my supervisors, Yana Fedortchouk and Richard Cox, for their continuing guidance and support throughout this project. I would like to express special thanks to Yana for her contagious enthusiasm for research and kimberlite geology. Thanks to Richard, who always made time to talk out a problem, and without whom a large part of the microprobe data collected for this study would not have been managed.

Many thanks to Dan MacDonald, for his endless patience, and his extensive expertise with the electron microprobe and all its functions. Thanks to Pat Scallion, for her expert knowledge and help with the scanning electron microscope.

Many thanks to Ryan Kressall, and the rest of the team at the Experimental Igneous Petrology Laboratory, for being so patient as I fought to understand the complex kimberlitic systems with many questions over the course of the year. Thanks also to Martin Gibling, for his notes and revisions through several drafts of this work.

Many thanks to Ingrid Chinn and De Beers Group Exploration for providing the mineral samples and reports on the geology of these kimberlites. Additionally, I would like to thank the Society of Economic Geologists Canada Foundation and NSERC Engage Grant (c/o Yana Fedortchouk) for funding this project.

1.0 INTRODUCTION

1.1 Kimberlite Geology

1.1.1 Diamond Deposits and Kimberlite Occurrences

Kimberlites are ultramafic, volatile-rich, extrusive igneous bodies that originate in the upper mantle (Dawson 1980). They are well known for containing diamonds and abundant xenoliths of upper mantle and crustal material. The xenoliths found in kimberlites have provided significant information on the mineralogy and petrology of the upper mantle. Other methods have been used to investigate the processes of the mantle; however none have produced the same volume or significance of results as studies of kimberlite rocks (Dawson 1980). First discovered in Kimberley, South Africa, kimberlites are emplaced into old continental cratons (Winter 2010). Kimberlites are most commonly 200 Ma or younger in age (Winter 2010), but the material they sample during their ascent is much older. Most diamonds formed between 900Ma and 3300Ma (dated from diamond inclusions) (Kirkley et al. 1992) and are stored at depths greater than 110km under continental cratons (Scott-Smith, 1995) where the lithospheric mantle is depressed beneath the diamond-graphite barrier (Winter, 2010). Mitchell (1986) noted that kimberlites with economic value are found in cratons of at least 2.4 Ga age.

Another primary source of diamond deposits is lamproites, a rock type similar to kimberlites. Both kimberlites and lamproites are rare, highly potassic rocks formed by explosive magmatic events with deep origins. They often carry diamonds to the surface (Winter 2010). These two types of deep crustal activity are differentiated by their chemical signatures and inferred tectonic settings. Lamproites occur predominantly in the areas with a deep subducted tectonic plate, with a composition specific to LREE-enriched fluids related to subduction magmatism. Kimberlites also have high LREE compositions, but are much more common in cratonic settings with thick

lithospheres (Winter 2010). Kimberlites and lamproites are both enriched in REEs, but lamproites slightly more than kimberlites. A major distinction between the two is the enrichment of CO_2 in kimberlites which is absent in lamproites (Kirkley et al. 1992).

There are two main classes of kimberlite: Group 1 and Group 2. Group 1 kimberlites are differentiated by their lower mica content than Group 2 kimberlites (Scott-Smith, 1995). Both can occur on- or off-craton (Becker and le Roex, 2006). Occasionally Group 2 kimberlites includes other classifications such as orangeites or lamproites because of their slightly differing mineralogy.

1.1.2 Mineralogy

There are four main sources of mineralogical material within a kimberlite: xenocrysts and xenoliths from the mantle and the crust, discrete nodule (or megacryst) crystallization, primary crystallization from the kimberlite melt (Mitchell 1986), and the crystallization of secondary material from interaction with fluids (Dawson 1980). The major minerals found in kimberlites include olivine, diopside, phlogopite, calcite, serpentine (secondary), and monticellite.

The addition and assimilation of mantle and crustal xenoliths to the kimberlite pipe contribute to the fragmental, brecciated texture of the kimberlite rock. The composition and volume of foreign material found in a specific pipe can vary widely based on the type and structure of the rock formations near the surface of the kimberlite eruption, and in the mantle, where eruption begins. Dawson (1980) identified the main sources of xenolithic material that can be present in a kimberlite. This list includes rocks believed to have been derived from the upper mantle (peridotites and pyroxenites), rocks that have undergone deep-seated metamorphism, probably the result of subduction (eclogites and granulites), and rocks derived from formations located along the kimberlite path to the surface. The mantle xenoliths in particular can provide large amounts of information about the conditions and processes occurring in the mantle. It is the fragmentation of

xenoliths assimilated during kimberlite ascent that results in xenocrysts within the diatreme. Common xenocrysts include diamonds, ilmenite, olivine, garnet, clinopyroxene, orthopyroxene and chromite (Mitchell, 1986, Kirkley et al. 1992).

The discrete nodule suite, also referred to as the megacryst suite, is somewhat of a mystery to kimberlite petrologists. Megacrysts are grains which are larger than the supposed phenocrysts of the kimberlite. As such, it is unclear whether megacrysts are cognate, or from an outside source.

Most commonly magnesian ilmenite, titanian pyrope, diopside, enstatite, phlogopite, and zircon are the minerals identified as the discrete nodule suite. Because the precise petrogenesis of this suite is largely unknown, Dawson (1980) adapted the term "megacrysts", to be used without connotations of a specific origin.

Minerals crystallizing directly from the kimberlite melt make up the aphanitic groundmass, as well as the phenocrysts and microphenocrysts found within the pipe. The groundmass mineralogy is very complex, and includes olivine, phlogopite, spinel, ilmenite, perovskite, and calcite (Mitchell, 1986, Roeder and Schulze, 2008). The phenocrysts and microphenocrysts of the primary kimberlite material are generally olivine, phlogopite and chromite (Mitchell 1986). Often during ascent of the kimberlite magma, the primary constituents of the system will be altered chemically and physically due to metasomatism and exsolution of volatiles in the pipe (Becker and Roex 2006). Late stage metasomatism and volatile exsolution (H_2O and CO_2 fluids) can also cause replacement of earlier crystallized minerals in the kimberlite pipe (Roeder and Schulze, 2008). Secondary exposure to meteoric water or groundwater often causes alteration of olivine to serpentine in-situ in the kimberlite pipe.

1.1.3 Kimberlite Facies

The classic kimberlite model is divided into three main facies: hypabyssal facies, diatreme facies and crater facies (Mitchell 1986). Hypabyssal facies kimberlites crystallize from the kimberlite magma in dykes and sills. They include the base or root zone of the kimberlite, which marks the transition from the diatreme above (the explosive facies of the pipe). Hypabyssal dikes and sills are considered the most similar to classic representations of igneous intrusions in texture and evidence for magma differentiation (Mitchell 1986). They have a massive texture ranging from aphanitic to coarse and macrocrystaline. Hypabyssal regions of the kimberlite can also be brecciated, though the rock fragments found in hypabyssal facies show evidence of magmatic interaction, whereas rock fragments in brecciated diatremes do not appear to have been influenced by the kimberlite magma (Mitchell 1986).

Diatreme facies is brecciated and makes up the primary pipe of the kimberlite. The diatreme facies is the expression of explosive kimberlite magmatism. It is composed primarily of a tuffistic breccia with an aphanitic groundmass, phenocrysts and microphenocrysts, as well as the discrete nodule suite (discussed in section 1.1.2) (Mitchell 1986). This tuff-breccia contains clasts from both the country rock and the kimberlite magma, in varying amounts. The inter-clast matrix of the diatreme is a uniform amalgamation of secondary hydrothermal minerals surrounding the primary and xenolithic clast material (Dawson 1980, Mitchell 1986).

The crater facies of the kimberlite comprises a tuffistic ring around the kimberlite pipe, tuff cones, and occasionally a lava flow (Dawson 1980).

Many kimberlite geologists have adapted a new terminology which groups the different kimberlite facies on their level of fragmentation. In this terminology, coherent, or hypabyssal, kimberlite (CK) would encompass dikes and sills. The diatreme and crater facies are termed volcaniclastic

kimberlite (VK) which includes the massive volcaniclastic kimberlite (MVK) in the bulk of the diatreme, pyroclastics (PK) and resedimented volcaniclastics (RVK) near the crater of the pipe (Kjarsgaard et al. 2009). Figure 1 shows a classic kimberlite pipe model with both the facies and newer terminologies displayed.

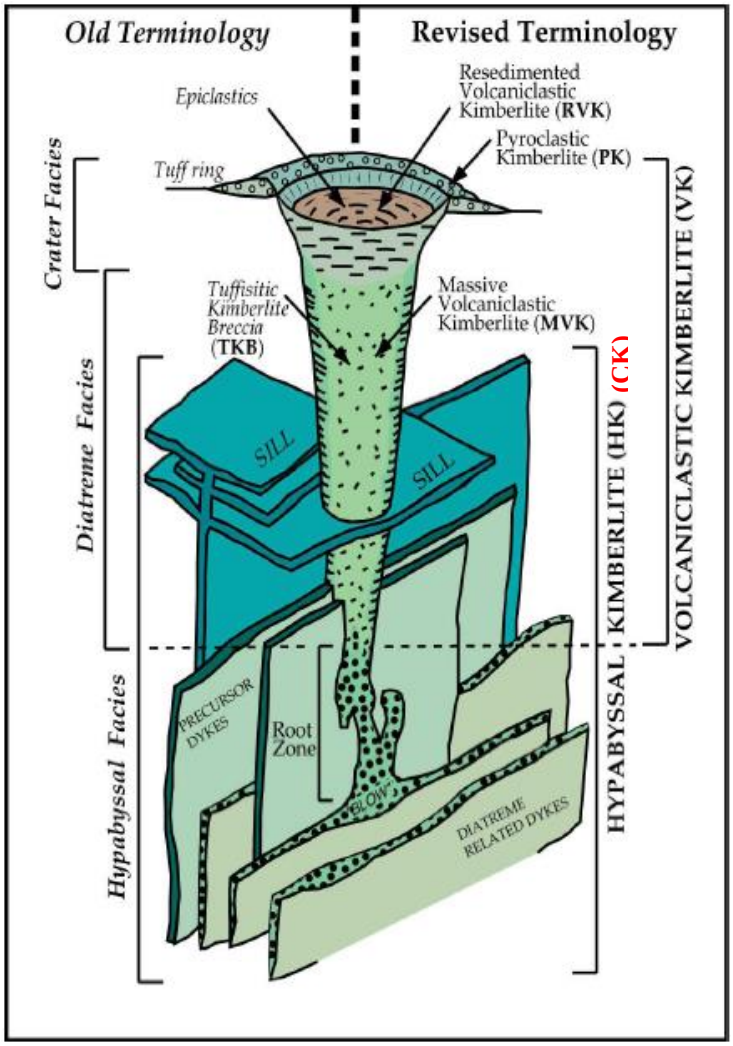

Figure 1.1 Classic kimberlite model depicting facies and newer kimberlite classifications. Modified from Kjarsgaard (2007)

Three classes of kimberlite eruption have been described (Field and Scott-Smith, 1999, Skinner and Marsh, 2004). The classic model (Class 1) depicted in Figure 1.1 is characteristic of South African kimberlites and was the only known model for kimberlitic eruption for many years. This model describes a steep-sided and deep pipe which excavates and is infilled almost simultaneously

by the fluid-driven diatreme. There is still much discussion about the mechanisms behind formation of the diatreme.

More recently, with discovery of kimberlites in North America, other types of kimberlitic eruptions have been identified. A Class 2 kimberlitic eruption is characteristic of the Prairies region of Canada, where only the crater facies of the pipe has formed in a shallow pipe (Field and Scott-Smith, 1999). Field and Scott-Smith (1999) attribute the different eruption style to differences in country rock geology, stating that the Prairies kimberlites have an easier route to the surface through soft sediment. They also propose that interaction of the magma with an aquifer is what drives the explosive eruption. In contrast, Skinner and Marsh (2004) argue that because the petrography of coherent kimberlite (CK) in Class 2 kimberlites is so variable, Class 2 kimberlite eruption is more influenced by fluids in the melt, rather than the surrounding geology. They also noted that the three classes of kimberlite eruption can occur within the same field, something that was not previously verified.

The third class of kimberlitic eruption, Class 3. The classic example of this eruption style is the Lac de Gras kimberlite in Northwest Territories, Canada. These pipes are shallow, similar to Class 2 eruptions, but they have steep sides, resembling smaller versions of the Class 1 kimberlite (Field and Scott-Smith, 1999). Class 3 pipes contain both coherent kimberlite (CK) facies, and volcaniclastic kimberlite (VK) facies. Unlike the Class 1 eruption, however, the pipe is supposed to have remained empty an open for some time, evidenced by the sedimentary material present very deep in the pipe (Field and Scott-Smith, 1999).

1.1.4 Primary Melt Compositions and Volatiles

Because of their deep origin, the composition of rocks resulting from kimberlite melts is highly influenced by assimilation of crustal and mantle material and the alteration effects of exsolved

volatiles within the melt. This can make it difficult to discern the composition of primary kimberlite melt. Whole rock analysis of kimberlite is not useful because of the abundance of xenolithic and secondary alteration materials present in the fragmental bodies (Canil and Bellis 2008). The most recent methods attempting to constrain initial kimberlite conditions have implemented precision trace-element measuring techniques on bulk samples of aphanitic portions of the pipe, what was considered low-contamination kimberlite (Kjarsgaard et al. 2009, Kopylova et al. 2007). These analyses were taken to represent the primary kimberlite melt, but most resulted in a compositions that were likely too high in Mg to have been in equilibrium with the mantle (Kopylova et al. 2007).

The high Mg content is attributed to the abundance of olivine in kimberlite rocks. Olivine is ubiquitous in all kimberlite classes and types, and so cannot be used to distinguish different magma sources (Scott-Smith, 1995). The unknown source of macrocrystal olivine in kimberlites, which are abundant, is also a problem to be considered. If the macrocrysts are cognate, then the primary crystallization fraction would be different than if the grains are of xenocrystic origin (Mitchell, 1986). This problem also applies to the discrete nodule suite. The uncertain source of these macrocrysts makes the proportion of fractionation from the primary melt uncertain.

1.2 Fe-Ti oxide Mineralogy and Chemistry

1.2.1 Oxide Mineralogy and Occurrence within Kimberlite

Chromite is part of the Spinel Group of minerals, which comprises three series: the spinel series, the magnetite series, and the chromite series. Each series is defined by the major trivalent cation present in the minerals of that series (Nesse, 1986). All of the spinel group are of the isometric octahedral crystal system. This crystal system becomes important when examining the surface dissolution on chromite grains. Chromite has the formula $FeCr_2O_4$ (Nesse, 1986). In the kimberlitic

system, chromite grains are particularly sensitive to changes in pressure (Gurney and Zweistra, 1995).

Ilmenite is an oxide mineral which follows the trigonal-hexagonal crystal system (Nesse, 1986). It very closely resembles magnetite in appearance and, though magnetite belongs to a different crystal system, it can be difficult to distinguish anhedral or very small grains of ilmenite from grains of magnetite. Ilmenite has the formula $FeTiO_3$ (Nesse, 1986). In the kimberlitic system ilmenites are sensitive to changes in oxygen fugacity. This makes them particularly important for determining the redox state of a kimberlite system (Gurney and Zweistra, 1995).

Fe-Ti oxides commonly occur as xenocrysts in kimberlites. Upon dissolution of the host xenolith, the oxide xenocryst becomes exposed to the kimberlite magma and reacts to establish equilibrium (Bearley and Scarfe, 1986). Chromite also precipitates from the kimberlite melt in the groundmass, as megacrysts and as phenocrysts. Chromite can be included in diamonds, and these chromites are considered important diamond indicators. Ilmenite occurs in kimberlites as megacrysts, but not as diamond inclusions (Gurney and Zweistra, 1995).

1.2.2 Chemical Composition and Trends

When examining oxide minerals, obtaining detailed compositional analyses can be hugely beneficial to understanding their petrogenesis (Wyatt et al. 2004). Particularly for oxides such as ilmenite. Kimberlitic and non-kimberlitic ilmenites are known to have a very similar appearance, so in the case of a secondary deposit of ilmenites, the chemical composition may be the best method to determine a grain's source. Ilmenite grains have been shown to display a very specific kimberlitic trend in relation to non-kimberlitic ilmenites (particularly high Mg, termed picro-ilmenites) (Wyatt et al. 2004). Chromites are less specific in their kimberlitic chemistry, showing a much wider range of compositions and variation within a single kimberlite. However, some

studies have attempted to use chemical analyses to constrain the petrogenesis of individual chromite grains within a kimberlite: xenocrystic, primary or metasomatised (Roeder and Schulze 2008). They have identified xenocrystic chromites as containing a wider range of Al-Cr proportions and very low Fe. Primary kimberlitic chromites have high Cr with some Fe. Metasomatised chromites are constrained to the higher Fe zone in the primary chromite field. The compositional divisions proposed by Roeder and Schulze (2008) are shown in Figure 1.2.

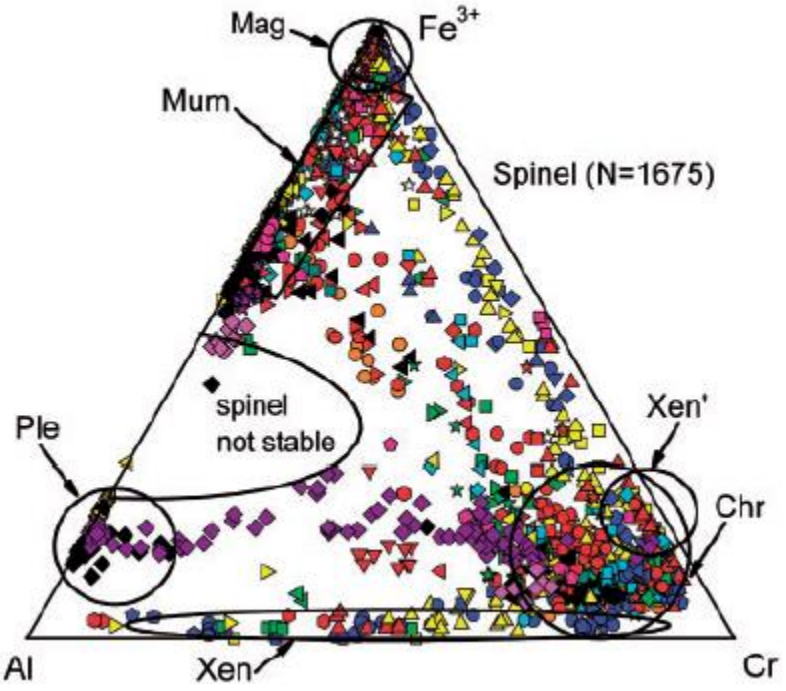

Figure 1.2 Composition of kimberlitic spinels with subdivisions: Cr = primary chromite, Xen = xenocrysts, Xen' = metasomatised, Ple = pleonaste spinel, Mum = mangesio-ülvo-spinel, Mag = magnetite, from (Roeder and Schulze, 2008)

1.2.3 Morphology and Surface Features

Lee et al. 2004 definitively established that chromite grains develop distinct surface features and morphologies when subjected to resorption in a kimberlite melt, different from chromites of other sources. In particular, they defined several morphologies which display elongation, a result plastic deformation from high temperature and pressure in the kimberlite pipe. This study, however, did not delve into the specific nature and morphology of the features themselves, beyond mentioning

their uniqueness to kimberlitic chromites. Lee et al. (2004) suggest that identification of the surface features seen on chromites as either kimberlitic or non-kimberlitic would be the most effective way of determining the source of a chromite, because of the similar compositions found in kimberlitic chromites and those from other sources.

Another study by LeBlanc (1980) began to establish a more comprehensive report of the surface features that occur on chromite grains, but from stratiform and podiform chromites. Part of the motivation for this current study of Orapa kimberlites is to classify the features seen on kimberlitic chromites and ilmenites, to determine how different or similar they are to surface features found on grains from other sources, and to investigate whether the composition of the kimberlite melt has an influence on the type of features seen on the grain surfaces.

A recent work conducted by Fedortchouk and MacIsaac (2013) used experimental methods to make some initial constraints on the fluid conditions in a kimberlitic melt which result in the development of surface features on chromite and ilmenite grains from kimberlites. They compared natural surface features on these minerals to experimentally induced features on the same grains (same composition with varied melt and fluid conditions). While this paper made significant contributions to the understanding of what causes features on oxide grain surfaces, a more inclusive and thorough classification and definition of chromite and ilmenite surface features is crucial.

1.2.4 Use of Fe-Ti Oxides in Kimberlite exploration

Fe-Ti oxides are of interest when studying kimberlites because of their resilience to surface weathering within the kimberlite pipe. Many other macrocrystal indicator minerals found in kimberlites, such as olivine, pyrope, pyroxene or diopside, survive transportation to the surface in the kimberlite but are lost during surface weathering. Oxides can be abundant in heavy mineral

concentrate trails within the kimberlite rock (Lee et al. 2004). These oxides become more important for diamond exploration where the abundance of recovered indicator minerals is low, and chromite and ilmenite grains become one of the more important sources for information about the kimberlite processes (Wyatt et al. 2004).

Chromite grains can also occur as inclusions within diamond. Chromite and garnet are considered the two most useful indicator minerals to be included in diamond (Gurney and Zweistra, 1995). This is because they reveal whether the diamond source for that kimberlite is peridotitic or eclogitic. The source of diamonds for a kimberlite can have a major impact on the economic value of a diamond deposit. Eclogitic diamond-bearing xenoliths are much more abundant in kimberlites than diamondiferous xenoliths of a peridotite source (Kirkley et al. 1992). Kirkley et al. (1992) suggest that peridotite xenoliths are more readily disaggregated by some resorption process in the kimberlite than eclogitic xenoliths.

Ilmenites do not occur as inclusions in diamond, but they are equally important for indicating the diamond potential of a kimberlite pipe. Gurney and Zweistra (1995) note that because diamonds and xenocrystal ilmenites do not have the same origin (i.e. composition of ilmenites is not affected by kimberlite conditions), their mutual occurrence or absence in a pipe must be due to late secondary processes, possibly resorption. Ilmenites have been known to reflect mantle conditions (Robles-Cruz et al. 2009) and, upon dissolution of the transport xenolith, react with the kimberlitic magma (Gurney and Zweistra, 1995). The change in ilmenite towards the rim of the grain therefore indicates how the grain adjusted to the conditions in the kimberlite pipe. In particular, changes in Mg and Fe^{3+} content distinguish the redox state of the kimberlite magma, which has implications for diamond resorption potential. Mg-rich ilmenites are indicators of a reduced kimberlite, which is more likely to preserve diamonds. Ilmenites rich in Fe^{3+} are characteristic of oxidized kimberlite

magmas, which have been correlated with higher grades of diamond resorption (Gurney and Zweistra, 1995, Robles-Cruz et al. 2009).

1.3 Motivation and objectives

There are several goals of this project, and several sources of motivation. One aim is to investigate the possibility of a connection between the dissolution features acquired by chromite and ilmenite grains during resorption and the composition of the kimberlitic melt. It is possible that specific chemical conditions will produce specific surface features during reaction between the grains and the kimberlitic melt. This kind of result could offer an explanation if, in fact, the surface features seen on kimberlitic oxides are specific to those from kimberlitic sources. Since Fe-Ti oxides in kimberlites are also diamond indicator minerals, the chemical composition of the grains will be used to infer the diamond preservation potential in the examined kimberlites. Using the experimental results from Fedortchouk and MacIsaac (2013) and the surface features observed on chromites and ilmenites, some inferences about the specific kimberlite conditions will be made, including constraining the fluid proportions and melt composition. Grains from two kimberlites in Botswana, supplied by De Beers Group, will be examined for surface dissolution features and chemical composition. The data will be examined in terms of reactions between the grain surface and the kimberlite melt. Information about the character of chromite and ilmenite resorption in kimberlites obtained from this project will aid in a better understanding of the processes that cause the dissolution of oxide minerals and the nature of their reactions with volatiles during a kimberlitic eruption.

2.0 GEOLOGICAL SETTING AND SAMPLES

2.1 Geologic and Tectonic History of the Area

The kimberlites chosen for this study are located in Botswana, Africa. The properties are owned by De Beers Group Exploration and they provided the mineral samples. These kimberlites are part of the Orapa kimberlite field of Cretaceous age, located in eastern Botswana, between the Zimbabwe craton and the Limpopo Belt (Archean) (Gernon et al. 2009). Both are diamond-bearing (Group 1) kimberlites (Chinn, 2013a, b). Due to issues of confidentiality with De Beers Group, specific information relating to the kimberlites and their locations is limited for disclosure in this study.

The Zimbabwe Craton is bordered by the Limpopo Belt to the south and is of Archean age (>3.5 Ga) (Khar'kiv, 2005). The Limpopo Belt was accreted during the Limpopo Orogeny, which occurred from 2.7-2.65 Ga (Barton and van Reenen, 1992). The Limpopo Belt comprises three zones of rocks which are much older than the orogen itself. The zones to the north and south are granite-greenstones metamorphosed to granulite facies. The Northern and Southern Zones are in contact with the Zimbabwe and Kapvaal cratons, respectively, and are each similar to the granulite facies of each adjacent cratonic terrane (van Reenen et al. 1992). The Central Zone of the Limpopo Belt comprises grey gneiss with an intrusive metagabbroic layered complex. The three zones are separated from each other and from the surrounding cratons by mylonitic shear zones (van Reenen et al. 1992).

The region is overlain by sediments of the Karoo Supergroup, ranging from the Late Carboniferous to Early Jurassic (Smith, 1990). The basal portion of the Karoo Supergroup is made up of the Dwyka Formation, formed from glacial deposition as Southern Gondwana passed over the South Pole in the Late Carboniferous (~270 Ma) (Smith, 1990). Variations between glacial and inter-glacial deposits (Ecca Group) followed to the beginning of the Permian, when the climate in now

Southern Africa shifted to semi-arid. The Ecca Group includes the bulk of the peat deposition which is the source of major coal reserves in South Africa (Smith, 1990). The semi-arid environment through the Permian and Triassic saw the deposition of dune-dominated sandstones with strata-bound uranium preserves. The Karoo Supergroup is capped by the Drakensberg tholeiitic basalt complex in the Early Jurassic (Smith, 1990).

The Orapa cluster of kimberlites was emplaced during the Cretaceous into the Limpopo mobile belt near the boundary to the Zimbabwe craton (Chinn, 2013b).

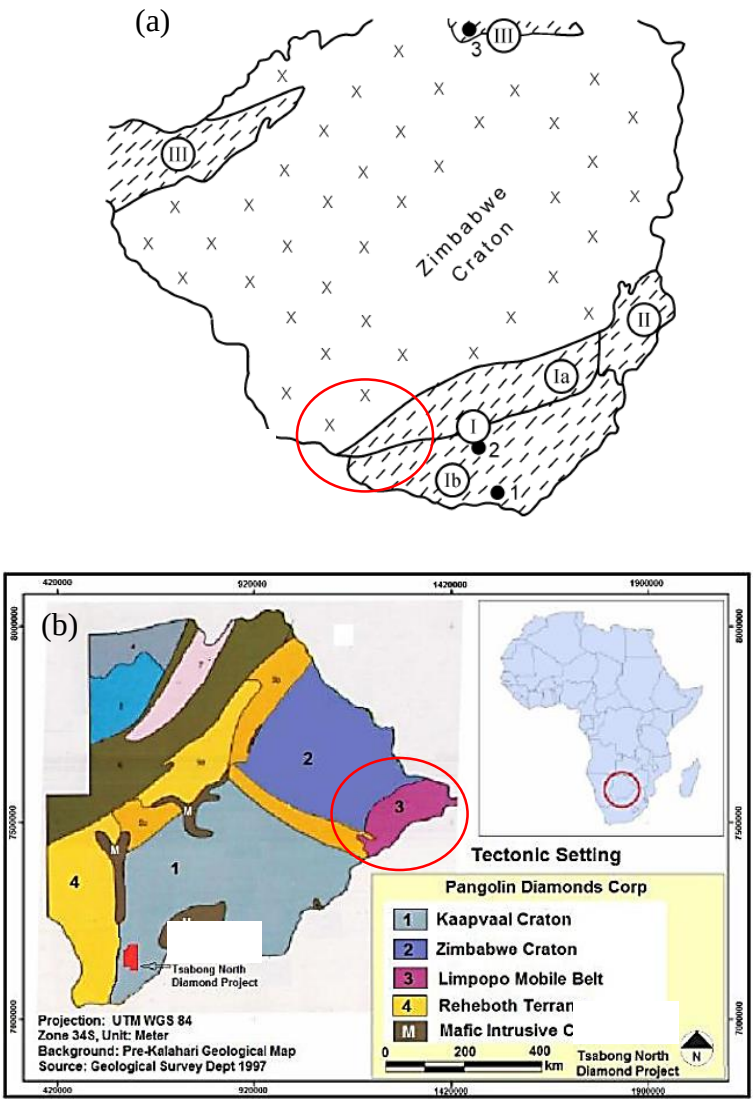

Figure 2.1 (a) Schematic of Zimbabwe craton showing boundaries with I-Limpopo Belt, Northern (Ia) and Central (Ib) zones, II-Mozambique Belt, and III-Zambezi Belt. Numbered points represent kimberlite belts. After (Khar'kiv, Roman'ko et al. 2005) (b) Diagram of the Republic of Botswana showing craton and mobile belt distribution through the country. Modified after (Daniels 2013) A red circle on each map highlights the location of the kimberlites used in this study.

2.2 Kimberlite A

Kimberlite A is a massive, uniform coherent kimberlite body partially overlain by Drakensberg Group basalt. The body is a sub-horizontal intrusive dyke which extends 160 metres beneath the surface and terminates in the Ntane Formation subarkosic sandstones. The contacts with the country rock are sharp with some minor brecciation. No volcaniclastic facies have been identified in association with this kimberlite. The coherent body has been classified as uniform in texture,

with xenolithic material ranging from 10-30 vol%, and mantle material constituting up to 70 vol% of the body. The olivine population in the kimberlite has been described as highly serpentinised along with other evidence of secondary alterations to the rock including the presence of segregated carbonate and some clay minerals (Chinn, 2013a).

2.3 Kimberlite B

Kimberlite B is a much more complex body than Kimberlite A. First identified by geophysical data, the kimberlite body has two main lobes that form adjacent coherent bodies located on a kimberlite root zone. One coherent lobe is confined to the north of the kimberlite area, and is the larger of the two lobes. The southern-most intrusive lobe has an associated and co-genetic massive volcaniclastic kimberlite (MVK) body. There is also a section of resedimented volcaniclastic kimberlite (RVK) material at the very south of the occurrence. In total, there are four phases of kimberlite facies identified in this kimberlite: the two coherent kimberlite (CK) facies, the MVK unit, and the RVK unit. The two coherent lobes as well as the MVK facies have altered or brecciated sub-units, most commonly in contact with the country rock. Geophysical information suggests that the southern portion of the kimberlite extends further to the south than is currently known (Chinn, 2013b).

Both coherent lobes of Kimberlite B are massive with crustal xenoliths. The northern lobe is coarser and contains fewer crustal xenoliths and secondary alteration products than the southern portion. The south coherent lobe contains abundant xenoliths with calcite and serpentine veins common. The RVK portion of the kimberlite is a smaller constituent. It has been described as a coarse-grained volcaniclastic kimberlite matrix with basalt clasts and a “reworked” texture. The MVK unit, located between the two coherent lobes, is a fragmental body with poor sorting and lithic clasts in a massive matrix. The composition of the whole kimberlite is stated to be uniform

within each unit (determined from magnetic susceptibility tests on the cores). Any chemical changes with depth are suggested to be due to variation in xenolith proportions (Chinn, 2013b).

2.4 Samples

These kimberlites are being used for this study because of their drastically different geological frameworks. The mineral samples sent to Dalhousie University from De Beers Group Exploration were extracted from additional screening of tailings at each site. The proportion of grains taken from different facies or locations in the kimberlite is unknown. Because of the lack of whole rock samples, further mineralogical assessment of these kimberlites cannot be commented on in this study. The number of samples sent of each mineral (chromite and ilmenite) from each kimberlite is annotated in Table 2.1.

Table 2.1 Number of mineral samples sent from De Beers Group Exploration from each kimberlite in this study.

	Kimberlite A “simple” single-facies kimberlite	**Kimberlite B** “complex” multi-facies kimberlite
Chromite	65	17
Ilmenite	76	257

3.0 METHODS

3.1 Sample Selection and Preparation

Several methods were applied in order to complete a full and effective analysis of the spinel and ilmenite grains. They include Scanning Electron Microscopy, Energy Dispersive Spectroscopy (SEM), Backscatter Electron imaging (BSE), microprobe quantitative chemical analyses (EMP) using Wavelength Dispersive Spectroscopy (WDS), and Elemental X-ray Mapping. All of the analyses were completed on two of Dalhousie University's Halifax campuses, the Sexton Engineering campus, which hosts a Hitachi S-4700 Field Emission Scanning Electron Microscope (FE-SEM), and the Studley campus, housing a JEOL 8200 Electron Microprobe (EMP).

Chromite grains (82) and ilmenite grains (333) were separated from mineral concentrates from two kimberlite bodies (A and B) and were supplied by De Beers for this study (Table 3.1). An optical stereo-microscope was used to select 52 chromite grains and 45 ilmenite grains with preserved original surfaces. The grains were cleaned in a dilute alcohol solution, mounted on carbon tape, photographed, and carbon coated.

Many ilmenite grains were covered with kimberlite groundmass and reaction material. Select grains were cleaned in a hydrochloric acid bath after the initial SEM examination in an attempt to partially remove any carbonaceous material from the grain surface. This process would have little to no effect on silicate groundmass and reaction material, or on oxide material. A solution of 10% hydrochloric acid was used and the grains were placed with the acid in a sonic bath for five minutes. These grains were then re-examined under the SEM. A fractured ilmenite surface with no features was used as a control in the acid bath to ensure the hydrochloric acid did not cause secondary etching or surface alteration on the ilmenite grains.

Table 3.1 Distribution of mineral grains from kimberlites and summary of methods applied.

Kimberlite	Mineral	Total grains	SEM	Polished	BSE	WDS	X-ray Map
Kimberlite A	Chromite	65	42	35	10	28	--
	Ilmenite	76	21	13	7	13	3
Kimberlite B	Chromite	17	10	8	3	8	--
	Ilmenite	257	24	16	8	16	3
Total	Chromite	82	52	43	19	36	0
	Ilmenite	333	45	29	16	29	6
	Total	415	97	72	35	65	6

3.2 SEM imaging

SEM involves the projection of electrons onto the sample being examined. An inelastic collision occurs with the sample, and excites electrons within the elements present (Swapp, 2013). As the excited electrons drop back to a lower energy state, they release secondary electrons, which are registered by a detector. SEM is not harmful to the sample, because there is minimal volume lost to the material during analysis. It is particularly useful for morphological and topographic analysis (Swapp, 2013).

SEM at Dalhousie's Sexton campus was used to catalogue the different surface features present upon the grain surfaces. Where a grain showed prominent surface features, several photographs were taken at magnifications ranging from x130 to x8000. SEM analyses were conducted with a 10keV accelerating voltage and a 15uA beam current. 97 grains were photographed (Table 3.1).

3.3 EDS analyses

Energy Dispersive Spectroscopy (EDS) methods were applied for surface identification. EDS involves a similar electron excitation method to SEM analysis. EDS measures characteristic X-rays that are emitted from the sample as the outer-shell electron drops an energy level. These X-rays are separated by the detector on the basis of their energy along a spectrum (Goodge, 2013).

This method was conducted on Hitachi S-4700 FE-SEM at Sexton and JEOL 8200 EMP at Studley Dalhousie University. EDS is a quick method of gaining a chemical composition and is often used for identification of unknown mineral phases. This method is not as precise as Wavelength Dispersive Spectroscopy (described in section 3.5); however, it does provide reliable verification of a mineral. It was used to confirm the presence of reaction products on many of the grain surfaces, particularly the ilmenite grains. First, the oxide composition was examined on unpolished grains during SEM work. A fractured surface inside of the grain was chosen to ensure that the original grain composition was analyzed and not a reaction phase. This type of initial analysis was also conducted on kimberlite matrix material and reaction products present on the surface of unpolished grains. After initial examination the grains were mounted in epoxy and polished. This allowed for re-examination of the reaction phases and any compositional zoning. Collection time for EDS spectra in this study was 60 seconds.

3.4 BSE imaging (from Goodge, 2012a)

BSE images display significant compositional variations but, do not provide quantitative verification of the different minerals. An electron beam is accelerated onto the sample in the EMP. Back scatter electrons are emitted during an elastic collision with the materials in the sample. The number of emitted back scatter electrons is registered by the receiver in the EMP. This number is proportional to the atomic number of the primary element present in the sample. Heavier portions appear brighter than lighter portions. This gives an image of general compositional variations within a sample.

Grains that had already been through the SEM process were selected for polishing to look for chemical zonation with back scatter electrons. A total of 43 chromites and 29 ilmenites were polished and examined for surface features and zonation. Some 19 chromites and 16 ilmenites showed these properties and were imaged in back scatter mode (See Table 3.1).

3.5 WDS analyses (from Henry, 2012)

WDS is a quantitative method of chemical analysis that detects the same characteristic X-rays analyzed during EDS, but the technique has higher spectral resolution and is more quantifiable. The WDS analysis involves an analytical crystal, which is precisely oriented within the machinery. The crystal filters the emitted X-rays according to Bragg's Law, and only lets past those which enter at a certain angle. The position of the crystal is adjusted for each element being analyzed, and in this way, the orientation allows for the entry of X-rays with the wavelength characteristic of the element being measured.

Single point analyses of the cores of chromite and ilmenite grains were completed on all of the polished grains. Where zonation or reaction products were detected in BSE, additional analyses were conducted. This included point analyses of rims or zones within a mineral, point analyses of different reaction phases, and profile collections that tracked a line of analyses through the core to the rim of a grain. WDS analysis was conducted on 36 chromites (28 from Kimberlite A, eight from Kimberlite B) and 29 ilmenites (13 from A, 16 from B).

The collection of quantitative analysis was conducted with a 20keV electron accelerating voltage, a 15uA probe current, and a beam width of 2um. The elemental standards run for these analyses were Ca, K, Nb, Mn, Fe, Nb, Zn, Mg, Na, Cr, V, Ti and Si.

3.6 Elemental X-ray Maps

The next method, applied to six ilmenite grains, was the acquiring of elemental X-ray maps. Several elements were chosen to show their trends through the grain: Ca, Fe, Mg, Si, Ti, Nb, Ni, V, Zn and Cr. The six grains used for this analysis were selected based on the presence of complex zoning and reaction phases (including perovskite and titanite, as well as kimberlitic groundmass material) occurring in the grains, determined from BSE images of the polished grains. X-ray maps provide a combined pictorial and quantitative representation of the chemical and elemental

interactions within the scale of a single grain. The technique was much more effective at demonstrating progressive and abrupt changes in composition than WDS or BSE alone. X-ray element maps are generated by completing a WDS analysis point-by-point over an area in a raster (Goodge, 2012b). These chemical results are then translated to the raster image in the form of a colour, representing concentration of the element measured. The resolution and time required for an X-ray map can be adjusted by changing the dwell time and strength of the beam, as well as the pixel size of the completed raster (Goodge, 2012b). The dwell time used for this study was 10 seconds, and the beam width and pixel size were each 1um.

4.0 RESULTS

This section will outline the major data collected during this study of kimberlitic oxides and detail the observations made regarding changes from the original grain morphology and composition. It will begin with grain composition and zonation toward the grain rims, then discuss dissolution and the related surface features, and will finish with a description of reaction phases present on the grain surface.

4.1 Chemical composition of oxide minerals

4.1.1 Composition of Chromian Spinel

Most of the spinel compositions from Kimberlites A and B correspond to magnesian chromian spinel and follow the Cr-Al compositional trend defined by Barnes and Roeder (2001) (Fig. 4.1). On a binary plot diagram with Cr-no vs Mg-no and a ternary diagram Cr-Al-Fe^{3+}, spinel compositions from this study plot within the xenolith, primary kimberlitic phenocrystal spinel, and pleonaste spinel groups defined by Roeder and Schulze (2008) for kimberlites (Figs. 4.1, 4.2).

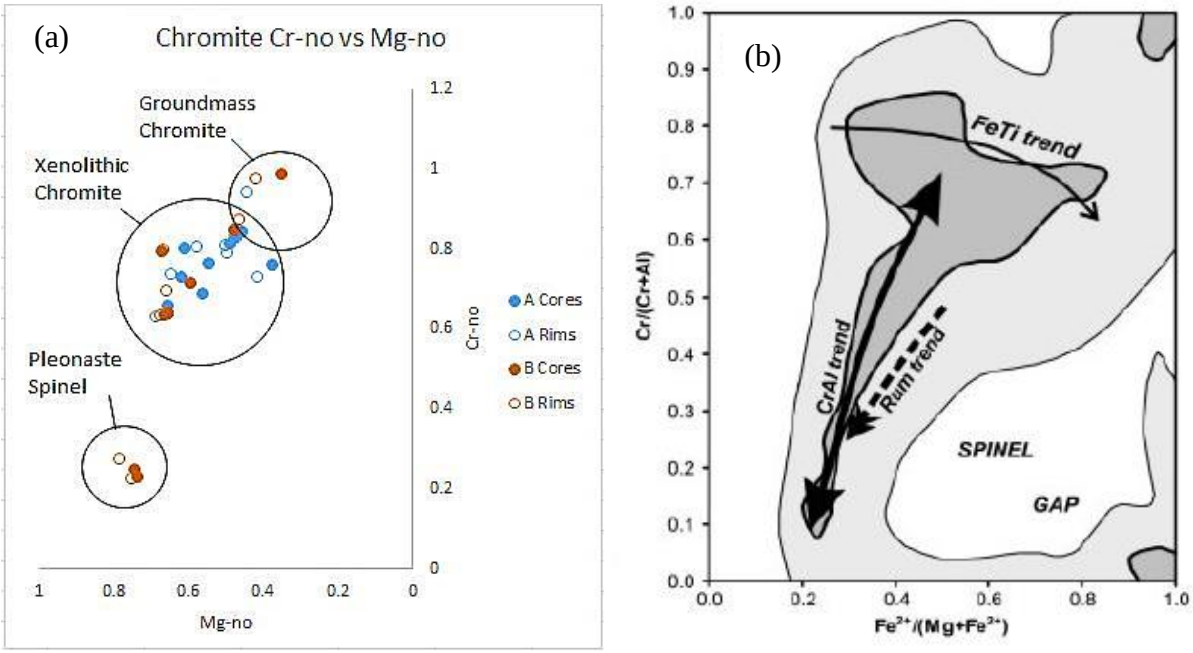

Figure 4.1 Composition of analyzed spinel grains (a) Cr-no showing chromite fields as defined in Roeder and Schulze (2008) compared to (b) Cr-Al and Fe-Ti trends described by Barnes and Roeder (2001).

The analyses of spinel grains (cores and rims) from Kimberlites A and B do not fit the magnesio-ülvo-spinel-magnetite (MUM) compositions and Fe^{3+} increase trend defined by Roeder and Schulze (2008) (Fig 4.2a) as the most common evolutionary trend for kimberlitic spinel (shown as "Kimberlite Trend" in Fig. 4.2b from Barnes and Roeder, 2001). All of the compositions from this study plot in the Cr-rich corner of the Cr-Al-Fe^{3+} diagram in the fields for xenocrystic spinel and primary kimberlite phenocrystal spinel (two extraneous grains). Pleonaste spinel (found in Kimberlite B only) plot towards the Al-rich zone of the diagram in a separate cluster. Looking at other variations in chemistry between the chromite grains reveals a slight negative trend. The chromites from Kimberlite B appear to have clustered Ti compositions, with mostly low Ti in all the chromites, excepting the two pleonaste spinel grains, which have high Ti. The chromites from Kimberlite A display a pattern much more akin to an evolutionary trend, with increasing Ti through crystallization, as can be seen in Figure 4.3.

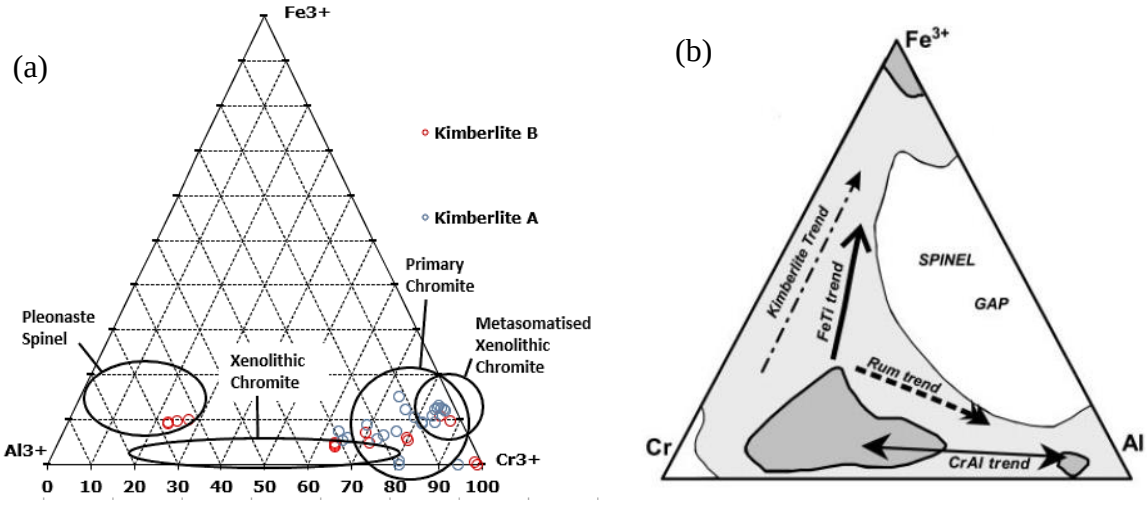

Figure 4.2 Composition of analyzed spinel grains (a) ternary Fe^{3+}, Al^{3+}, Cr^{3+} showing chromite fields as defined by Roeder and Schulze (2008) compared to (b) Cr-Al ad Kimberlite trends described by Barnes and Roeder (2001).

Chromites from both kimberlite pipes show up to 2.7 wt% of TiO_2 (Fig. 4.3). The highest Ti in Kimberlite B is recorded in the two pleonaste spinel grains. Chromian spinel from Kimberlite A

forms a continuous trend of Ti increase, whereas the limited number of analyses (eight grains) form a cluster at <0.5 wt% TiO2.

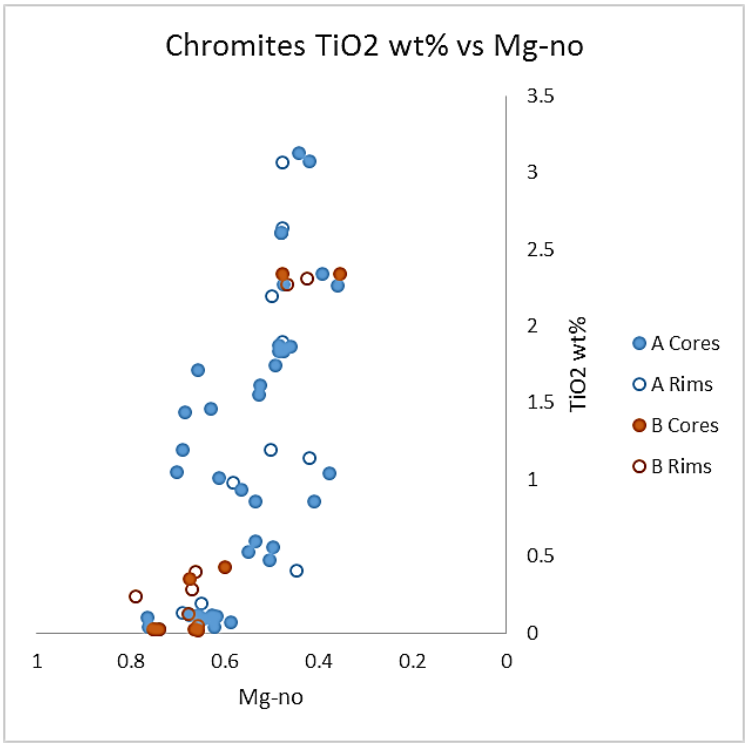

Figure 4.3 Composition of analyzed chromites, TiO_2 wt% vs. Mg-no.

Both Kimberlites A and B show zonation in the chromite grains, with a slight increase in Cr and Ti toward the rim. Most of the zonation displayed on chromite grains seems to be associated with pitting around the edge of the grain (Figs. 4.4, 4.5). The grains in Kimberlite A show thicker rims (up to 50µm) than Kimberlite B (<10 µm).

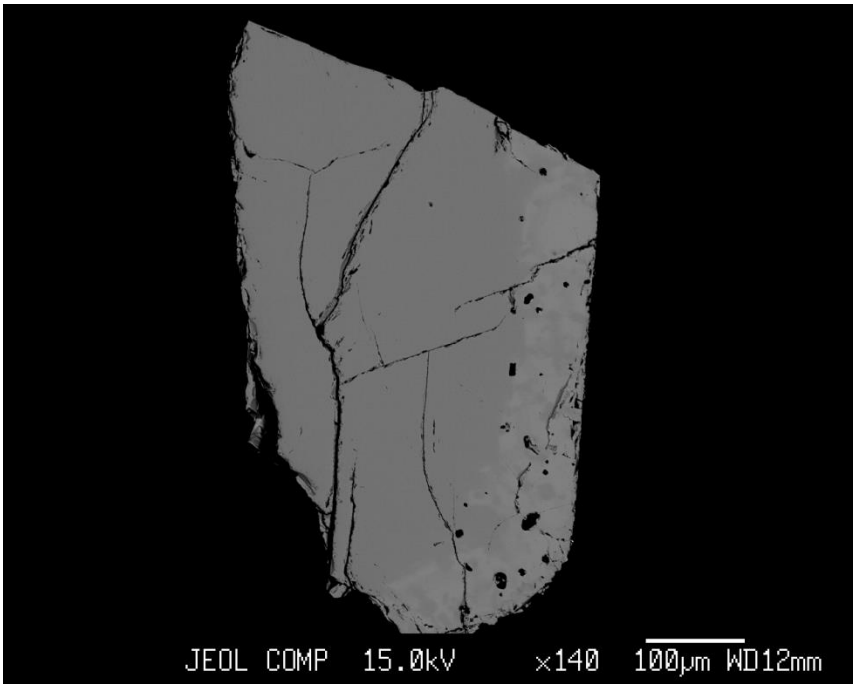

Figure 4.4 Back scatter electron image of a chromite grain from Kimberlite A showing slight zonation around the grain edge.

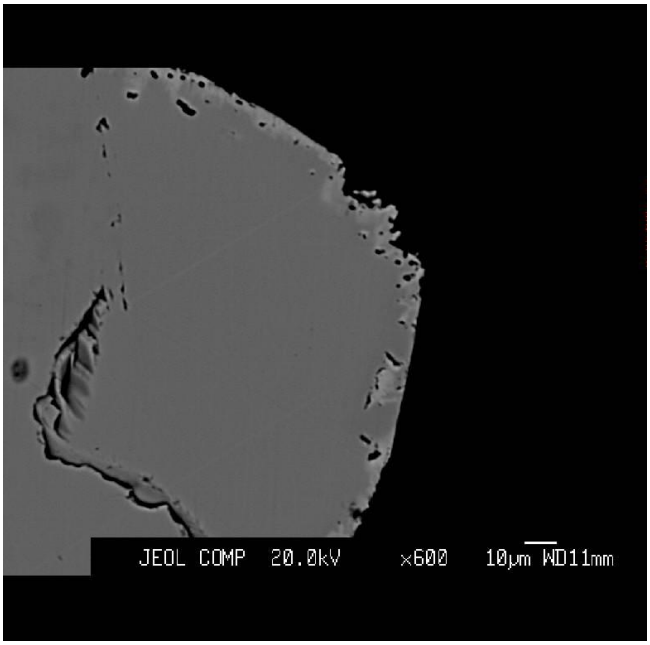

Figure 4.5 Back scatter electron image of a chromite grain from Kimberlite B showing a very thin zonation rim.

4.1.2 Composition of Ilmenites

The ilmenites examined in this study are Mg-rich and plot within the kimberlite field, as defined by Wyatt et al. (2004) (Fig 4.6). Ilmenites from Kimberlite A consistently have higher MgO content (up to 16 wt%) and both cores and rims form a positive Mg vs Ti trend. Ilmenites from Kimberlite B have lower Mg (up to 10wt% MgO) and separate into more Ti-rich core and Ti-poor rim clusters (Fig. 4.6). Ilmenites from Kimberlite A also show significantly higher Cr content than ilmenites from Kimberlite B (Fig. 4.7a). Similar to the chromian spinel, ilmenites from Kimberlite A show evolutionary compositional trends, whereas ilmenite compositions from Kimberlite B are clustered (Figs. 4.6, 4.7).

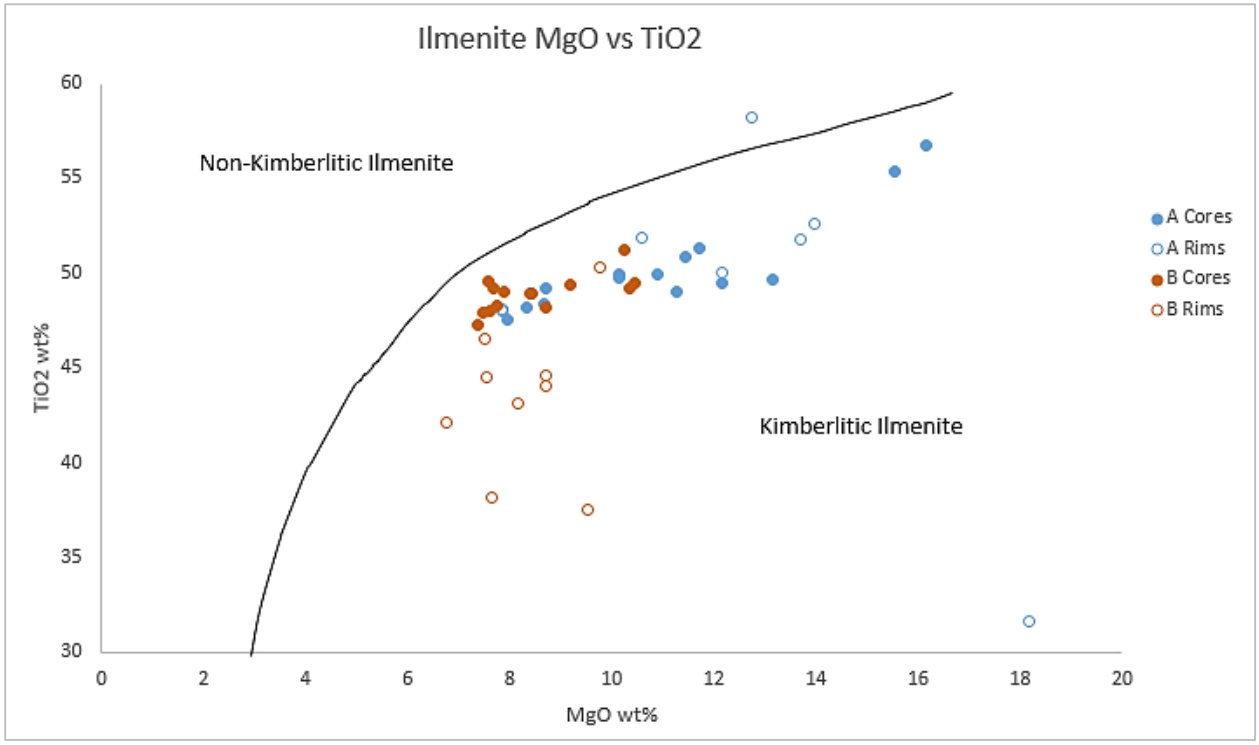

Figure 4.6 TiO_2 vs MgO of the studied ilmenites compared to the "kimberlite field" defined by Wyatt et al. (2004)

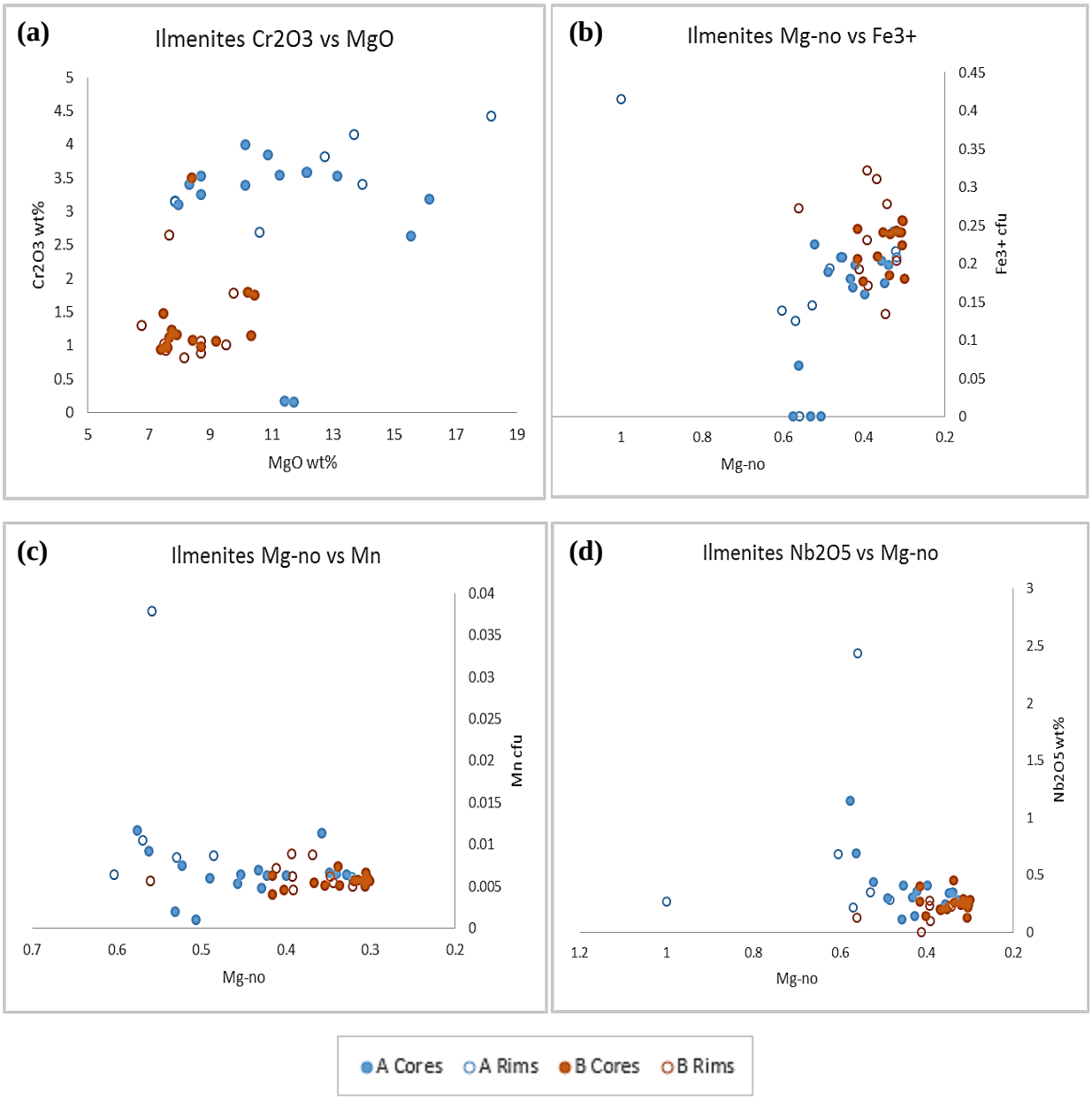

Figure 4.7 Compositional plots of examined ilmenite grains (a) Cr_2O_3 vs. MgO (b) Fe^{3+} vs. Mg-no (c) Mn vs. Mg-no and(d) Nb_2O_5 vs. Mg-no

There is apparent zonation in the ilmenite grains from both kimberlites. To examine compositional zonation, the cores and rims of 13 grains from Kimberlite A and 16 grains from Kimberlite B were analysed. Though it is not apparent in the plots, examination of individual grain compositions revealed some patterns. Both Kimberlite A and Kimberlite B have rims depleted in Nb and slightly enriched in Mn (see Tables A1 and A2). The ilmenite rims appear to be depleted in Ti and Cr, particularly those from Kimberlite B. In addition, ilmenites from both kimberlites have significant

reaction rims consisting of perovskite and titanite and occasionally Ti-magnetite (Fig. 4.8, 4.9). The reaction products are described further in section 4.2.3.

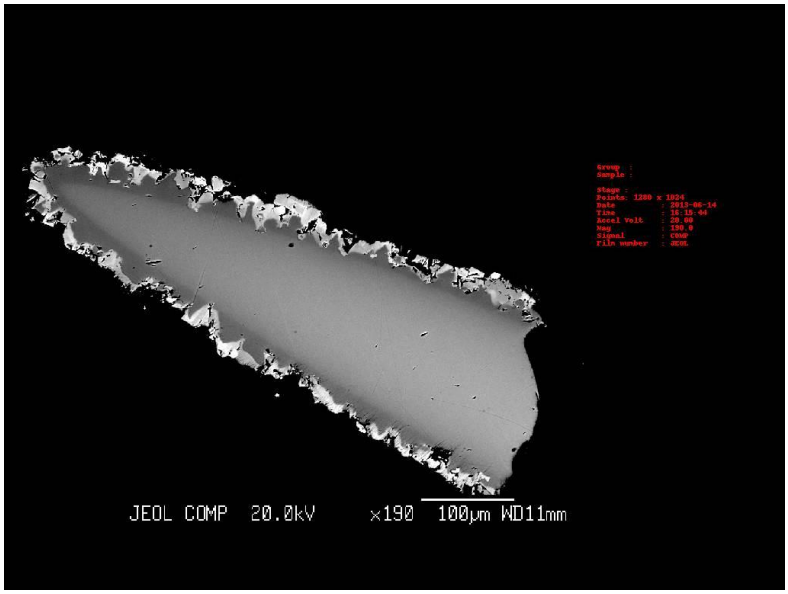

Figure 4.8 Back scatter electron image of an ilmenite grain from Kimberlite A with visible grain zonation and some reaction phases on grain surface.

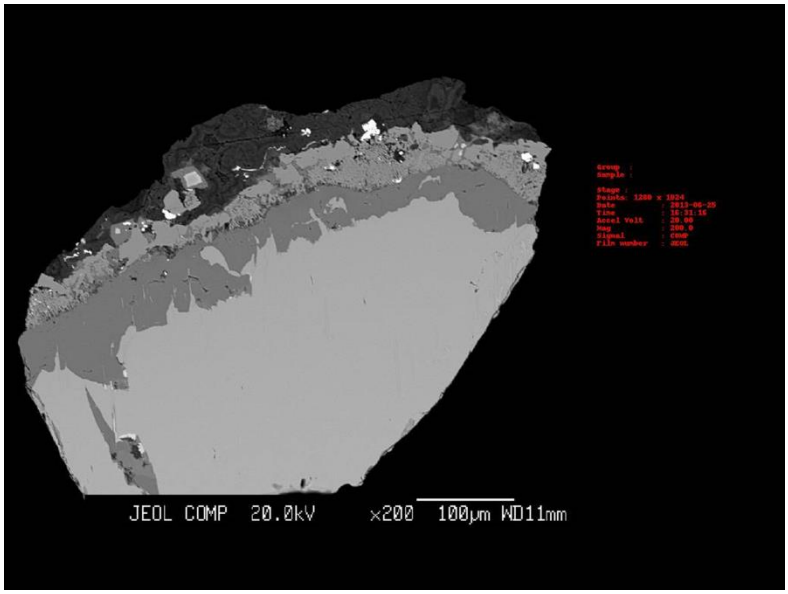

Figure 4.9 Back scatter electron image of an ilmenite grain from Kimberlite B with no visible grain zonation and large volume of reaction phases on grain surface.

Visible zonation in BSE images was only observed on ilmenite grains from Kimberlite A (Fig. 4.8) due to an increase in Mg/(Mg+Fe) in the rim of the grains, confirmed by elemental X-ray mapping. This trend was not evident in the ilmenites from Kimberlite B.

4.1.3 Compositional Grain Profiles

In order to gain a better understanding of the nature of the zonation occurring in the chromite and ilmenite grains, profiles were traced through three grains. WDS spectra were collected at every 10 micrometres along the trace from the core to the rim of each grain. Elemental variations were plotted against distance from the core. This process was completed on one chromite grain from Kimberlite A, one ilmenite from Kimberlite A and one ilmenite from Kimberlite B. In Kimberlite B, the zonation seen in chromite grains is too thin to produce an effective profile. The profiles and plots are shown in Figs. 4.10-4.12. The WDS spectra for these profiles are given in Appendix C.

The chemical profile from the chromite grain (Fig. 4.10b) shows that the compositional variations evident in back scatter images are the result of decreases in Mg and Al, and increases in Ti and Fe towards the rim of the grain. The variations do not appear in a uniform pattern around the grain rim, the zonation is patchy, and could be associated with the pitting and/or fracturing also present around the grain edge (Fig 4.10a).

The compositional profile from the Kimberlite A ilmenite grain has a very complex signature. The core of the grain has a similar composition to other ilmenites from both kimberlites, with slightly higher Mg and Ti, and lower Fe. The next portion of the grain stands out very clearly in the back scatter image (Fig 4.11a) as a lighter coloured zone with a darker exsolution pattern. This distinct type of zonation has not been seen in any other grains from either kimberlite. This lighter zone has significant Ti and Nb (70 and 15 wt% TiO_2 and Nb_2O_5 respectively) and increased Cr proportions (up to 6 wt% Cr_2O_3) (Fig 4.11b). This phase is likely leucoxene, a high titanium oxide mineral

mentioned by Mitchell (1986) as being a reaction phase with kimberlitic megacrystal ilmenites. Mitchell also mentions the occurrence of ilmenite exsolution within kimberlites. The exsolution seen in the leucoxene phase rim of this ilmenite grain could be lamellae of ilmenite, or another phase which contributes the unusually high Nb content.

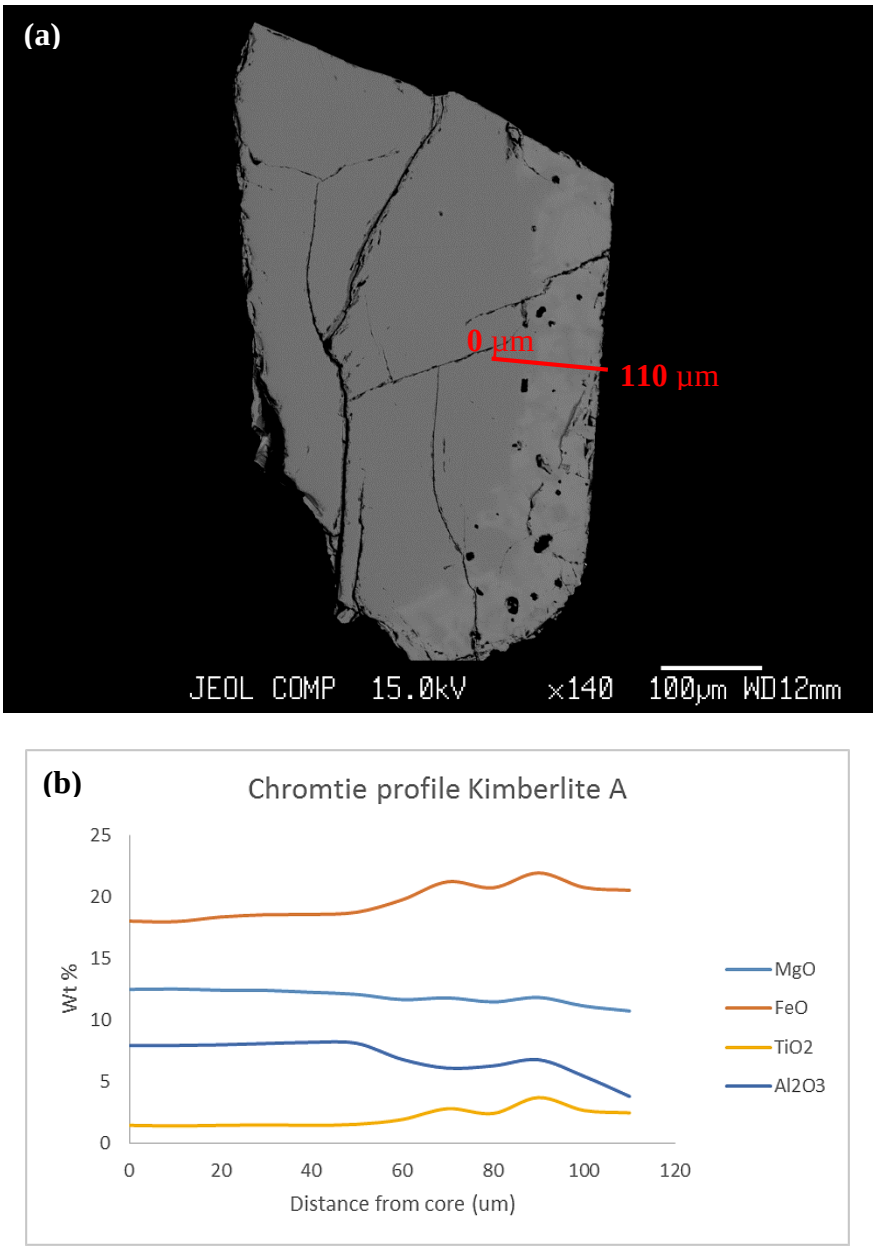

Figure 4.10 Chromite grain from Kimberlite A (a) WDS profile trace (b) elemental variation plots from core to rim.

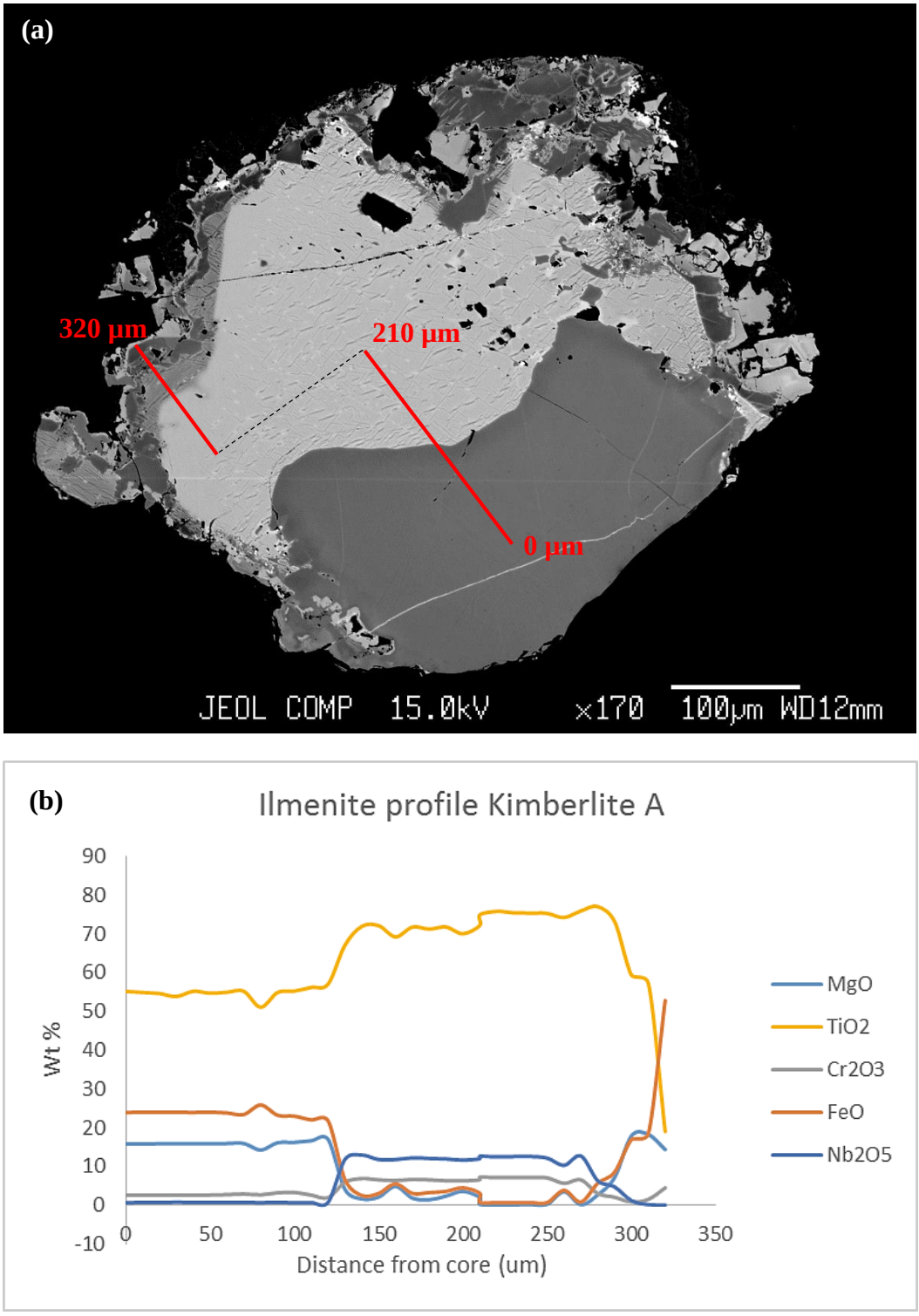

Figure 4.11 Ilmenite grain from Kimberlite A (a) WDS profile trace (b) elemental variation plots from core to rim.

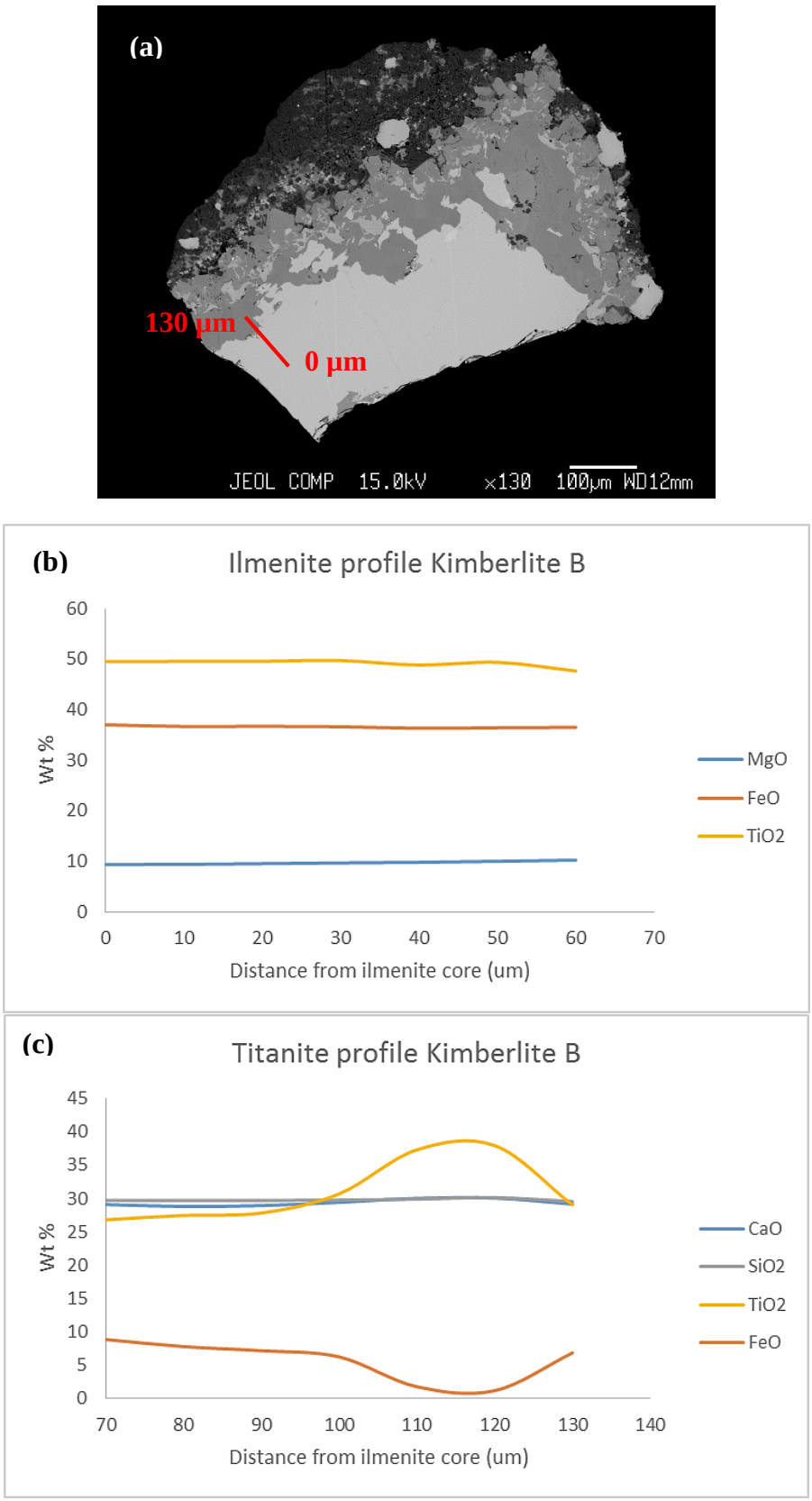

Figure 4.12 Ilmenite grain from Kimberlite B (a) WDS profile trace (b) elemental variation plots in ilmenite from core to titanite contact (c) elemental variation plots in titanite from ilmenite contact to core of titanite.

Another compositional profile transects both ilmenite and reaction phase titanite in a grain from Kimberlite B (Fig 4.12). The profile starts in the core of the ilmenite, moves to the rim, and then into the titanite rim to the margin of the grain (Fig 4.12a). The compositional profile within ilmenite reveals a slight depletion in Ti towards the titanite contact at the rim. The rest of the elements remain fairly constant through the grain profile (Fig 4.12b). The titanite shows variations in Ti and Fe away from the ilmenite contact (Fig 4.12c).

4.2 Dissolution features and reaction products on Fe-Ti oxides

4.2.1 Description of dissolution features on Chromian Spinel

The chromian spinel group observed in this analysis consistently displayed regular and patterned dissolution features on the surface of the grains. The chromite grains in this study were categorised based on grain shape and dissolution type. The majority of the chromite grains had rounded ovoid shapes, an elongation of the chromite octahedral grain shape. Other grains had a more equant shape, though still some rounding of the corners and edges which gave the grain a truncated appearance and a few were too fractured to discern a shape. The categorical chromite grain shapes derived from these observations were octahedral, truncated, ovoid-elongate and grains that were fractured or indeterminate (Table 4.1). The main dissolution types seen were edge/corner dissolution, full grain dissolution, and grains that were fractured or the dissolution patterns were indeterminate (Table 4.1). Grains that displayed edge/corner dissolution had preserved {111} faces with minimal alteration, the majority of the resorption focused around the corners and edges. Full grain dissolution describes grains where the faces {111} were attacked equally to the edges and corners. Table 4.1 shows distribution of the different grain shapes and dissolution patterns between the two kimberlites. The majority of the population from Kimberlite A had an ovoid-elongate grain shape, and the most common dissolution style was edge-corner dissolution. In Kimberlite B, the

primary shape and dissolution styles were indeterminate because most of the grains were too fractured to identify a pattern.

Table 4.1 Distribution of chromite grain shapes and dissolution styles in Kimberlites A and B, determined from SEM images.

Kimberlite	Dissolution style	Total	Grain Shape			
			octahedral	truncated	ovoid-elongate	fractured/indeterminate
A	edge/corner dissolution	21	3	9	8	1
	full grain dissolution	17	--	5	9	3
	fractured/indeterminate	4	--	1	3	
	Total	42	3	15	20	4
B	edge/corner dissolution	2	--	--	2	--
	full grain dissolution	5	--	--	3	2
	fractured/indeterminate	3	--	--	--	3
	Total	10	--	--	5	5

Part of the aim of this project was to investigate a possible relationship between the surface features and compositions of grains found in kimberlites. To that affect, the chromite grain shape and dissolution style groups, as described above, were plotted against the chemical compositions. The result did not yield any particular pattern, in either the grain shape divisions or the dissolution style divisions. Figures 4.13 and 4.14 show the plots of Mg-no versus Cr-no. Mg-no versus TiO_2wt% comparisons were also plotted, with a similar result. It is interesting to note, however, that only Kimberlite A has grains which display octahedral and truncated grain shapes. This could be a product of the much smaller sample size available for Kimberlite B.

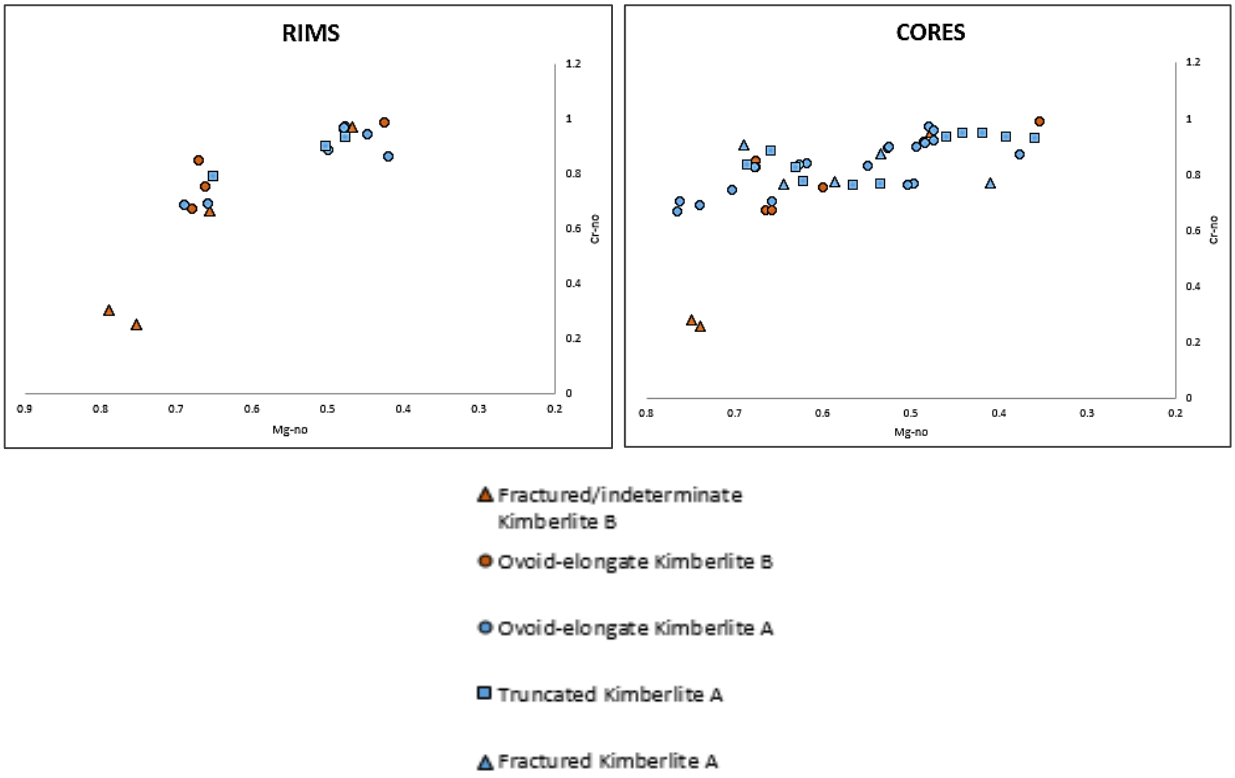

Figure 4.13 Chromite grain shape group compositions

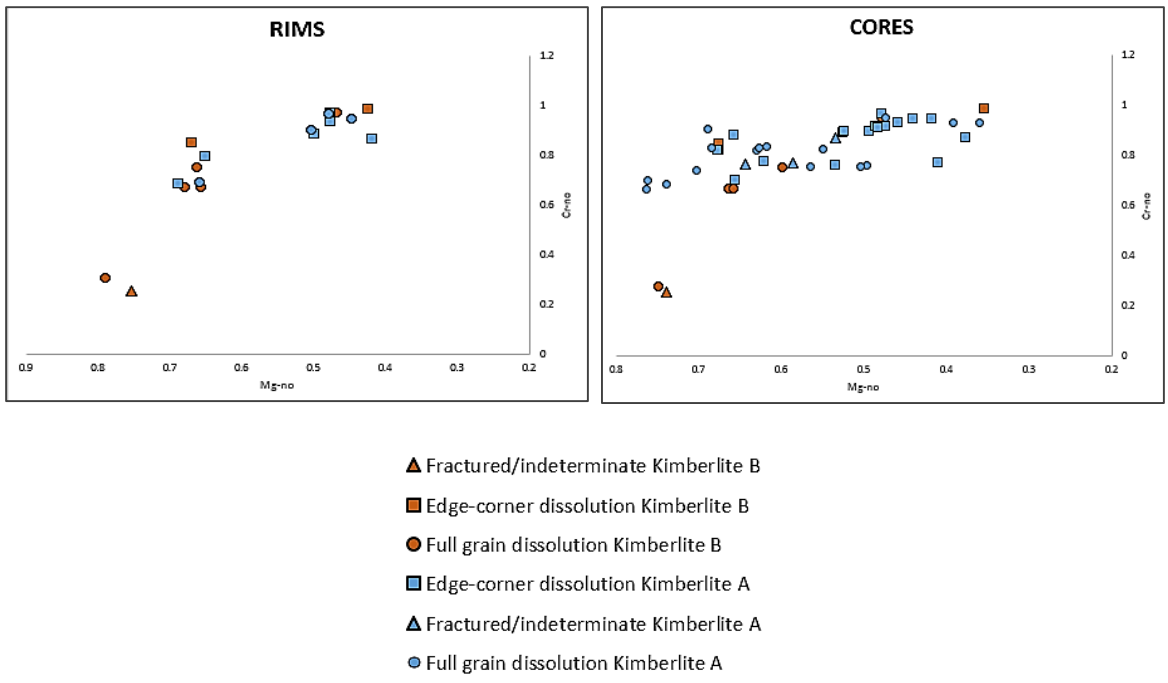

Figure 4.14 Chromite dissolution style group compositions

The following sections will more completely depict the features seen on the {111} faces, on [100] vertices and along the edges perpendicular to the [110] direction of the chromite grains from both kimberlites.

4.2.1.1 Resorption of {111} face

The {111} faces have only been preserved on chromite grains from Kimberlite A. The grains of Kimberlite B are either too extensively fractured or too resorbed to identify any {111} faces. Dissolution of {111} results in pitting, most commonly forming triangular shapes (trigons). The trigons are consistent in size on all the studied grains, varying from 4-10 μm. Some pits are much deeper than the rest of the trigons (Fig. 4.15b). Back scatter images revealed kimberlitic groundmass material sitting in some of the pits on the grain surface (Fig. 4.15d). Overall, the {111} face showed much less resorption than the other faces of the grain, even in the case of the full grain dissolution style, where the trigons and pits extended across the whole face.

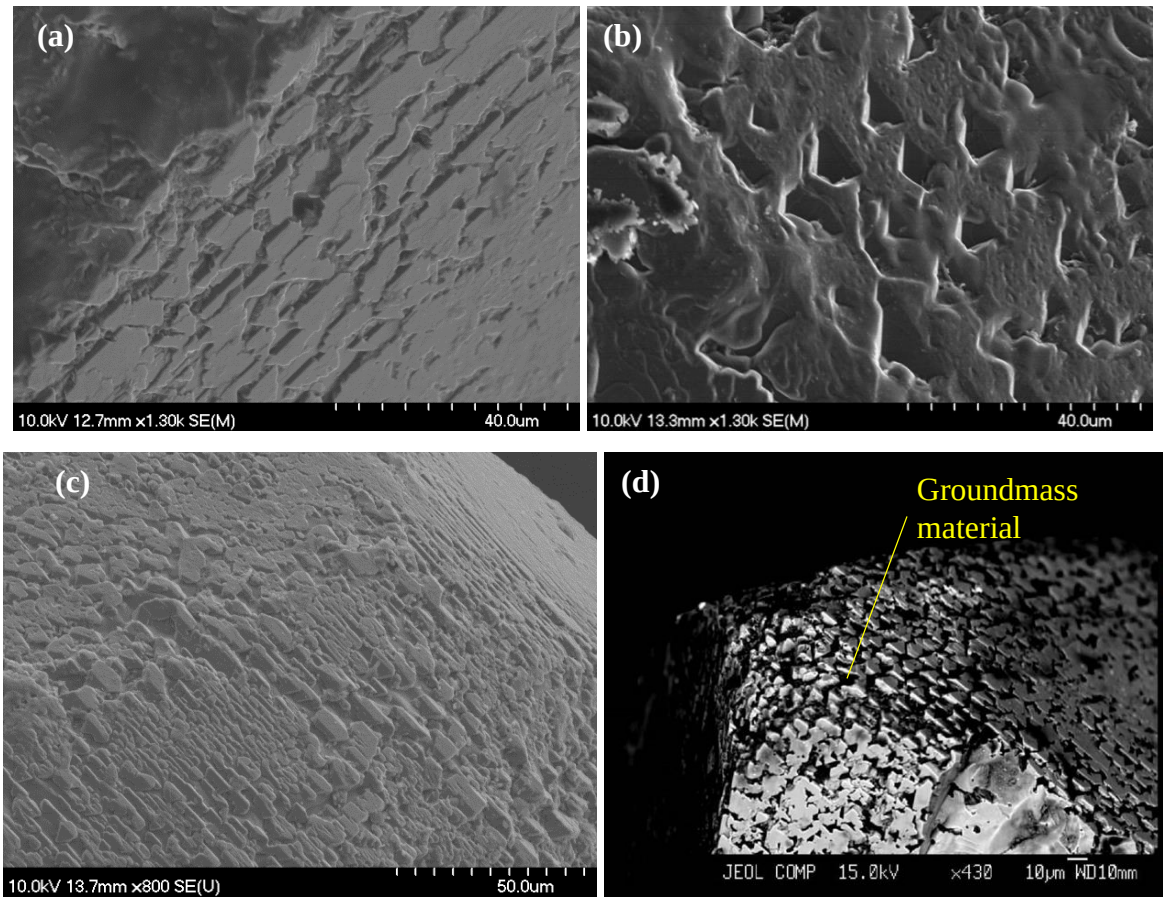

Figure 4.15 Examples of triangular dissolution pits on [111] face of chromite grains from Kimberlite A (a,c) shallow triangular pits, (b) deep triangular pits and (d) BSE image with kimberlite groundmass material filling pits on grain surface.

4.2.1.2 Resorption along [110] edge

Resorption of the [110] edge results in grain rounding. Many of the examined grains are almost fully rounded with very small {111} faces preserved. In cases where the edges are clear, dissolution produces a stepped pattern. This elongate feature appears to extend to the corners where the terminations of each step form the protruding nodules found on the [100] vertices. Grains from Kimberlite A typically show more rounded and thinner steps, approximately 1-2 µm (Fig. 4.16a). The steps seen on Kimberlite B are more protruding, sharper and wider, about 4 µm (Fig. 4.16b). In some cases on grains from Kimberlite B, the [100] direction was not preserved, and elongate steps covered the whole of the grain surface (Fig. 4.16c). Examples of elongate edge steps from each kimberlite are shown in Figure 4.16 (a,b).

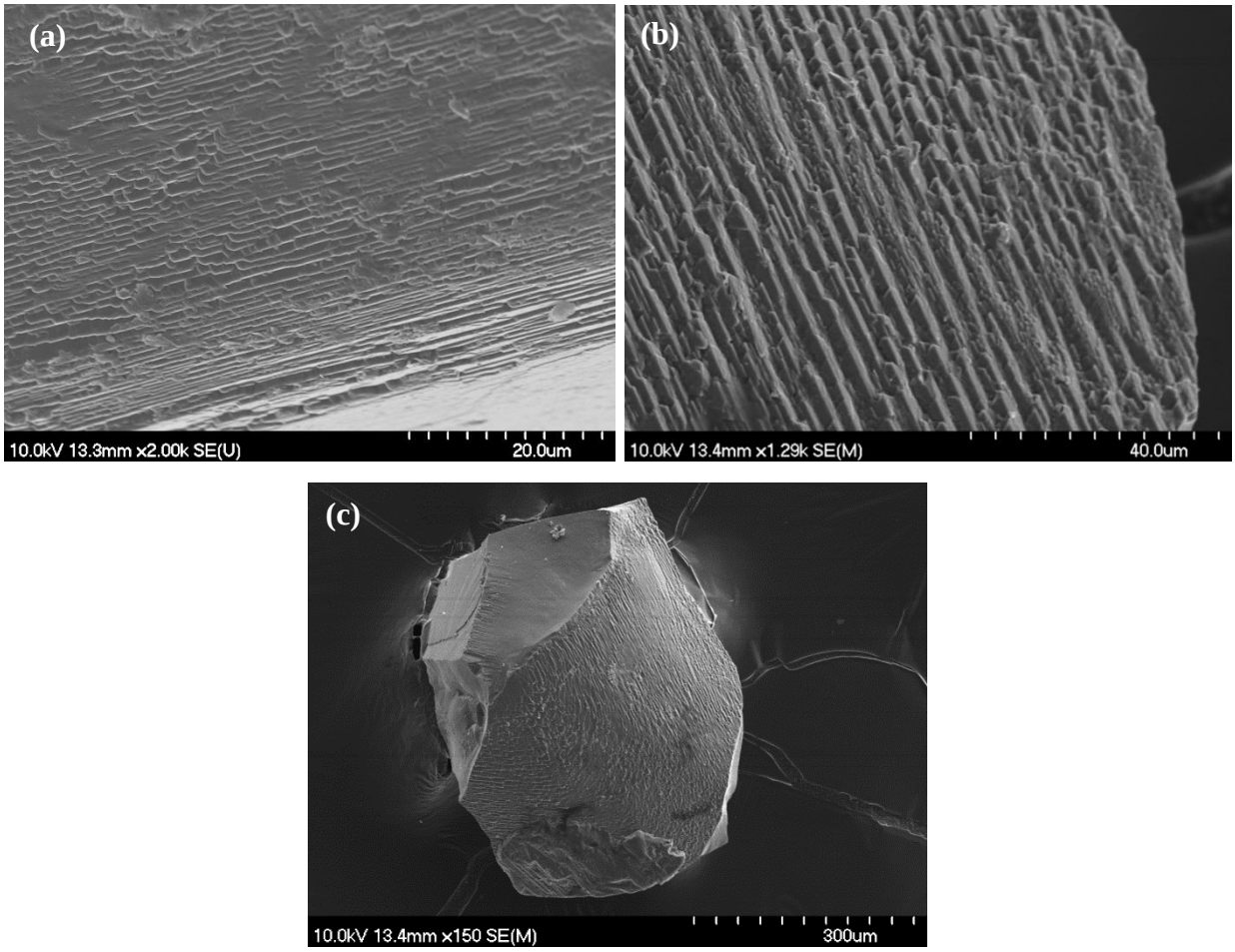

Figure 4.16 Examples of {110} edge dissolution from (a) Kimberlite A, showing rounded, thin steps, (b) Kimberlite B, with sharper, wider steps and (c) showing a grain with complete dissolution of [100] direction.

4.2.1.3 Resorption of [100] vertices

The [100] direction of the chromite grains showed the most resorption. The corners of the grains consistently display the most regular features: protruding octahedral nodules, or pyramids (Fig 4.17). These nodules are oriented on the corners of the grains similar to what has been observed in other studies (LeBlanc, 1980). The [100] corner direction of the chromite grains is less often preserved in Kimberlite B, however, where there is a preserved corner, the nodules are rounded, small and anhedral (Fig 4.17 c,d). There were two or three grains from Kimberlite A which presented a similar rounded quality to the nodules found on the resorbed corners; however, the most common corner resorption seen in Kimberlite A was very sharp and prominent (Fig 4.17 a,b).

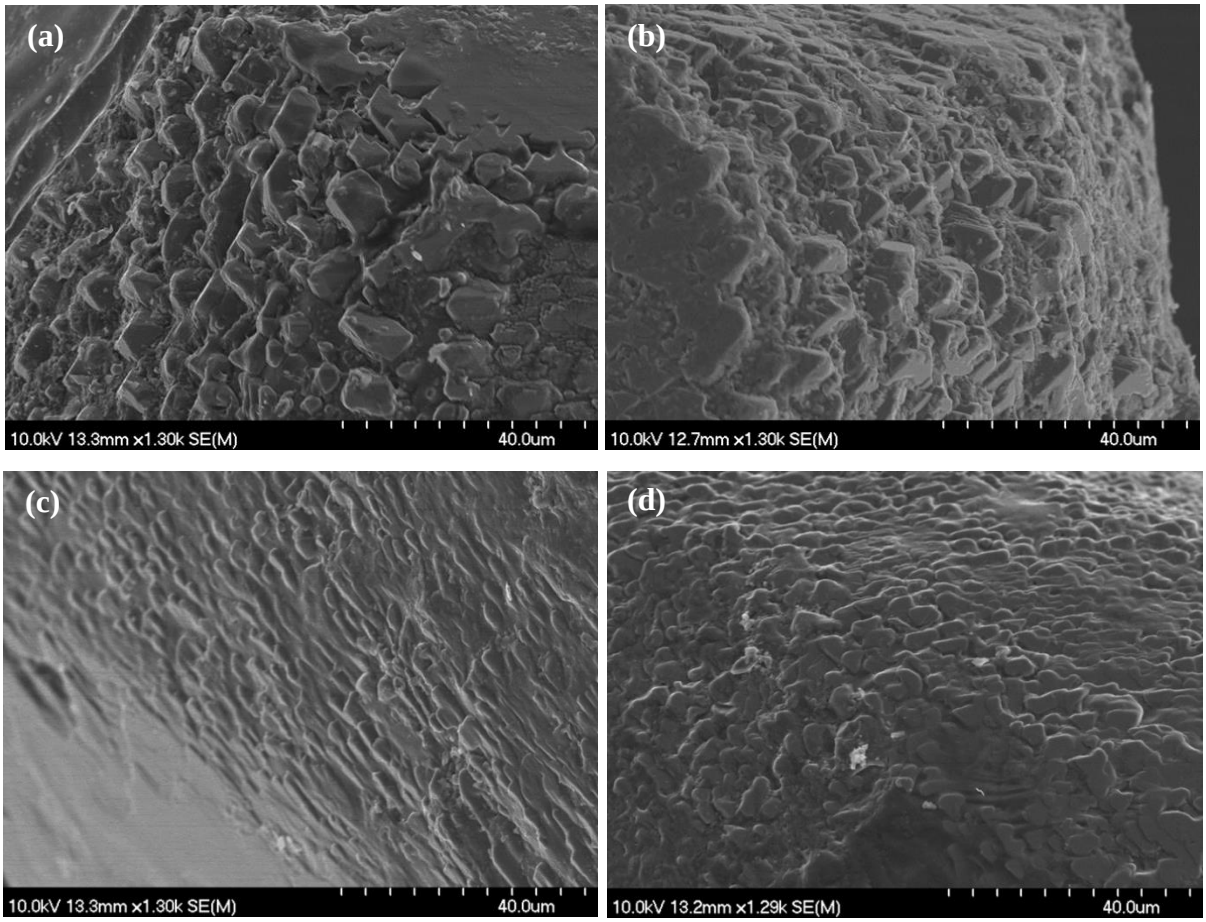

Figure 4.17 Examples of chromite dissolution in {100} direction (a,b) prominent octahedral dissolution of corners in Kimberlite A (c) less-common rounded corner dissolution of grains in Kimberlite A (d) rounded anhedral corner dissolution of chromites in Kimberlite B.

A schematic representation of the resorption occurring on the octahedral chromite grain is shown in Figure 4.18. The [100] vertices develop pyramid nodules, the [110] edges develop elongate step patterns, and the {111} faces develop triangular pits around the edges and corners.

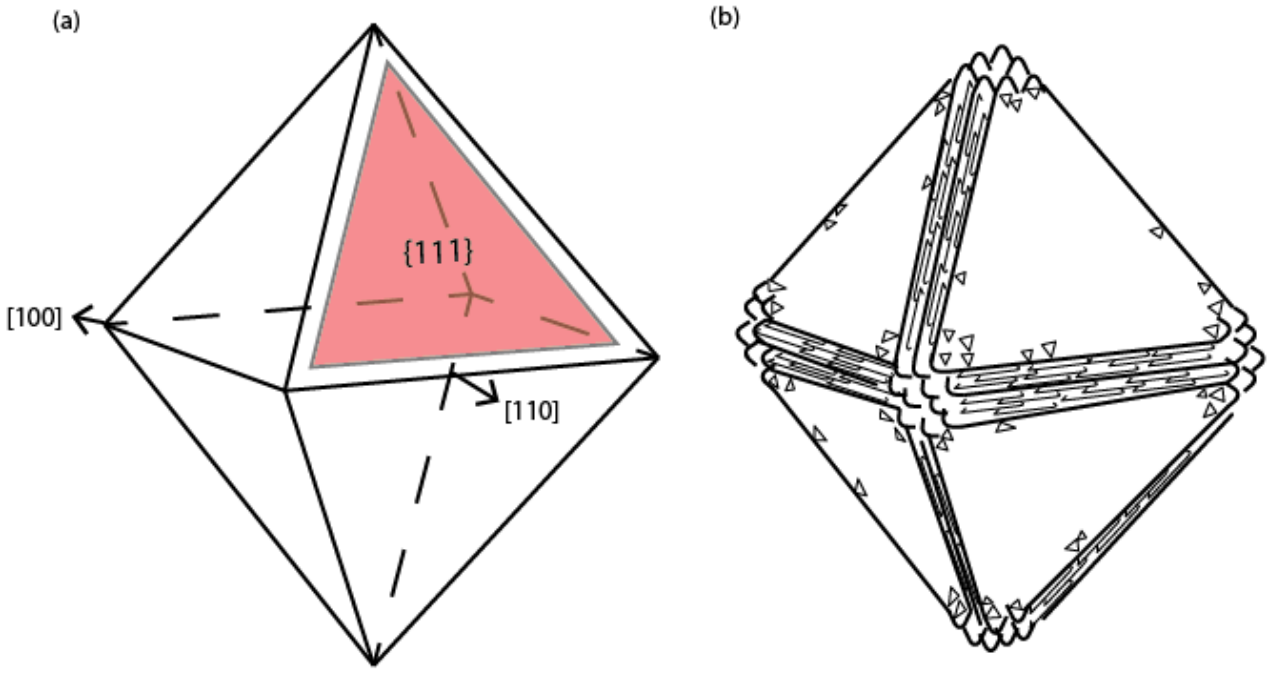

Figure 4.18 (a) Schematic of chromite grain showing primary directions of dissolution {111}, [110] and [100]. (b) Schematic representation of dissolution occurring in each direction on chromite grain undergoing edge-corner dissolution.

4.2.2 Description of dissolution features on Ilmenite

All of the examined ilmenite grains show only partial grain surfaces which were in contact with the kimberlite melt. Most of the grains were highly fractured or the original grain surface was covered with reaction products. Nor do the grains preserve any shape reflective of their hexagonal crystal system; they are predominantly anhedral. These observations were seen on the grains from both of the studied kimberlites (Fig 4.19). The most common interaction of the ilmenite grains with the kimberlite melt was the crystallization of reaction products. The main reaction products that were observed were titanite ($CaTiSiO_5$) and perovskite ($CaTiO_3$). This result will be discussed further in section 4.2.3.

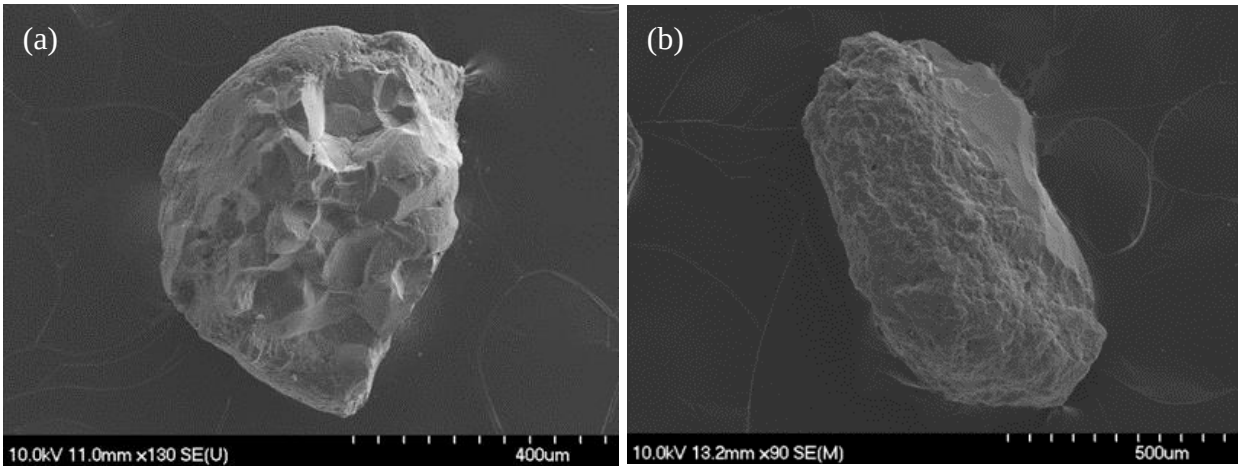

Figure 4.19 (a) Ilmenite grain from Kimberlite A with anhedral shape and fractured surfaces. (b) Ilmenite grain from Kimberlite B with anhedral shape, fractured surfaces and reaction products.

Fourteen grains do carry some dissolution features on ilmenite surface such as pitting, both triangular and circular. These pits were seen on both kimberlites, though there were some evident distinctions. The pits seen on four grains from Kimberlite A were usually smaller than the pits found on the 10 grains from Kimberlite B (ranging 1-3 μm and 5-20 μm, respectively). In Kimberlite A, circular and triangular pits could be found on the same grain (Fig 4.20 a,b), however, in Kimberlite B, where there was pitting of an ilmenite grain, it would be one shape or the other (Fig 4.20 c,d). The pitting on ilmenites from Kimberlite B was also much denser on the grain surface than those from Kimberlite A. In Kimberlite B ilmenites with circular or triangular pitting were often covered in the pits, whereas Kimberlite A ilmenites showed sporadic pitting clustered in small areas.

Some ilmenite grains from Kimberlite B showed surface features which had more resemblance to the resorption observed on the chromite grains. Protruding nodules were found on some corners of ilmenite grains (Fig 4.20d), though the grains do not show the same octahedral shape, or their own regular crystal habit.

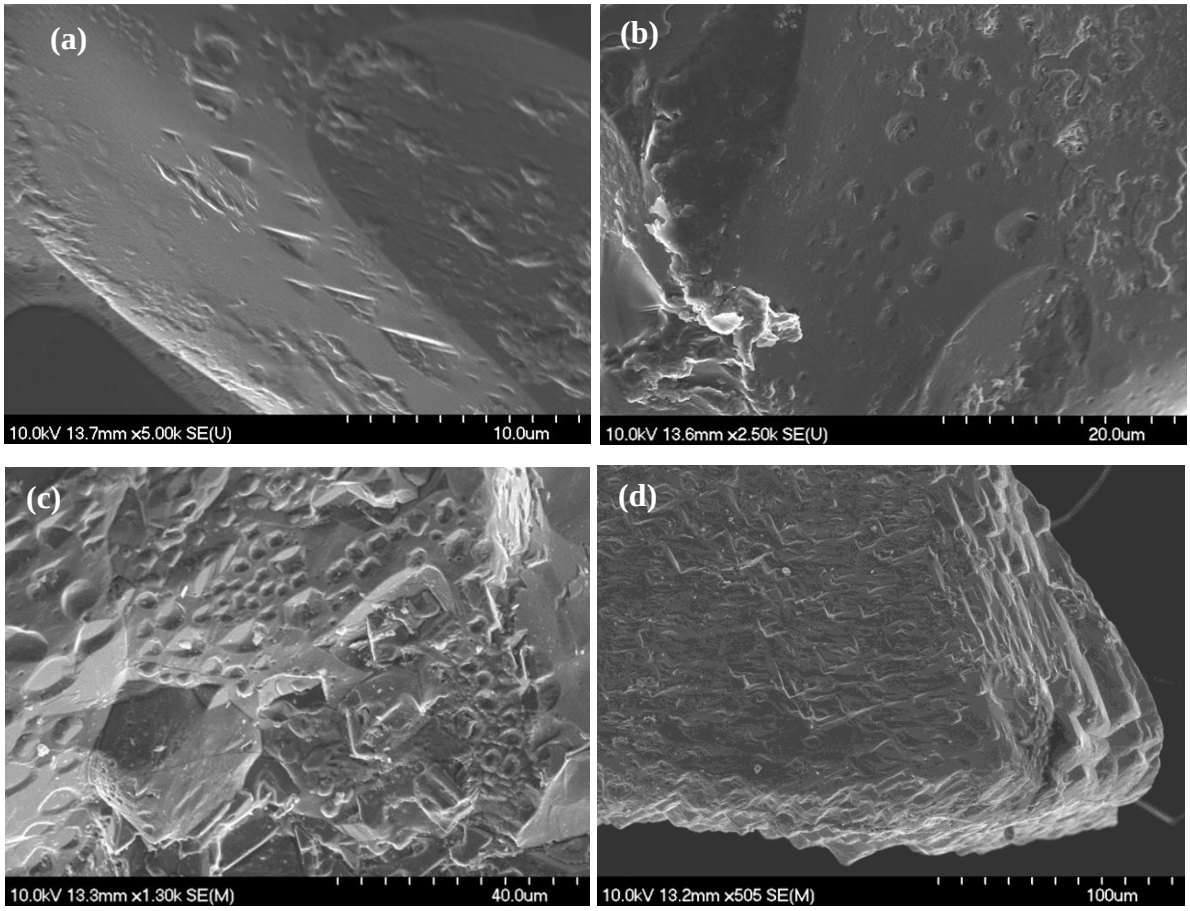

Figure 4.20 Examples of dissolution of ilmenite grains (a,b) small triangular and circular pitting from a single grain in Kimberlite A, (c) high density, large circular pitting on ilmenite grain surface from Kimberlite B and (d) high density triangular pitting and protruding nodules from ilmenite in Kimberlite B.

4.2.3 Reaction products on Ilmenites

Almost all of the studies ilmenite grains have a rim of reaction products, titanite and perovskite. These were identified on the grain surface with EDS during the SEM photographing process (Fig 4.21a), and were later analyzed by EMP. Some ilmenites also have an outer rim of Ti-magnetite. The titanite displayed a rounded habit, while the perovskite appeared more angular and slightly tabular in shape. These reaction products were more easily distinguishable from the ilmenite when examined in back scatter images (Fig 4.21 b,c) and in the elemental X-ray maps (Figs 4.22-4.27), both of which clearly outline portions of different composition within the grain.

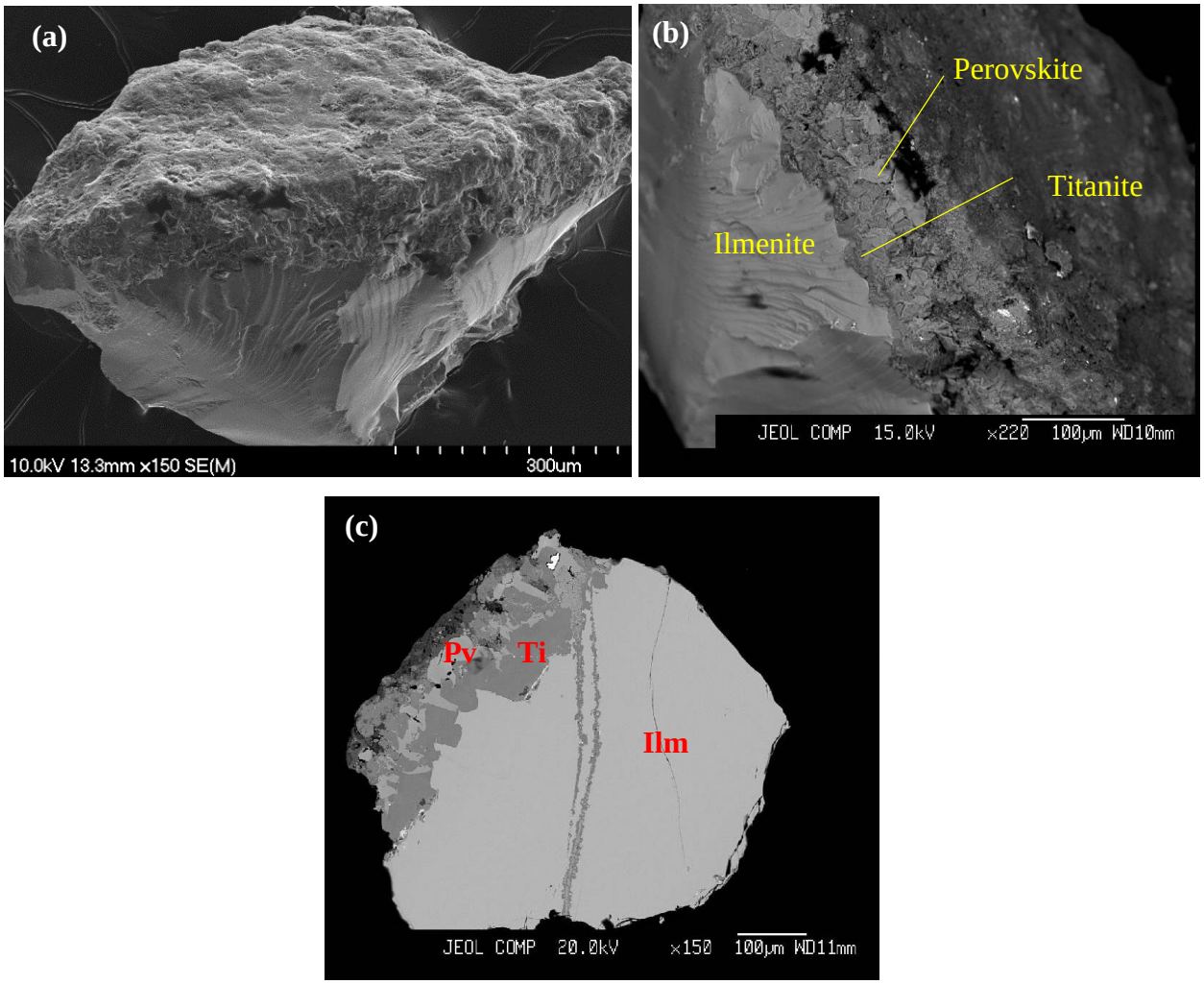

Figure 4.21 A single ilmenite grain from Kimberlite B with a large volume of reaction products shown (a) under SEM, (b) a back scatter image under SEM, and (c) a polished back scatter image showing ilmenite (Ilm), titanite (Ti) and perovskite (Pv).

Polished sections through the grain surface and reaction products revealed a pattern of reaction sequences, particularly on grains from Kimberlite B. In Kimberlite A there is not much titanite; however, ilmenite zonation is obviously pronounced (as was mentioned in section 4.1.2), with minor perovskite on the grain surface. The reaction products are seen with some distinct shapes along the ilmenite grain boundary. In Kimberlite B, the titanite is often in direct contact with the grain surface, this is followed by an outward zone of perovskite, and finally, the groundmass aggregate sitting on the outermost surface. These observations are supported by the elemental X-ray maps conducted on six ilmenite grains. The minor amounts of reaction products and obvious

zoning are exemplified in grains from Kimberlite A in Figures 4.23-4.25. The large volume of reaction products present on the surface of grains from Kimberlite B can be seen in Figures 4.26-4.28.

4.2.4 Volume Dissolution

Several of the polished grains displayed a highly pitted habit when observed under the EMP. These coarse pits were very irregular and often covered a large portion of the grain. These pits could represent volume dissolution through whole grain, as opposed to only dissolution of the outer grain surface. This texture was confined to chromite grains from Kimberlite A (Fig. 4.22). These grains showed up to 25-30% volume dissolution through the polished section.

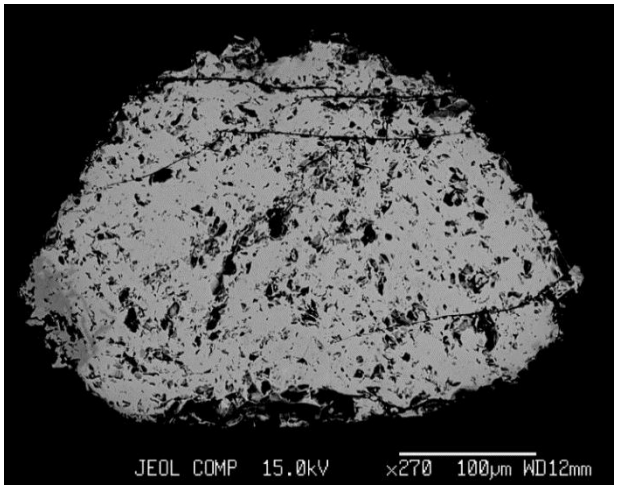

Figure 4.22 Chromite grain from Kimberlite A with total volume dissolution.

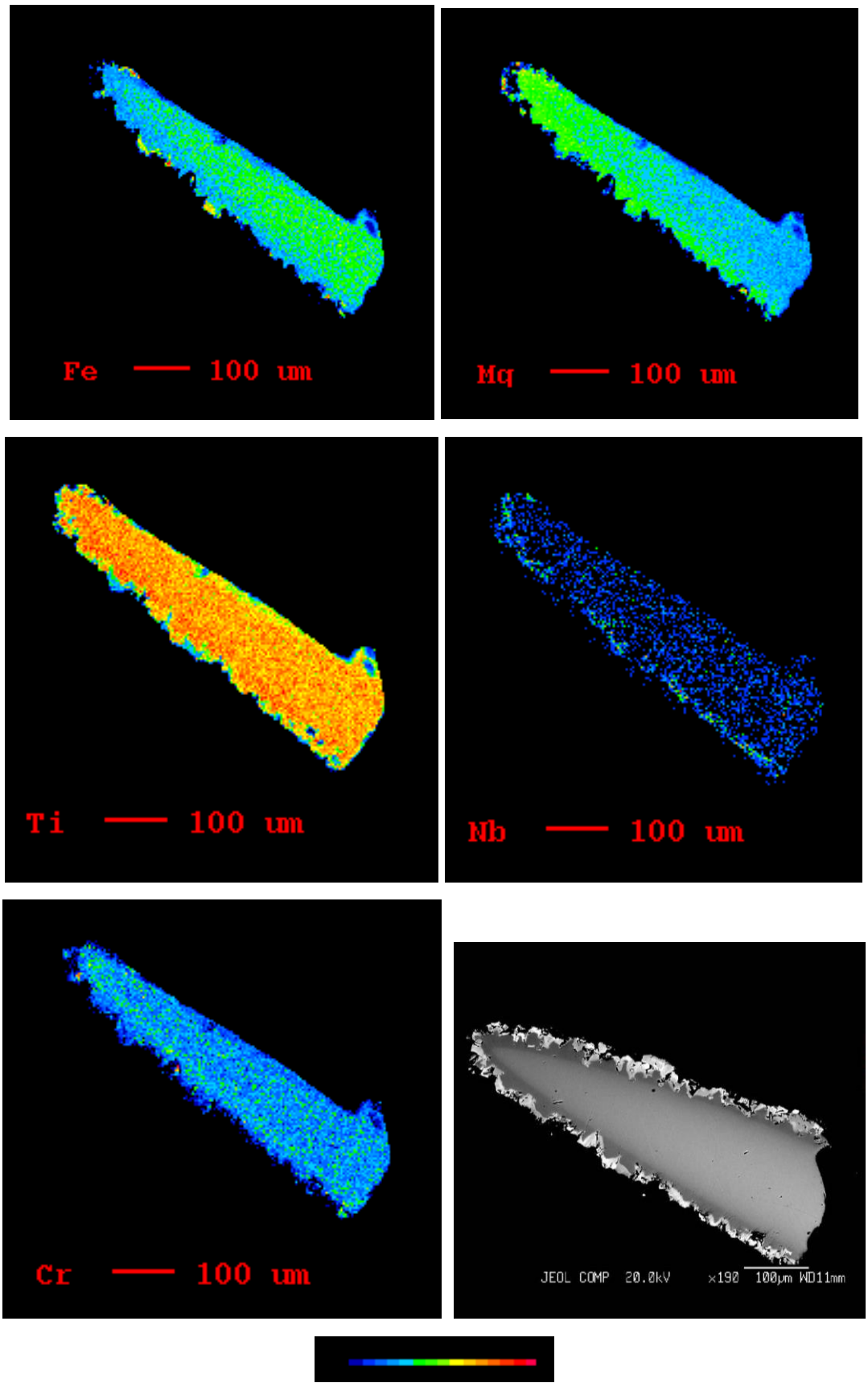

Figure 4.23 Elemental X-ray maps and back scatter image of an ilmenite grain from Kimberlite A

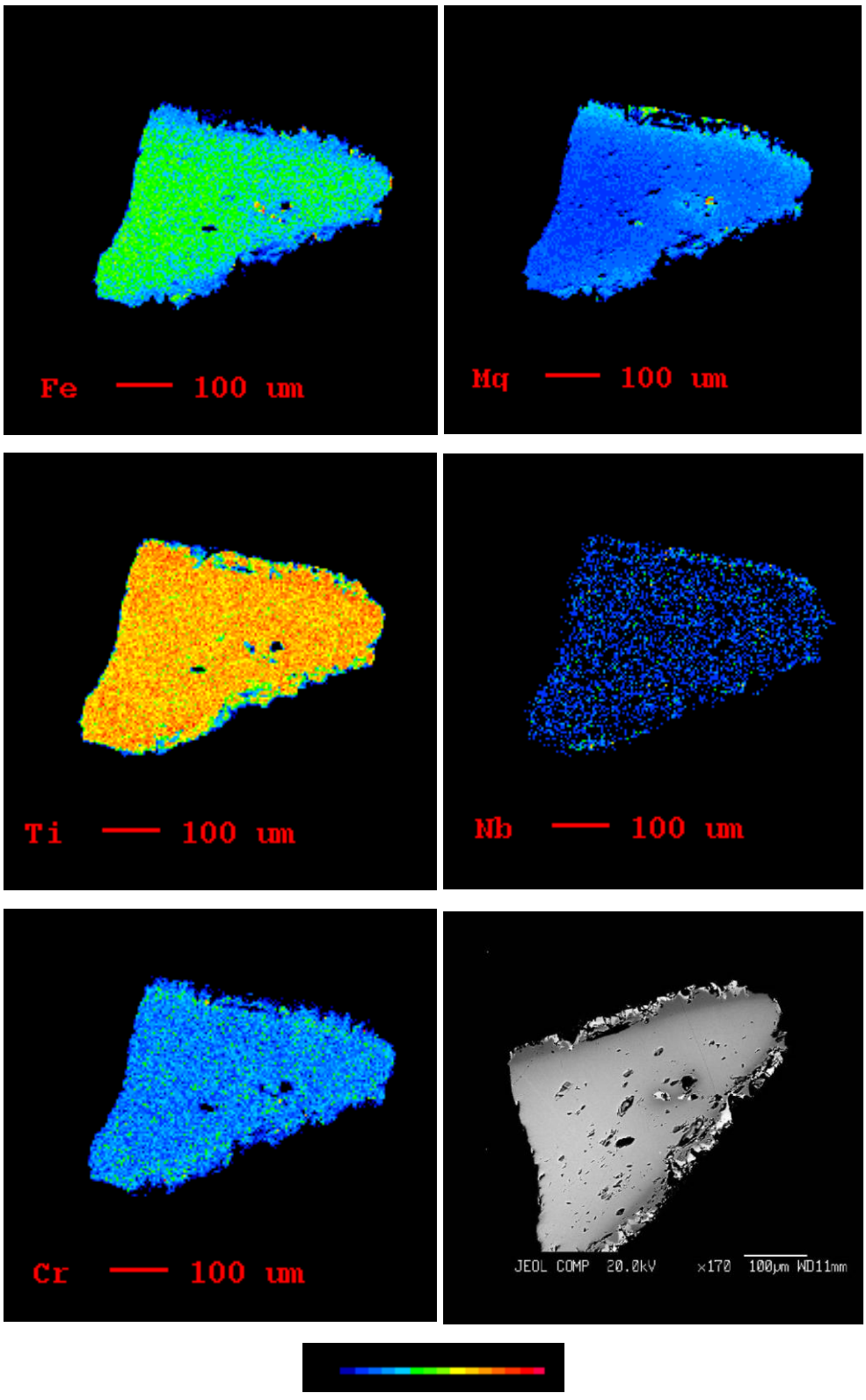

Figure 4.24 Elemental X-ray maps and back scatter image of an ilmenite grain from Kimberlite A.

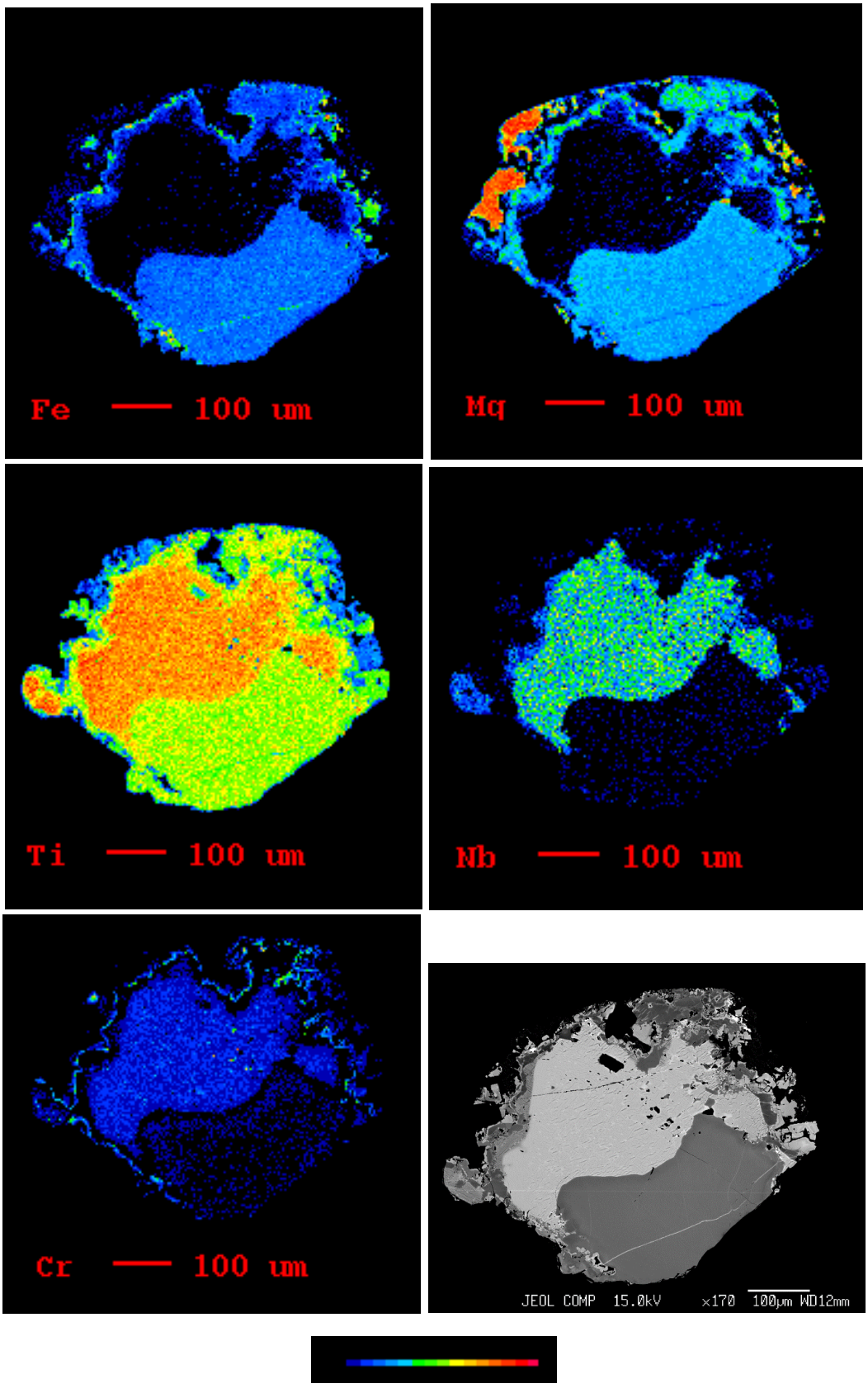

Figure 4.25 Elemental X-ray maps and back scatter image of an ilmenite grain from Kimberlite A.

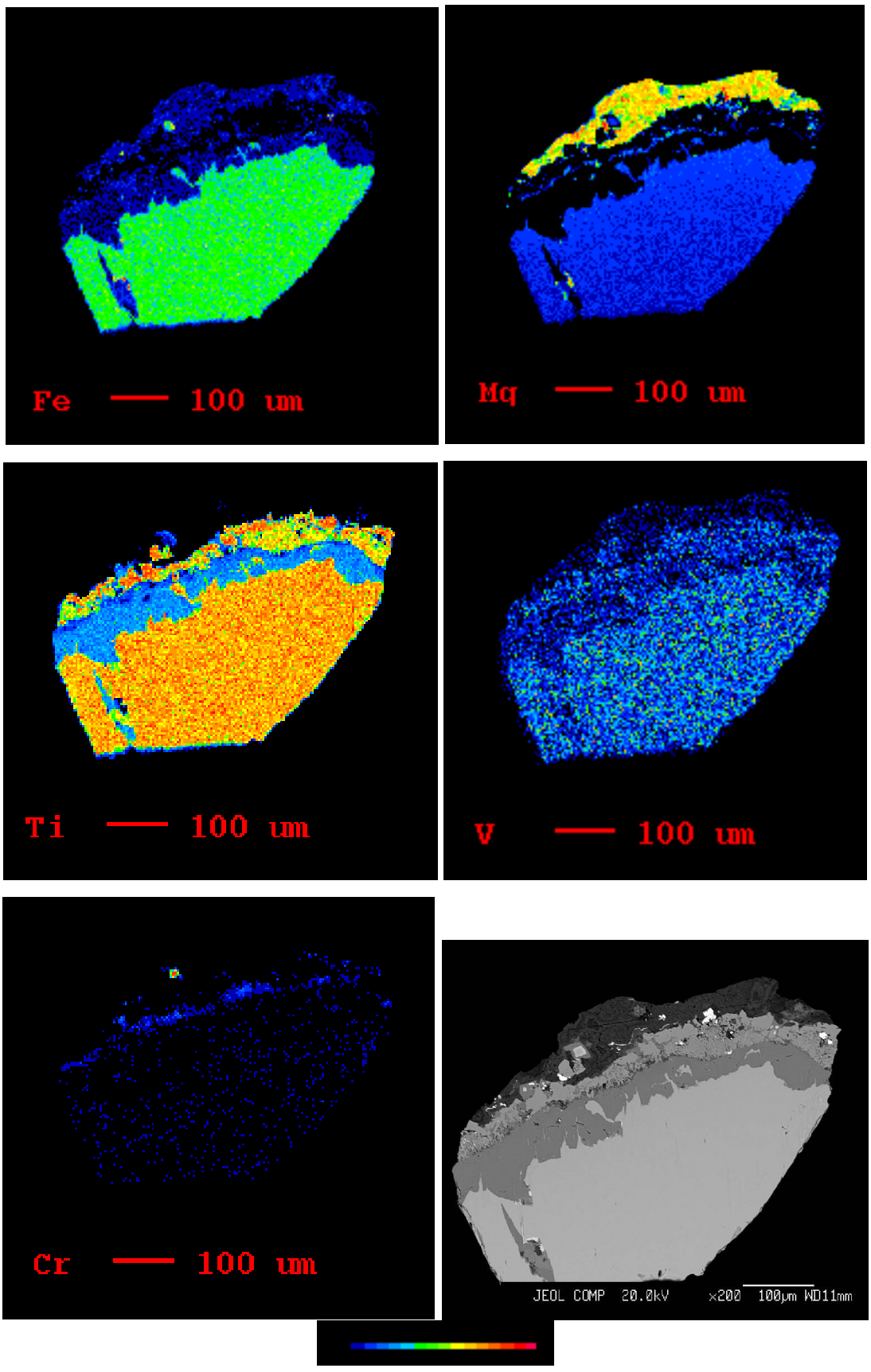

Figure 4.26 Elemental X-ray maps and back scatter image of an ilmenite grain from Kimberlite B.

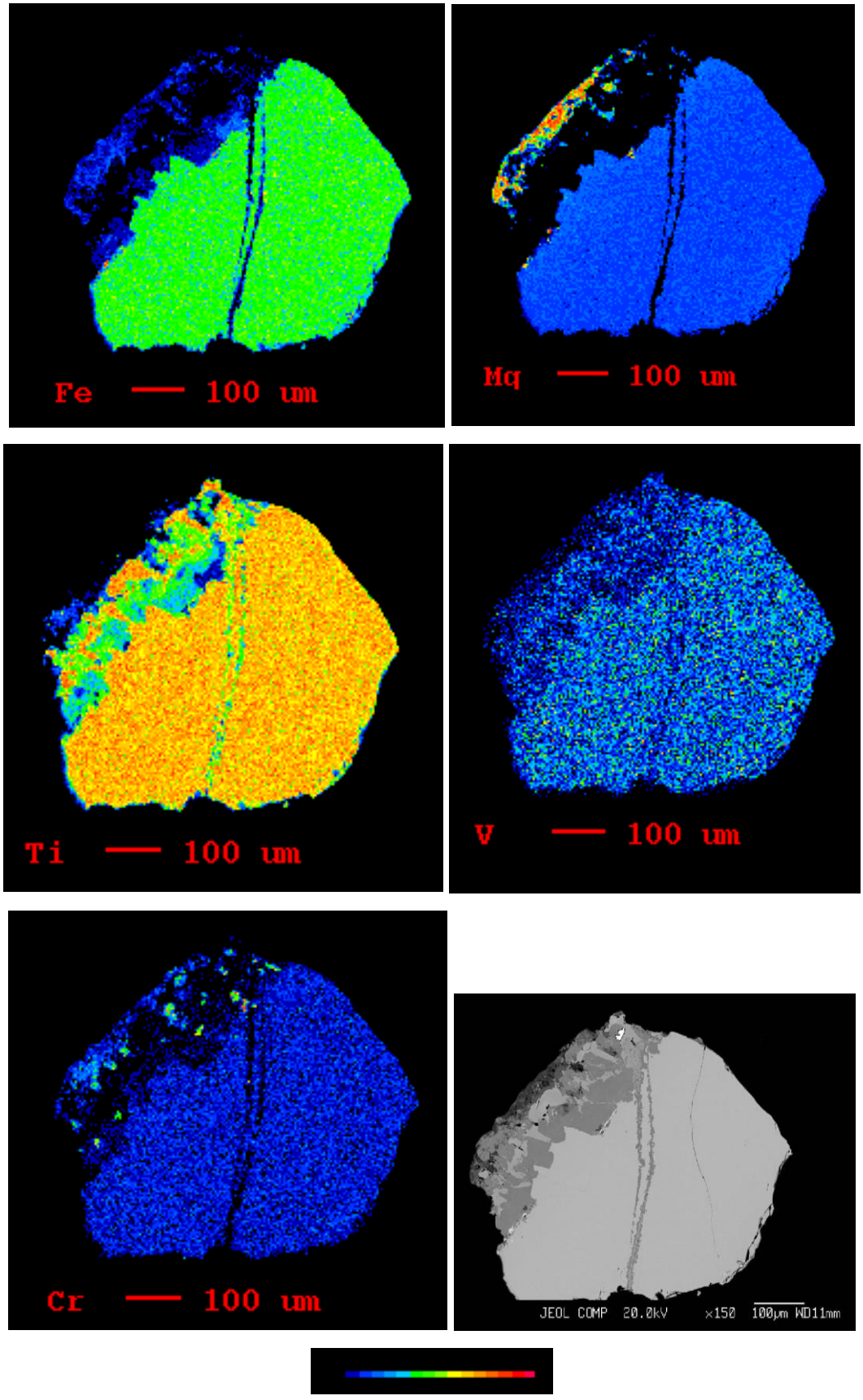

Figure 4.27 Elemental X-ray maps and back scatter image of an ilmenite grain from Kimberlite B.

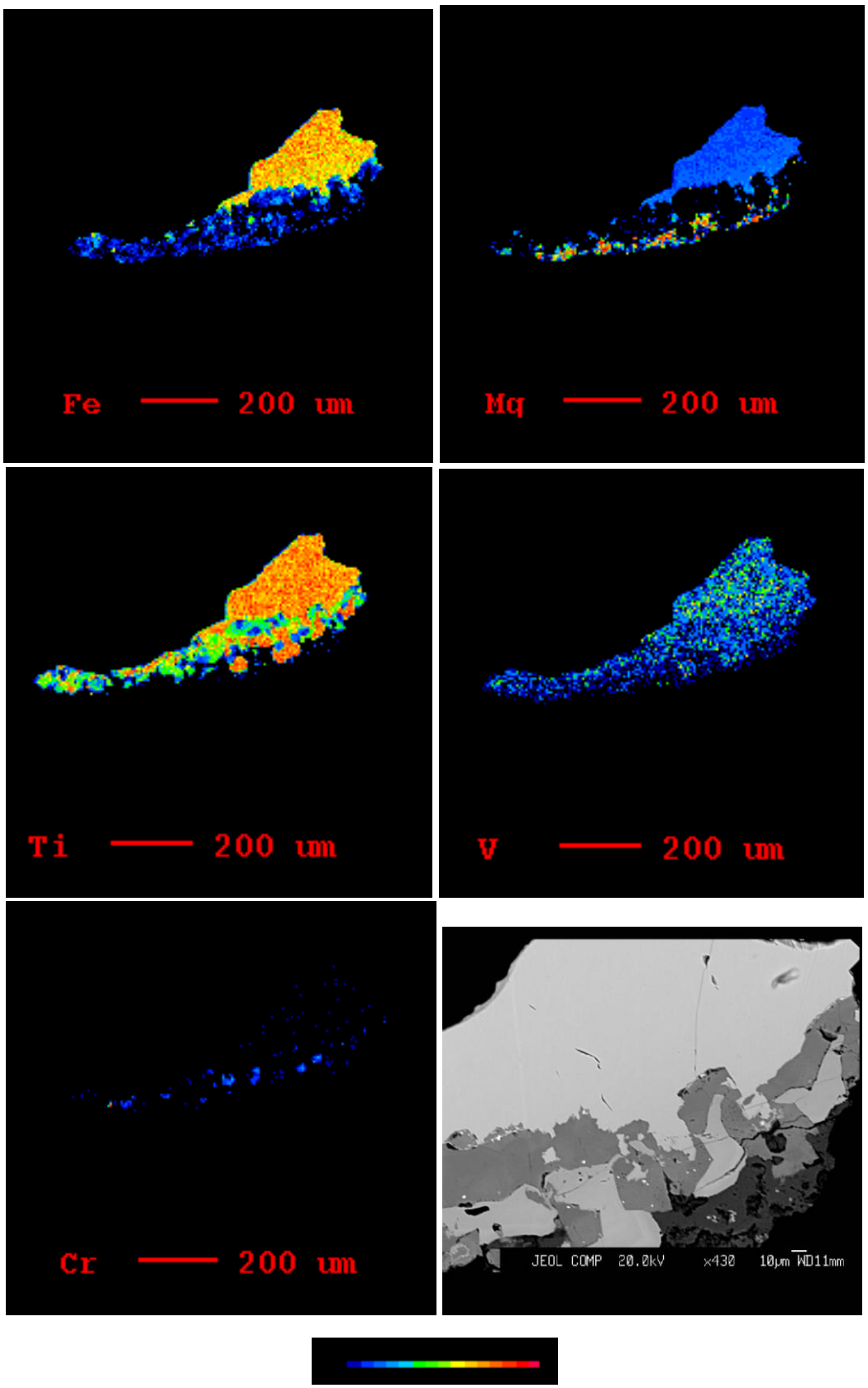

Figure 4.28 Elemental X-ray maps and back scatter image of an ilmenite grain from Kimberlite B

4.3 Summary of Results

The results, as described in this section, are summarised in Table 4.2, comparing the two kimberlites based on compositional trends, presence of zonation, reaction products, and styles of dissolution.

Table 4.2 Summary of results comparing Kimberlites A and B.

Kimberlite A "simple" single-facies kimberlite		**Kimberlite B "complex" multi-facies kimberlite**	
Chromite	**Ilmenite**	**Chromite**	**Ilmenite**
Trending compositions	Trending compositions	Clustered compositions	Clustered compositions
Patchy zonation	Clear zonation rims	Very thin zonation	No visible zonation
No reaction phases	Minor reaction phases (perovskite)	No reaction phases	Large volume of reaction phases (perovskite and titanite)
Ovoid-elongate morphology	Irregular and some fracturing	Highly fractured	Highly fractured
Well preserved {111} faces and regular surface features	Small scale pitted surface features, two types of dissolution on one grain	Few {111} faces preserved and varying surface features	Inconsistent and varying surface features, only one type of dissolution on a single grain

5.0 DISCUSSION

5.1 Comparison of resorption features on oxide minerals from South African kimberlites and oxide minerals from Ekati Mine kimberlites

The chromite surface features observed in this study were compared to those observed on oxides from Ekati Mine kimberlites (Northwest Territories, Canada) (unpublished data from Kressall, 2014a) and, the following scheme was proposed for the classification of the morphologies and features seen on kimberlitic chromites:

1. The overall morphology of the grains can be classified as:
    - Octahedral (grains which maintain their chromite octahedral shape with minimal distortion
    - Truncated (the octahedral shape is recognisable, but does not form a perfect octahedron
    - Elongate (have preserved {111} faces, but the octahedral shape is elongated or flattened, creating an ovoid morphology
    - Rounded (little to no identifiable octahedral shape because of excessive dissolution
    - Fractured (no specific morphological identification can be made)
2. A subsection of the morphological classification allows for the adage of a fractured portion to the grain. “None”, “partially”, or “fully” are used to describe the amount of fracture eliminating grain surface.
3. Focusing on resorption, the first step is to identify the type (or rather location), of resorption. Using the three main areas of the chromite grain, the edge, the corner, and the face, the specific directions of attack on the grain can be identified.
    - The most common dissolution combinations seen on kimberlitic chromite grains were Edge-Corner (EC) dissolution, and Edge-Corner-Face (ECF) dissolution.

- The degree of dissolution is described on a 0-3 scale as follows:
  - 0 – shows no resorption on any grain surface
  - 1 – has slight resorption, with the primary grain shape still identifiable
  - 2 – grains with resorption which has distorted the primary grain shape
  - 3 – grains with the most resorption, may have some {111} faces still preserved, but the majority of the grain has been resorbed.

4. The classification scheme continues to describe specific features in each location (edge, corner, face) on the grain. The type case resorption style has been identified in each case and separated into a few descriptions.
   - On the grain edges, the characteristic stepping pattern can be classified as not present, wavy, smooth, sharp, or other, in the case where another type of resorption has occurred on the grain edge.
   - There is a further sub-description which identifies the relative size of the edge features as fine or coarse (this is somewhat subjective).
5. A similar scheme has been applied to the classification of the commonly occurring pyramids on the corners of the grains. They are depicted as either not-present, bumpy, smooth, sharp, or possibly another type of resorption has occurred. Again, these are further described as being fine or coarse on the scale of the grain.
6. Features on {111} faces have been identified as a few different types, in particular, trigons, polygons, pits, or lineations. Several sub-features have been noted (cracking, pitting) on the chromite grains in North American kimberlites, however none were observed in the South African chromites of this study.

(a)

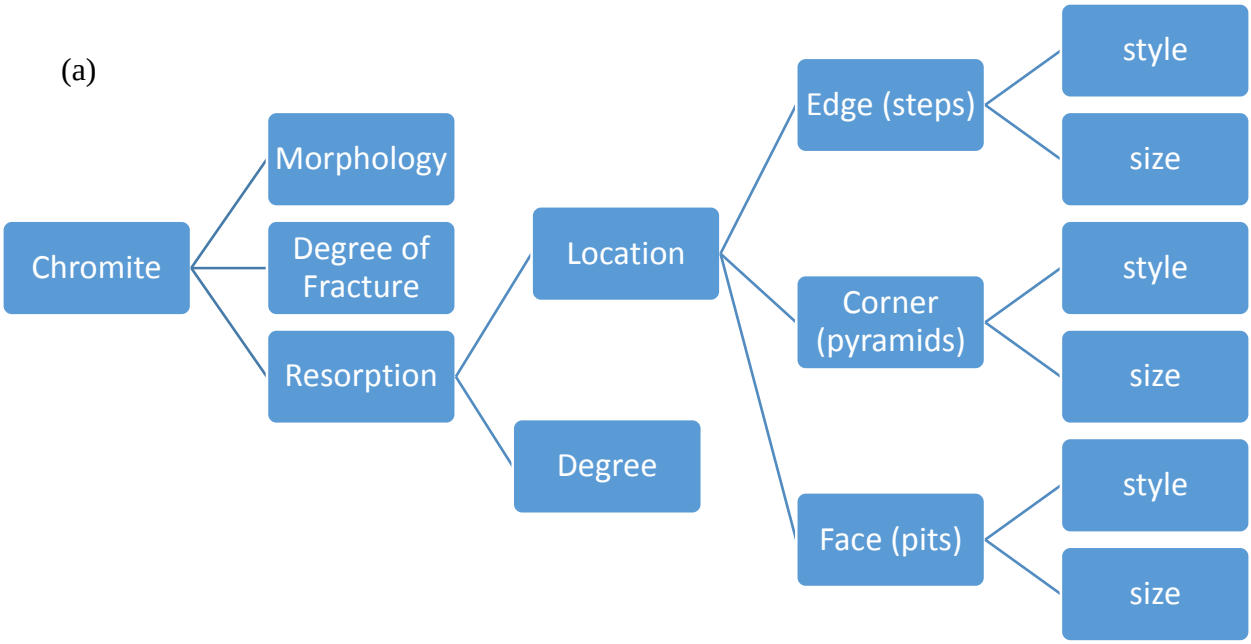
Chromite
Morphology
Degree of Fracture
Resorption
Location
Degree
Edge (steps)
Corner (pyramids)
Face (pits)
style
size
style
size
style
size

(b)

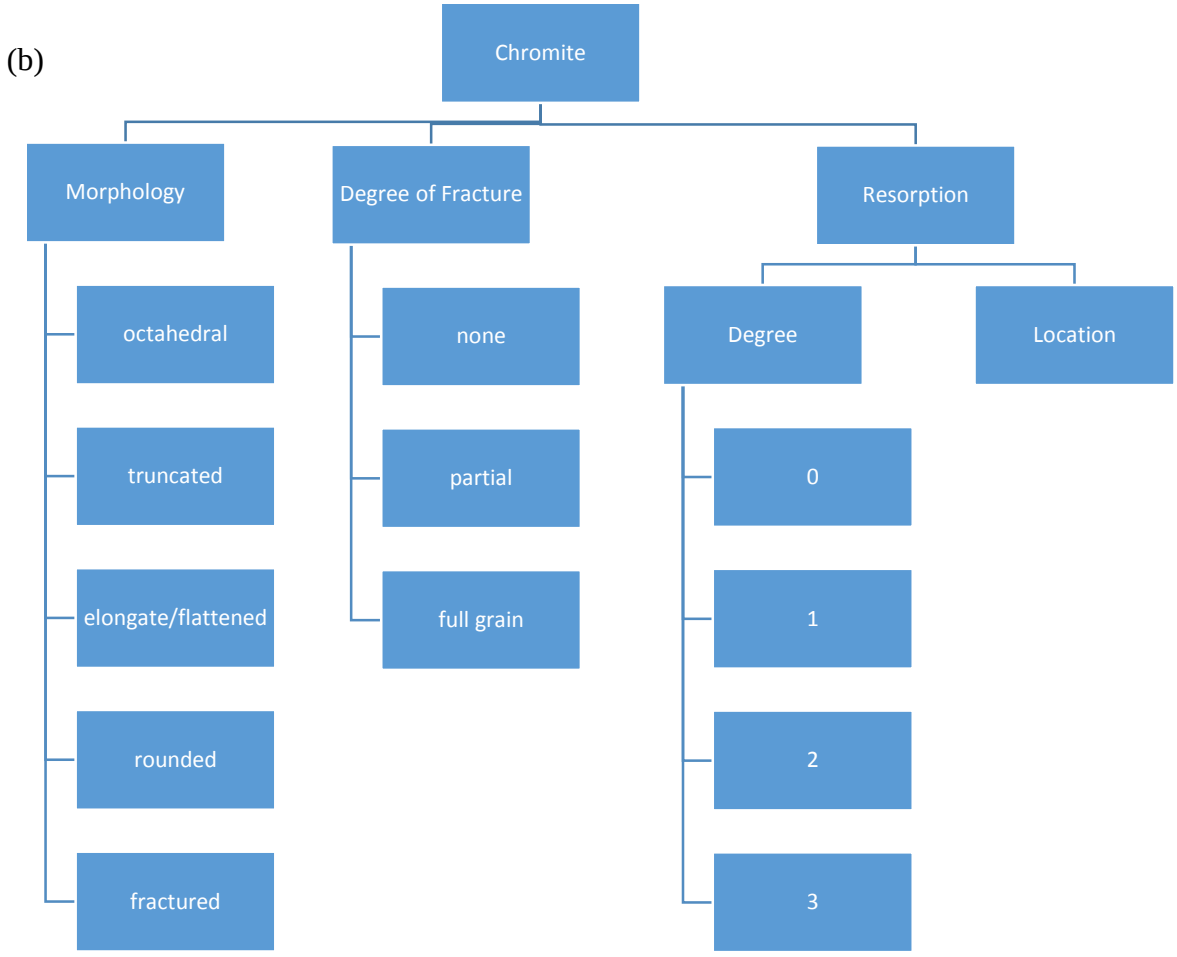
Chromite
Morphology
Degree of Fracture
Resorption
octahedral
truncated
elongate/flattened
rounded
fractured
none
partial
full grain
Degree
Location
0
1
2
3

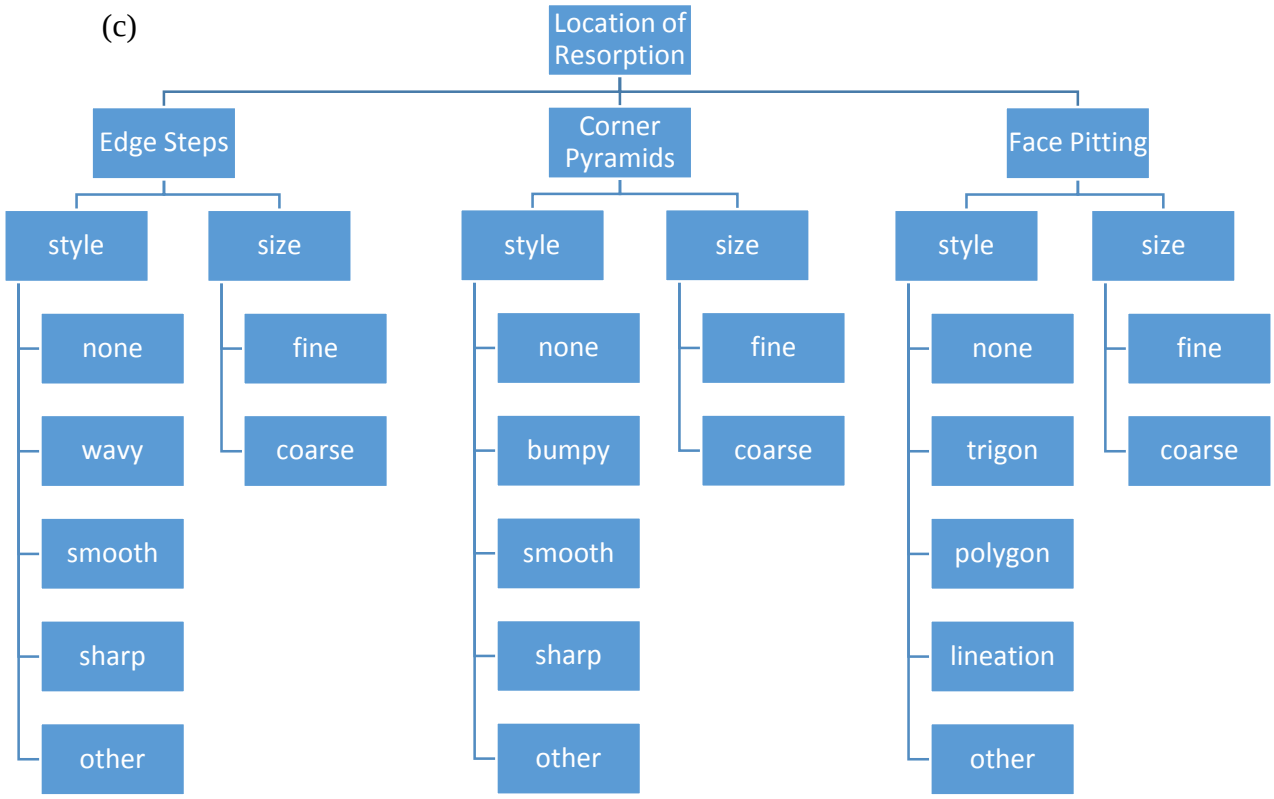

Figure 5.1 (a) Classification scheme for resorption features of kimberlitic chromite grains (b) Break-down of morphology types and degrees of fracture and resorption (c) Break-down of resorption styles in specific locations.

Using the classification provided above, the two Orapa kimberlites, A and B were compared to three kimberlites from the Ekati Mine in Northwest Territories, Canada (from Kressall, 2014a). Two of the kimberlites were of hypabyssal facies, and one was resedimented volcaniclastic (RVK). The two hypabyssal kimberlites from Ekati had chromites that were too resorbed to identify a particular morphology, and were classified as "rounded". Where the morphology was discernable, the grains had a flattened/elongate shape. Most of the Ekati hypabyssal chromites were very irregular, with edge-corner-face dissolution, and most with a resorption degree of 3 (Kressall, 2014a). This is somewhat different to what was observed on the South African kimberlitic chromites, where most of the grains had well preserved faces, and there was a bimodal distribution of the edge-corner and edge-corner-face resorption styles (see Table 4.1). The small scale features seem to be similar on chromites from Orapa and chromites from Ekati. Both sets of grains display wavy edge steps and bumpy corner pyramids, with trigon pitting/protrusion relief patterns on the

faces (where resorbed). The features on grains from Orapa, however, were often better defined than those from Ekati, where some trigons and pyramids, though present, might be described as globular in shape.

The volcaniclastic Ekati kimberlite could not easily be compared to the two Orapa kimberlites from this study because the proportion of volcaniclastic facies was so low in Kimberlite B. Kressall (2014a) reported that the chromite grains from the volcaniclastic kimberlite were skewed towards octahedral and truncated morphologies, and nicely preserved grains. The resorption style was still predominantly edge-corner-face, however the degree of resorption was often lessened to 2. The corner pyramids on the volcaniclastic facies chromites were bumpy, however the edge steps were slightly more defined, and classified as smooth. One interesting feature seen on Ekati chromites was fine cracking on the grain faces in an irregular, sometimes triangular configuration (Kressall, 2014a). This was also seen on chromites from Orapa, but much less abundant, only on one grain from Kimberlite A.

The ilmenites from the Ekati kimberlites were largely lacking in surface features (Kressall, 2014b). Kressall (2014a) reported very fine circular pitting (<5 μm) with a vermicular texture surrounding the pits on one grain.

Overall, the types of surface features (edge steps and corner pyramids) seen on kimberlitic chromites from Ekati and Orapa are similar. The variation between kimberlites lies in the degree of resorption, the definition of the small scale features and the consistency of one style of resorption within each kimberlite.

Resorption features on chromites from Orapa kimberlites A and B were also compared to surface features reported on chromites from stratiform and podiform deposits, from (LeBlanc, 1980). Stratiform deposits are continental layered mafic and ultramafic intrusions, and podiform deposits

are massive nodular deposits found in ophiolite ultra-mafic complexes. Stratiform cumulate chromites were examined from two different deposits, and reported equant grains (average 200 μm diameter) with clearly defined faces, and sharp edges. LeBlanc (1980) also noted two different dissolution styles, similar to what was observed in this study: dissolution on only the edges and corners with well-preserved faces, and dissolution on the faces, as well as the edges and corners, with the primary grain shape preserved. The podiform chromites are described as having a morphology more reminiscent of deformation, with elongate, or stretched, shapes (LeBlanc, 1980). They are also described as having rounded, rough surfaces, which appear similar to some of the grains seen in the current chromite examination. The study by LeBlanc (1980) principally highlights features caused by grain slip defects. There was, however, one noted surface feature on a podiform chromite which appeared similar to a feature seen on an ilmenite grain from the Orapa field kimberlites. LeBlanc (1980) describes this feature as pyramidal pitting (5 μm), and it was noticed on one ilmenite grain from Kimberlite A.

Observed features on chromites from oxide study

Observed results from (LeBlanc, 1980)

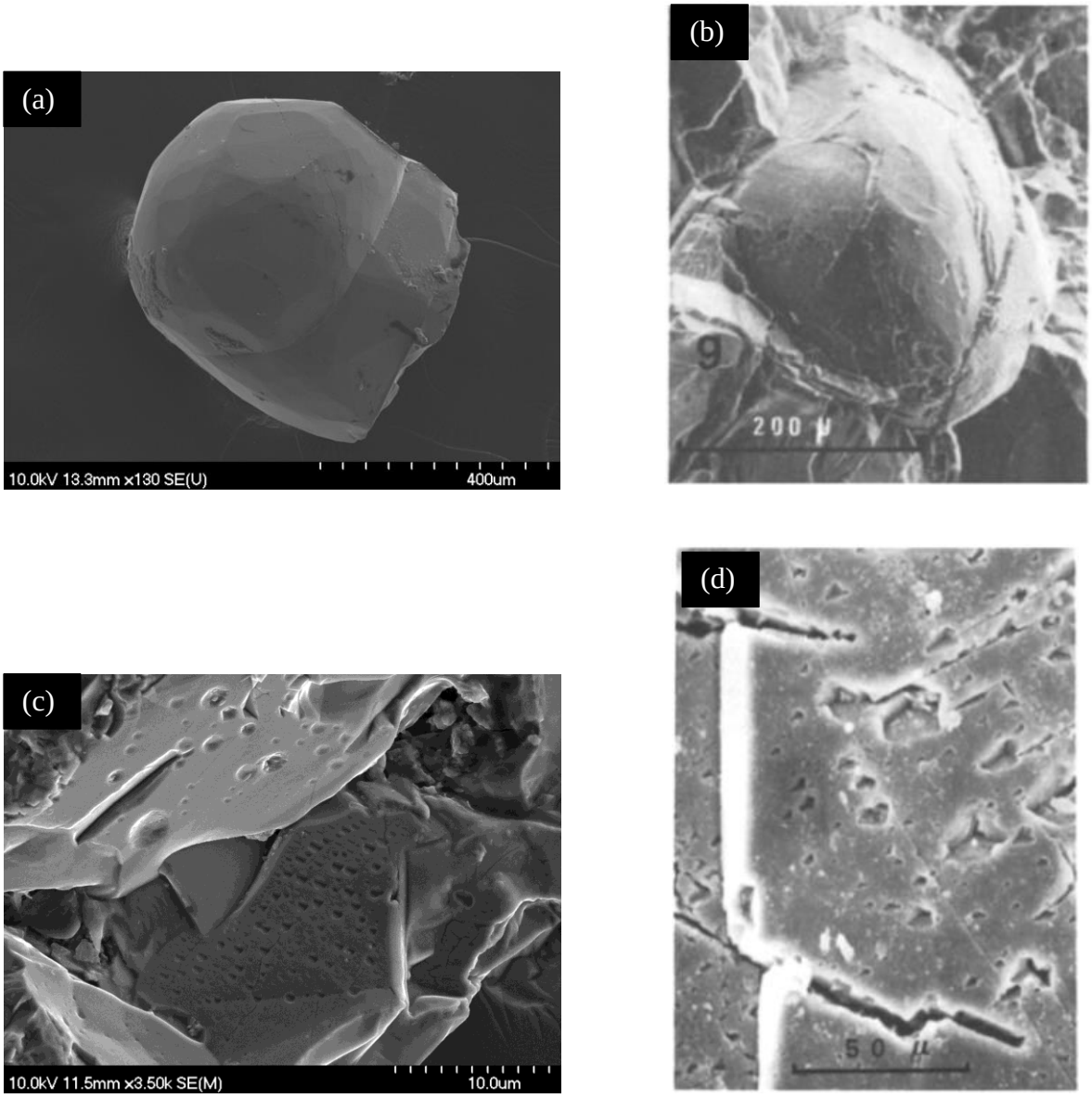

Figure 5.2 Comparison of kimberlitic chromite grains (a, c) and podiform deposit chromites (b, d) (from LeBlanc, 1980) showing (a, b) well rounded grains with rough surfaces and (c, d) pyramidal pitting described by LeBlanc on a kimberlitic ilmenite (c) and a podiform chromite (d).

The morphologies observed on kimberlitic chromites are most similar to those from podiform deposits. The styles of dissolution seen on chromites from kimberlites most resembles the dissolution seen on chromites from stratiform deposits.

5.2 Comparison of resorption features on natural kimberlitic oxides to experimentally induced features

Some previous work has been conducted investigating the fluid composition effect on oxide dissolution features - (Fedortchouk and MacIsaac, 2013). In particular, they examined the differences resulting in variations in H_2O-CO_2 fluid proportions and compared the results to surface features found on natural kimberlites. For full details of experimental methods, see Fedortchouk and MacIsaac (2013). Looking at the experiments run where H_2O content was varied in the melt, the compositions most congruent with the chromite dissolution seen in this study are the features produced on chromites in diopside melt with 5 wt%, 13 wt% and 15 wt% H_2O content.

Table 5.1 Summary of H2O experimental conditions from Fedortchouk and MacIsaac (2013).

H_2O fluid experiments	
5 wt% H_2O	H_2O dissolved in diopside melt
13 wt% H_2O	In diopside melt with free aqueous fluid phase
15 wt% H_2O	In diopside melt with free aqueous fluid phase

The experiments with 5 wt% H_2O dissolved in diopside melt produced surface dissolution features very similar to those seen in Kimberlites A and B. The authors describe small nodular features on smooth surfaces which resemble the rounded nodules seen on the {100} corners of chromites from Kimberlite B (Figure 5.1a, b). This run also produced edge step patterns that were wavy, similar to some wavy edges seen on chromites from Kimberlite A. The 13 wt% H_2O experiments in diopside melt with free aqueous fluid produced features which were typical of the most common features seen in Kimberlite A, namely the sharp, protuberant nodules on the corners of chromites (Figure 5.1c, d). The experiments conducted with 15 wt% H_2O also produced a feature that was observed in Kimberlite A, but only on one grain (Figure 5.1 e, f). The resemblance of resorption

features on grains from Kimberlite A to the experimental products from the two runs with diopside melt equilibrated with aqueous fluid (runs with 13 and 15 wt% H_2O), and the resemblance of features from Kimberlite B to those on the 5 wt% H_2O run, undersaturated in H_2O, may indicate higher content of aqueous fluid phase in Kimberlite A. The surface features produced in the experimental study by varying CO_2 content were not congruent with any features found on the examined chromite grains form either kimberlite. The experiments with CO_2 did produce some reaction around the grain, though the grains did not undergo any compositional changes with dissolution (Fedortchouk and MacIsaac, 2013).

Similar experiments were conducted using ilmenite grains and varied volatile proportions (MacIsaac, 2009). The results of dissolution in H_2O fluid produced a features described as "micropyramidal" protrusions on the grain surface. This feature is similar to features observed on a single ilmenite grain from Kimberlite B. The CO_2 experiments did not yield any preserved ilmenite grains at higher concentrations, indicating complete resorption of the grains under these conditions. Because of the high preservation rate of ilmenite in both of the studied kimberlites, it is likely that the proportion of CO_2 in both was relatively low.

Observed features on chromites from oxide study

Experimental results from (Fedortchouk and MacIsaac, 2013)

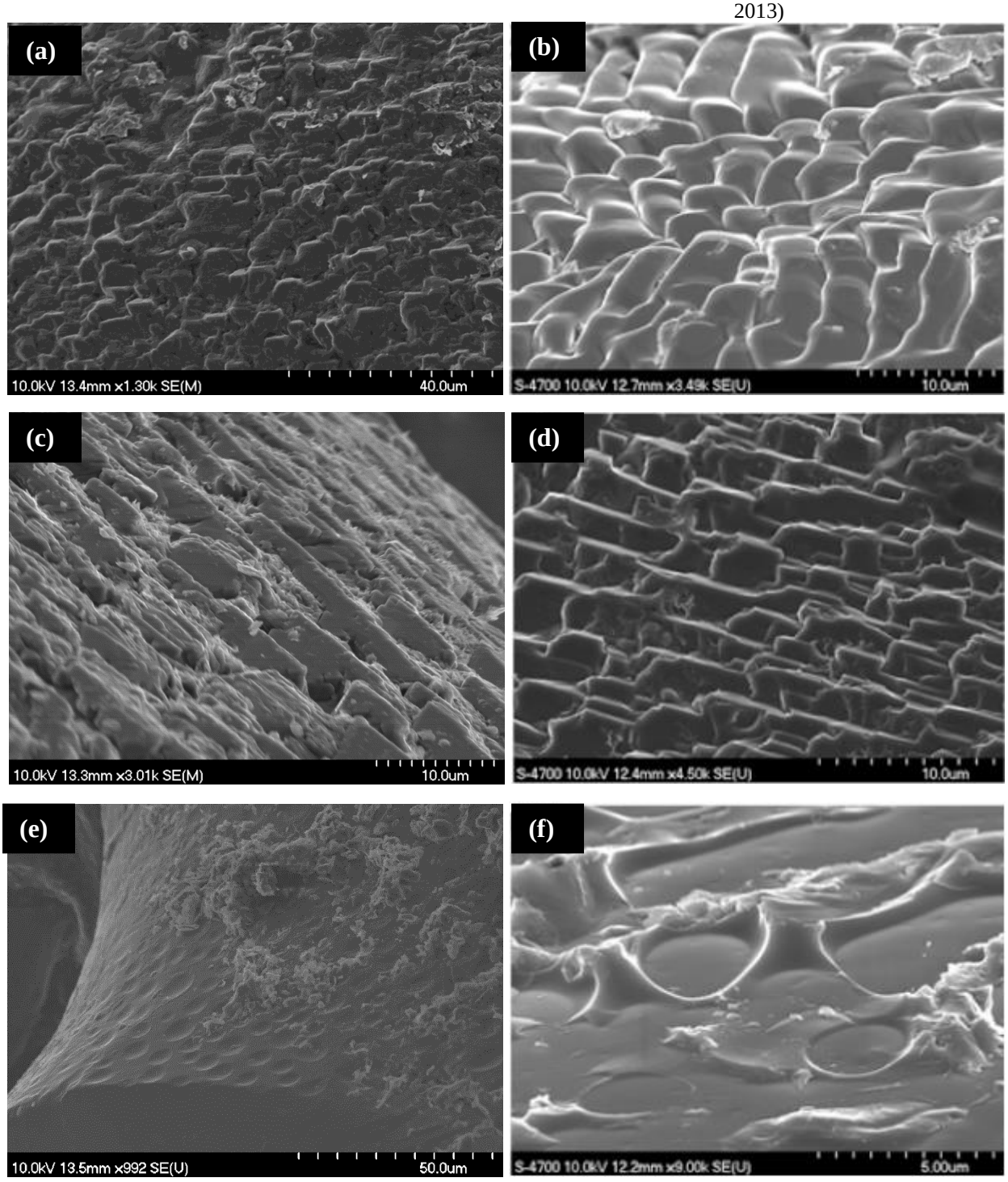

Figure 5.3 Comparison of chromite dissolution features from experimental study (Fedortchouk and MacIsaac, 2013) with observed features on studied grains (a) rounded {100} direction nodules in Kimberlite B and (b) experimental result of 5% H_2O fluid, (c) sharp elongate steps on {110} in Kimberlite A and (d) experimental results of 13% H_2O fluid (e) circular depressions in Kimberlite A and (f) experimental results of 15% H_2O fluid

The absence of an apparent relationship between the surface features found on chromite grains in kimberlites and their compositions suggests that:

1. The chemistry of the melt does not affect the reaction or mechanism of dissolution
2. The resorption features mostly represent the late magmatic history of the kimberlite emplacement, when oxides entrained at various depths (from the mantle and the crust) are interacting with kimberlite magma in a similar fashion.

5.3 Relationship between the characteristics of oxides and kimberlite geology

The chemical composition of oxides can provide some insights into the conditions of kimberlite crystallization. From comparison with experimental results on chromite and ilmenite grains, it has already been inferred that both kimberlites likely had low proportions of CO_2 fluid in the melt. It was also interpreted that Kimberlite A perhaps had a higher H_2O content and presence of free aqueous fluid phase, compared to the lower H_2O content and lack of free fluid phase interpreted in Kimberlite B. Because of the presence of titanite and perovskite (both Ca bearing phases) on the ilmenite grains, there would have been carbonaceous activity in both kimberlites (melt or fluid). In Kimberlite B, there must also have been an event of high siliceous activity, needed to crystallize titanite in reaction with the ilmenite grain surface.

The ilmenite grains from Kimberlite A had clear visible zonation in both the back scatter images and the elemental x-ray maps, which show an Fe-depletion and Mg-enrichment in the rims of the grains. This description seems to fit an overprinting trend depicted by Haggerty et al. (1979) as a magmatic trend. This trend comprises an enrichment of MgO and Cr_2O_3 at the rims of the ilmenites, as well as trending towards a more reduced environment (decrease in Fe^{3+}). Zoning in ilmenites from Kimberlite A suggests that they follow the magmatic trend - with slight increases in both Mg and Cr, and decreases in Fe^{3+} near the rims. The shift to a more reducing environment

(decrease in oxygen fugacity, *fO2)* is associated with pressure decrease within the system (Haggerty et al. 1979, Mitchell, 1986).

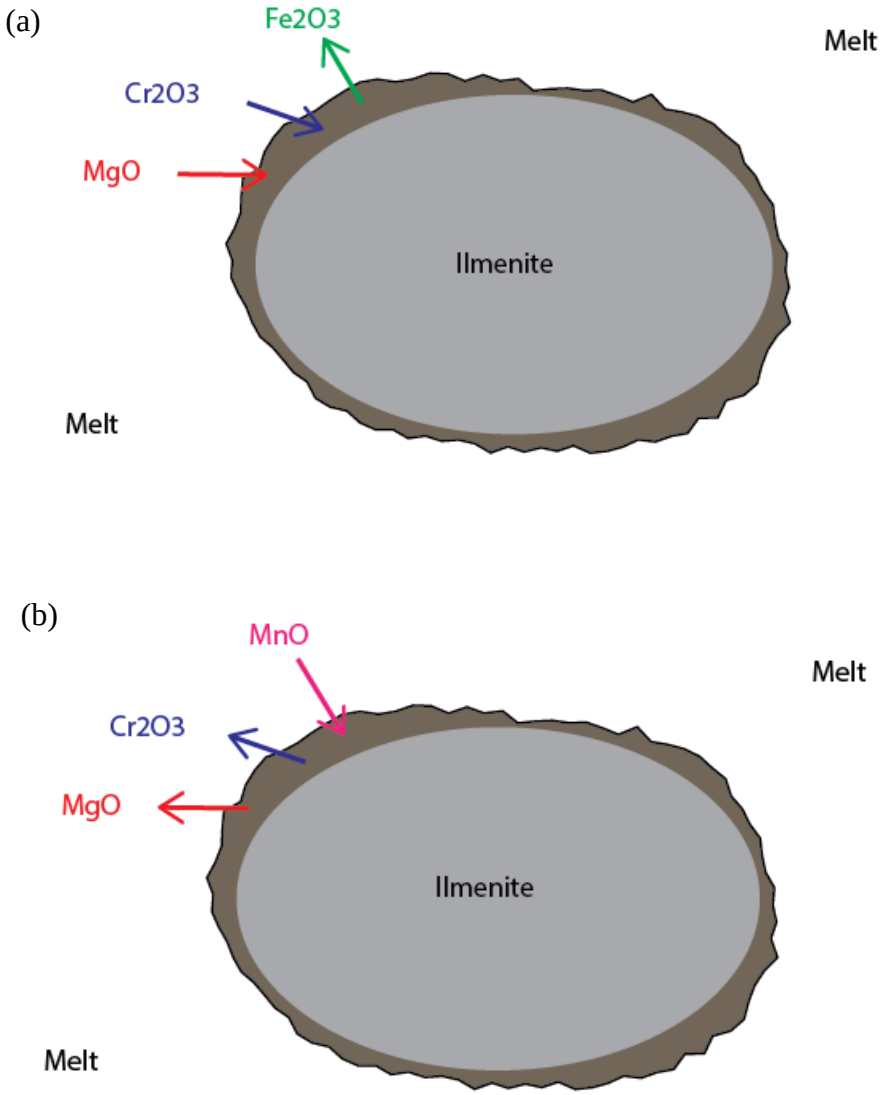

Figure 5.4 (a) Schematic ilmenite grain developing diffusive zonation following the magmatic trend described by Haggerty et al. (1979). (b) Schematic ilmenite grain developing diffusive zonation following the kimberlite reaction trend described by Haggerty et al. (1979).

The ilmenites from Kimberlite B seem to follow a trend called the kimberlite reaction trend (Haggerty et al. 1979). This trend is defined by decreases in MgO and Cr_2O_3 at the rims, and an increase in Mn. The decrease in Cr is clear on the compositional plots of ilmenites from Kimberlite

B. The decrease in Mg is less apparent, though still present in the majority of grains when examining the data. The plots also show a slight increase in Mn near the rim of some of the grains. This change in Mn is specifically important to kimberlites because it signifies a carbonate fluid immiscibility in the kimberlite melt. Haggerty et al. (1979) have stated that the presence of a sudden increase in Mn in the rim of an ilmenite signifies the fluidization event within a kimberlite.

The ilmenites from Kimberlite B show a slight increase in Fe_2O_3 near the rims, indicating movement towards a more oxidising environment. Gurney and Zweistra (1995) have determined that higher proportions of Fe_2O_3 in kimberlitic ilmenites is associated with increased diamond resorption. This could imply that Kimberlite A has a higher potential for diamond preservation; lower *fO2* marked by lower Fe_2O_3 content of the ilmenite grains. The potential for diamond resorption in Kimberlite B could be higher than Kimberlite A because of the trend towards a more oxidised melt as seen in the ilmenites.

Concerning the ilmenite grain described in the compositional profiles with high Nb and Ti zonation, the partitioning of Nb into the ilmenite could give an indication of the melt conditions. A study of compatibility of trace elements in carbonatite and kimberlitic melts with reference to perovskite (Beyer et al. 2012) states that the Nb partition coefficient in perovskite is higher in silicate than carbonate melts. Relating this paper to the high Nb zone in the ilmenite grain from Kimberlite A, the unusual Nb content could indicate a reaction with silicate melt.

5.4 Processes affecting chromite and ilmenite grains during magma ascent

There are a number of reactions that occur simultaneously with a mineral reacting with kimberlite magma: dissolution, diffusional exchange and development of zoning, reaction producing secondary mineral phases, and overgrowth with the same mineral of liquidus composition. The

rate of reaction and the resultant product is controlled by the relative rates of each of these processes.

5.4.1 Dissolution

Dissolution of minerals in a melt system is known to be a steady-state process which transports material away from the crystal-melt interface (Bearley and Scarfe, 1986). In a system where dissolution is occurring faster than diffusion of materials from the grain into the kimberlite melt, no zonational rim develops on the grain (see Figure 5.5).

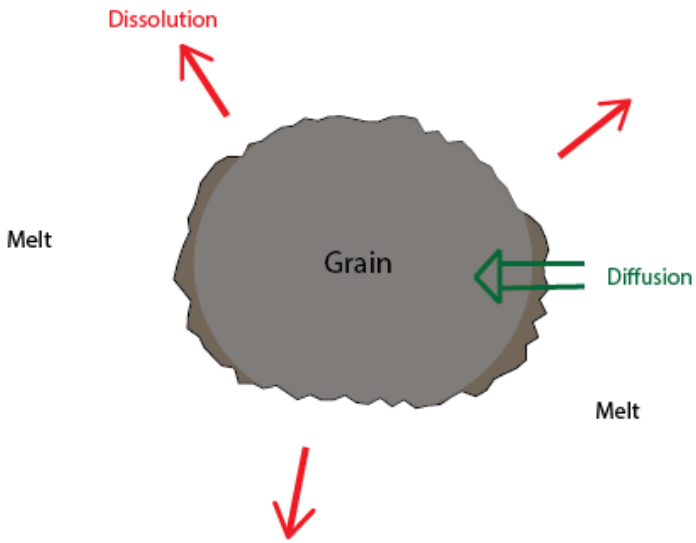

Figure 5.5 Diffusive zonation minimal to absent where dissolution (red arrows) is occurring faster than diffusion (blue dots).

5.4.2 Diffusion

When a xenocryst grain is exposed to the kimberlitic magma, the compositions are different and the system will try to equilibrate. The kimberlite magma will begin to have a diffusive reaction with the outer surface of the grain, creating a smooth zonational rim effect. Diffusion in the case of these two kimberlites has not been quantified, but a relative rate can be established with the grain dissolution. Where a diffusive zonation is present at the rim of the grain, it can be said that diffusion was occurring faster than dissolution in the kimberlite (see Figure 5.6). In the case of

Kimberlites A and B, diffusion was likely occurring at a fast rate relative to dissolution in Kimberlite A, where there were definitive zonational rims on the ilmenite grains, in particular. In Kimberlite B, diffusion occurs at a slower rate relative to dissolution, where there were no zonational rims

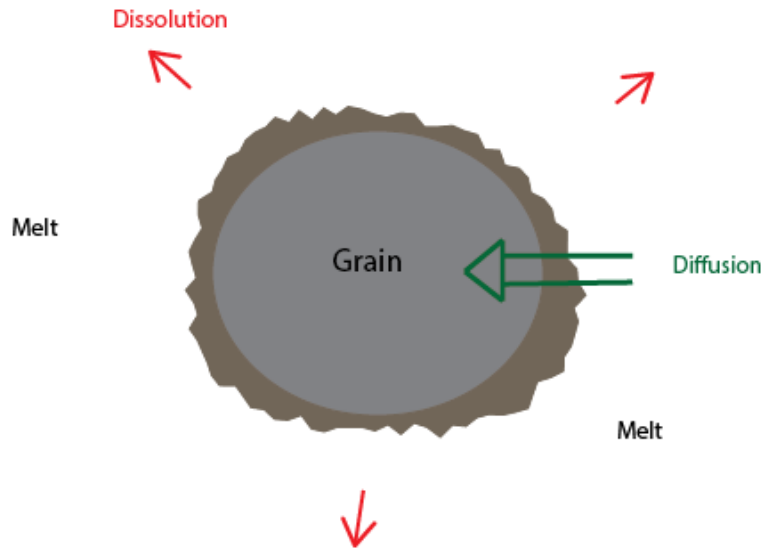

Figure 5.6 Diffusive zonation developing where diffusion (blue dots) is occurring faster than dissolution (red arrows).

5.4.3 Reaction

Many of the grains observed in this study exhibited reaction textures and phases on the grain surface. These phases are a result of interaction with the grain surface and melt as it is exposed to the kimberlite. This is particularly apparent in ilmenite grains. Bearley and Scarfe (1986) conducted multiple experiments at different pressures with mafic basalt melts. They suggest that reaction of the grain surface with the melt occurs where the grain being resorbed is not of the melt liquidus composition. This means that the further from liquidus composition a grain is when it is

exposed to the kimberlite melt, the greater reaction it will have as the system attempts to equilibrate the two contrasting compositions.

Using this supposition for the two kimberlites from the Orapa field, it can be inferred that the Kimberlite A melt was likely not crystallising a primary ilmenite phase because of the titanite reaction products on the grain surface. Because of the low volume of reaction products compared to the other kimberlite, the ilmenite composition may not have been far from the melt liquidus. Kimberlite B ilmenites display a large volume of reaction products on the grain surface. It is likely that this melt was not crystallizing any primary ilmenite, and that the xenocrystal ilmenite was far from the melt liquidus. Because neither kimberlite showed any reaction products on the chromite grain, it can be interpreted that both pipes were crystallising primary chromite grains of a similar composition.

The specific sequence of reaction products seen on ilmenite grains is quite unusual, because of the variations in silicic activity which would have occurred in the kimberlite to produce this line of crystallization events. This odd progression of reactions became apparent from the chemical composition, and the elemental x-ray maps. Figure 4.17b, an increase in silica activity between the two zones of lower silica activity. This is a rather curious phenomenon which seems to be unique to Kimberlite B. After the introduction of a silicate fluid, the proportion of silicate would be expected to increase, but in this case, there is a dissipation of the silica activity where the perovskite (oxide $CaTiO_3$) crystallizes, before a re-introduction of the silica fluid.

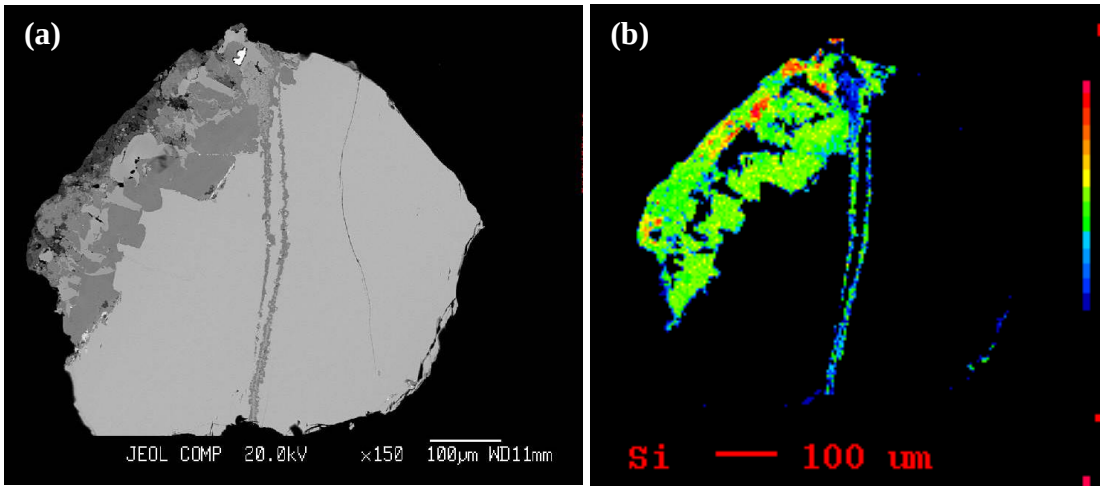

Figure 5.7 Ilmenite grain from Kimberlite B showing (a) BSE image of polished grain and (b) x-ray map of Si variations within the grain.

5.4.4 Overgrowth of same mineral

Overgrowth of the same mineral can occur where the grain composition is near to the melt liquidus, and the reaction between the melt and grain is minimal. Instead of causing a voluminous reaction texture, the kimberlite melt would crystallize the same mineral surrounding the original grain, perhaps of a slightly different composition. This could be the type of reaction occurring on the chromite grains from both kimberlites. Even though a rim or zonation is not apparent in the grain, diffusion between the two mineral compositions would have equilibrated any compositional variations between the two crystallizations.

6.0 CONCLUSIONS

1. Kimberlite A is a small "simple" kimberlite, with only one facies (coherent kimberlite) which is relatively uniform in texture. This kimberlite housed chromite grains that were well preserved with minimal dissolution, mostly on the edges and corners of the grains. The chromites often displayed a deformational elongate morphology. The ilmenite grains had diffusional zonation and some minor reaction products on the grain surface (mostly perovskite). Diffusion through the grain-melt interface was likely occurring at a faster rate than dissolution of the grains. Xenocrystic ilmenite was not at liquidus composition of the kimberlite melt, however, the kimberlite was likely crystallizing primary chromite. It is interesting to note that this relatively uniform kimberlite body displayed more varied and trending compositions than Kimberlite B, which is a much more complex body. In this kimberlite, it was possibly a silicate magma with a low wt% of dissolved CO_2 fluid and an H_2O free fluid phase that reacted with the oxides. The reduced state of Kimberlite A implies that diamond resorption in this melt was low, and there is a high potential for diamond preservation. These conclusions are summarized in Table 6.1.
2. Kimberlite B is a larger "complex" kimberlite, with several kimberlite facies present in the pipe (two coherent kimberlite lobes, a massive volcaniclastic facies, and a resedimented volcaniclastic facies). This kimberlite had few preserved chromites, and most were highly fractured. Where they were preserved, they showed highly resorbed textures, with very few {111} faces preserved. The ilmenite grains showed no diffusional zonation, and had large volumes of reaction products on the grain surface (perovskite and titanite). Dissolution was likely occurring faster than diffusion of material through the grain-melt interface. The ilmenite was possibly even further from liquidus composition than in Kimberlite A because of the large volume of reaction phases on the grain surfaces. Again, the kimberlite was likely crystallizing a primary chromite phase (lack of reaction products on chromite grains),

however, like the ilmenite grains, the resorption is more extensive than in Kimberlite A. Kimberlite B displayed two compositional populations of chromite and ilmenite, but no compositional trends as in Kimberlite A. This kimberlite probably had higher silica activity. It also had low wt% dissolved CO_2 and H_2O phases. The oxidizing state of Kimberlite B indicates that there was likely some diamond resorption occurring, and the potential for diamond preservation is lower than for Kimberlite A. These conclusions are summarized in Table 6.1.

Table 6.1 Comparison of inferences made about Kimberlites A and B from examination of Fe-Ti oxide reaction with kimberlite magma.

Kimberlite A **"simple" single-facies kimberlite**	**Kimberlite B** **"complex" multi-facies kimberlite**
Free fluid H_2O phase	Dissolved fluid H_2O phase
Low wt% dissolved CO_2 phase	Low wt% dissolved CO_2 phase
Possibly a silicate melt	High intermittent silica fluid activity
Reduced kimberlite melt – high diamond preservation potential	Oxidized kimberlite melt – lower diamond preservation potential than Kimberlite A
Diffusion through grain-melt boundary faster than grain dissolution	Grain dissolution faster than diffusion through grain-melt boundary
Ilmenite closer to liquidus composition than in Kimberlite B	Ilmenite further from liquidus composition than in Kimberlite A
Chromite close to liquidus composition	Chromite close to liquidus composition

3. Dissolution morphologies and features seen on kimberlitic chromites can be classified based on the style, or location (edge-corner or edge-corner-face), of dissolution attacking the grain, and further based on small-scale features developing in each location on the grain surface. Comparison with chromites from stratiform chromite deposits in ophiolites revealed similar dissolution features to those seen in kimberlitic chromites: edge-corner

dissolution, and edge-corner-face dissolution. This similarity could indicate similar chemical/fluid environments of dissolution Comparison with podiform chromites revealed a similar deformational morphologies to the elongate shapes seen in Kimberlite A, indicating notable deformation in both settings.

4. There does not seem to be any definitive correlation between the composition of chromite and ilmenite grains and the particular dissolution style or features. This was examined primarily in the chromite grains, where the dissolution features were the most distinctive. This non-correlational inference is supported by the observation of similar dissolution attack styles occurring in stratiform and podiform chromites, namely, the edge-corner and edge-corner-face resorption patterns. The rounded, rough morphology of the chromites seen in podiform deposits was also very similar to some of the shapes observed on kimberlitic chromites. This suggests that the morphologies and resorption developed on chromite grains is not related to the composition of the dissolving oxide but to other factors such as temperature or composition of fluids. Based on comparison with North American kimberlitic chromites and discussion with Kressall (2014b), the saturation of fluids could be a factor influencing the type and degree of resorption observed on kimberlitic Fe-Ti oxides.
5. Kimberlite emplacement with free-fluid phases, and well preserved chromites with edge-corner dissolution could indicate a reduced kimberlite melt and higher diamond preservation potential.
6. Fe-Ti oxides are important constituents in the kimberlitic system and are very useful indicators of processes occurring within the kimberlite magma during eruption. Because of their sensitivity to conditions in the melt such as oxygen fugacity, temperature, pressure, fluid phases and liquidus composition, the reactions that take place at the grain-melt

boundary are highly indicative of kimberlitic melt conditions. Fe-Ti oxides can also be useful for indirectly predicting diamond preservation potential from the redox state of the kimberlite.

7. Further work examining the reaction of Fe-Ti oxides with kimberlite magma would help to establish the consistency of chromite surface features in kimberlite settings, as well as their occurrence on chromites of other sources. Some studies have compared the resorption of chromites to other kimberlitic indicator minerals such as olivine and pyroxene (Leblanc, 1980, Gurney and Zweistra, 1995). Investigation of the resorption of these minerals along side Fe-Ti oxides would aid in further constraining the conditions and influences that cause resorption and affect the resultant surface features and reaction textures.

   The reaction products seen on the grain surfaces of ilmenite grains has also proved very useful for interpreting kimberlite magma conditions such as redox state, which is important for estimating diamond preservation, and liquidus composition. Future studies looking at the reaction of ilmenites with kimberlite magma could further the understanding of the reliability of ilmenites for interpreting the level of diamond resorption in kimberlites.

7.0 REFERENCES

Barnes, S. J., & Roeder, P. L. (2001). The Range of Spinel Compositions in Terrestrial Mafic and Ultramafic Rocks. *Journal of Petrology, 42*(12), 2279-2302. doi: 10.1093/petrology/42.12.2279

Barton, J. M. Jr., & van Reenen, D. D. (1992). When was the Limpopo Orogeny? *Precambrian Research,* 55, 7-16.

Bearley, M., & Scarfe, C. M. (1986). Dissolution of Upper Mantle Minerals in an Alkali Basalt Melt at High Pressure: An Experimental Study and Implications for Ultramafic Xenolith Survival. *Journal of Petrology, 27*(5), 1157-1182.

Becker, M., & A. P. le Roex (2006). Geochemistry of South African On- and Off-craton, Group I and Group II Kimberlites: Petrogenesis and Source Region Evolution. *Journal of Petrology, 47*(4), 673-703.

Beyer, C., Berndt, J., Tappe, S., & Klemme, S. (2012). Trace element partitioning between perovskite and kimberlite to carbonatite melt: New experimental constraints. *Chemical Geology*. doi: 10.1016/j.chemgeo.2012.03.025

Canil, D., & A. J. Bellis (2008). Phase equilibria in a volatile-free kimberlite at 0.1 MPa and the search for primary kimberlite magma. *Lithos 105,* 111-117.

Chinn, I. (2013a). *A--- Kimberlite*. DeBeers Group.

Chinn, I. (2013b). *B--- Kimberlite*. DeBeers Group.

Daniels, L. (2013). *Kimberlites, diamonds, the craton and the mantle?* Paper presented at the Botswana Resource Sector Conference, Gaborone.

Dawson, J. B. (1980). Kimberlites and Their Xenoliths. New York, Springer-Verlag.

Fedortchouk, Y., & MacIsaac, E. (2013). *Surface Features on Kimberlitic Chromites as Indicators of Magmatic Fluid and Diamond Quality*. Paper presented at the Proceedings of the 10th International Kimberlite Conference, Bangalore, India.

Field, M., & Scott-Smith, B. H. (1999). *Contrasting Geology and Near-Surface Emplacement of Kimberlite Pipes in Southern Africa and Canada.* Paper presented at the The 7th International Kimberlite Conference, Cape Town.

Gernon, T. M., Fontana, G., Field, M., Sparks, R. S. J., Brown, R. J., & Mac Niocaill, C. (2009). Pyroclastic flow deposits from a kimberlite eruption: The Orapa South Crater, Botswana. *Lithos, 112, Supplement 1*(0), 566-578. doi: http://dx.doi.org/10.1016/j.lithos.2009.04.016

Goodge, J. (2012a). Back-scattered Electron Detector (BSE). 2013, from http://serc.carleton.edu/research_education/geochemsheets/bse.html

Goodge, J. (2012b). Element Mapping. 2013, from http://serc.carleton.edu/research_education/geochemsheets/elementmapping.html

Goodge, J. (2013). Energy-Dispersive X-Ray Spectroscopy (EDS). 2013, from http://serc.carleton.edu/research_education/geochemsheets/eds.html

Gurney, J. J., & Zweistra, P. (1995). The interpretation of the major element compositions of mantle minerals in diamond exploration. *Journal of Geochemical Exploration 53*, 293-309.

Haggerty, S. E., Hardie, R. B. III, & McMahon, B. M. (1979). The Mineral Chemistry of Ilmenite Nodule Associations from the Monastery Diatreme. *The Mantle Sample: Inclusion in Kimberlites and Other Volcanics, 16*, 249-256.

Henry, D. (2012). Wavelength-Dispersive X-ray Spectroscopy (WDS). 2013, from http://serc.carleton.edu/research_education/geochemsheets/wds.html

Khar'kiv, A. D., Roman'ko, E. F., & Zubarev, B. M. (2005). Kimberlites of Zimbabwe: Abundance and Composition. *Russian Geology and Geophysics, 46*(3), 318-327.

Kirkley, M.B., Gurney, J.J., & Levinson, A.A. (1992). Age, origin and emplacement of diamonds: a review of scientific advances in the last decade. *The Canadian Mining and Metallurgical Bulletin, 85*(956), 48-57.

Kjarsgaard, B. A., et al. (2009). "Geochemistry of hypabyssal kimberlites from Lac de Gras, Canada: Comparisons to a global database and applications to the parent magma problem." *Lithos 112, Supplement 1*(0), 236-248.

Kopylova, M. G., Matveev, S., & Raudsepp, M. (2007). Searching for parental kimberlite melt. *Geochimica et Cosmochimica Acta, 71*(14), 3616-3629. doi: http://dx.doi.org/10.1016/j.gca.2007.05.009

Kressall, R. (2014a) Unpublished data.

Kressall, R. (2014b) P. Comm.

Leblanc, M. (1980). Chromite growth, dissolution and deformation from a morphological view point: SEM investigations. *Mineralium Deposita, 15*(2), 201-210. doi: 10.1007/bf00206514

Lee, D. C., et al. (2004). The Importance of Chromite Morphology in Diamond Exploration. 8th International Kimberlite Conference Long Abstract. R. H. Mitchell, H. S. Grutter, L. M. Heaman, B. H. S. Smith and T. Statchel, Elsevier.

McIsaac, E. M. (2009). Experimental Study of Surface Dissolution Features on Kimberlite Indicator Minerals. (Bachelor of Sciences, Honours), Dalhousie University, Halifax.

Mitchell, R. H. (1986). Kimberlites: Mineralogy, Geochemistry, and Petrology. New York, Plenum Press.

Nesse, W. D. (2000). *Introduction to* Mineralogy. New York: Oxford University Press.

Robles-Cruz, S. E., Watangua, M., Isidoro, L., Melgarejo, J. C., Gal, S., & Olimpio, A. (2009). Contrasting compositions and textures of ilmenite in the Catoca kimberlite, Angola, and implications in exploration for diamond. *Lithos, 112, Supplement 2*(0), 966-975. doi: http://dx.doi.org/10.1016/j.lithos.2009.05.040

Roeder, P. L. and D. J. Schulze (2008). "Crystallization of Groundmass Spinel in Kimberlite." *Journal of Petrology 49*(8), 1473-1495.

Scott-Smith, B. H. (1995). Petrology and diamonds. *Exploration and Mining Geology, 4*(2), 127-140.

Smith, R. M. H. (1990). A review of stratigraphy and sedimentary environments of the Karoo Basin of South Africa. *Journal of African Earth Sciences, 10*(1/2), 117-137.

Skinner, E. M. W., & Marsh, J. S. (2004). Distinct kimberlite pipe classes with contrasting eruption processes. *Lithos, 76*(14), 183-200. doi: http://dx.doi.org/10.1016/j.lithos.2004.03

Swapp, S. (2013). Scanning Electron Microscopy (SEM). 2013, from http://serc.carleton.edu/research_education/geochemsheets/techniques/SEM.html

van Reenen, D. D., Roering, C., Ashwal, L. D., & de Wit, M. J. (1992). Regional geological setting of the Limpopo Belt. *Precambrian Research, 55*, 1-5. doi: http://dx.doi.org/10.1016/0301-9268(92)90009-D

Winter, J. D. (2010). Principles of Igneous and Metamorphic Petrology. Upper Saddle River, New Jersey, Pearson Education Inc.

Wyatt, B. A., et al. (2004). "Compositional classification of "kimberlitic" and "non-kimberlitic" ilmenite." *Lithos 77*(14), 819-840.

APPENDIX A: Compositions of Ilmenite grains

Table A1: Kimberlite A, C = core analysis, R = rim analysis All Fe given as FeO

Sample	MgO	Al_2O_3	SiO_2	CaO	TiO_2	V_2O_3	Cr_2O_3	MnO	FeO	Na_2O	K_2O	Nb_2O_5	NiO	Total	Mg-no	Fe^{3+}/Fe^{tot}
a-a-4 C	11.26	0.053	0.018	0.009	48.98	0.278	3.543	0.323	33.65	0.031	0.027	0	0.085	98.67	0.453	0.305
a-a-4 R	10.6	0.245	0.059	10.75	51.88	0.214	2.696	0.325	19.15	0.385	0.022	0	0.042	97.05	0.603	0.367
a-b-2 C	8.683	0.098	0.007	0.012	48.39	0.331	3.255	0.562	36.76	0.016	0.027	0	0.073	98.46	0.357	0.268
a-b-2 R	12.15	0.145	0	0.055	49.99	0.349	3.587	0.44	31.94	0.02	0.009	0	0.049	99.01	0.485	0.303
a-b-3 C	13.15	0.148	0.062	0.046	49.62	0.276	3.535	0.385	31.96	0.033	0.028	0	0.079	99.78	0.523	0.355
a-b-3 R	13.97	0.245	0.261	2.388	52.57	0.217	3.41	0.545	24.93	0.049	0.022	0	0.046	98.91	0.569	0.259
a-c-1 C	11.44	0.607	0.049	0.026	50.89	0.351	0.174	0.24	34.8	0.021	0.021	0.14	0.107	98.9	0.429	0.241
a-c-2 C	10.13	0.035	0.002	0.041	49.91	0.322	3.386	0.317	34.33	0.023	0.016	0.407	0.072	99	0.399	0.229
a-c-3 C	7.964	0.071	0	0.014	47.55	0.323	3.097	0.317	39.53	0.019	0.016	0	0.068	99.29	0.328	0.295
a-c-3 R	7.836	0.056	0.009	0	48	0.35	3.165	0.299	38.77	0.024	0.008	0	0.084	98.89	0.322	0.268
a-c-3 R	7.844	0.066	0	0.009	48.06	0.321	3.145	0.282	38.61	0	0.003	0	0.076	98.67	0.321	0.26
a-c-4 C	10.88	0.06	0	0.014	49.97	0.303	3.842	0.351	33.64	0.022	0.026	0	0.056	99.48	0.433	0.267
a-c-4 R	13.69	0.192	0	0.065	51.79	0.306	4.145	0.44	28.62	0	0.018	0	0.07	99.69	0.529	0.259
a-c-5 C	10.15	0.054	0.059	0.013	49.78	0.346	4.003	0.318	33.71	0.013	0.016	0.355	0.072	98.92	0.422	0.29
a-c-6 (3)	2.133	0.07	0.077	0.014	72.23	0.469	6.679	0.108	3.358	0.004	0.018	12.27	0	97.44	0.531	0
a-c-6 (4)	0.949	0.053	0.037	0.035	76.63	0.417	6.352	0.055	1.649	0	0.021	11.35	0	97.55	0.506	0
a-c-6 C	15.55	0.112	0	0.047	55.36	0.268	2.632	0.484	24.84	0.011	0.015	0	0.106	100.15	0.562	0.141
a-c-6 C	16.15	0.09	0.003	0.036	56.71	0.316	3.192	0.613	21.19	0.013	0.02	0	0.061	99.55	0.576	0
a-c-6 R	12.74	0.379	0.313	0.41	58.24	0.266	3.825	1.974	17.92	0.015	0.024	0	0.047	98.61	0.559	0
a-c-6 R	18.17	1.943	9.048	6.737	31.66	0.209	4.43	1.731	23.14	0.08	0.026	0	0.074	97.59	1	1
a-c-7 C	8.324	0.042	0.016	0	48.15	0.285	3.407	0.323	37.42	0.011	0.012	0.352	0.083	98.44	0.34	0.255
a-d-6 C	11.72	0.754	0.028	0.024	51.28	0.402	0.15	0.272	34.43	0.028	0.024	0.113	0.123	99.35	0.457	0.303
a-e-5 C	8.692	0.048	0.023	0.014	49.23	0.276	3.535	0.327	36.62	0.01	0.016	0.341	0.092	99.23	0.349	0.233
a-e-6 C	12.17	0.269	0.034	0.029	49.48	0.348	3.581	0.303	31.24	0.006	0.023	0.296	0.111	97.93	0.49	0.299

Table A2: Kimberlite B, C = core analysis, R = rim analysis All Fe given as FeO

Sample	MgO	Al_2O_3	SiO_2	CaO	TiO_2	V_2O_3	Cr_2O_3	MnO	FeO	Na_2O	K_2O	Nb_2O_5	NiO	Total	Mg-no	Fe^{3+}/Fe^{tot}
b-a-3 C	8.397	0.046	0	0.027	48.92	0.297	3.507	0.368	37.39	0.002	0.024	0	0.087	99.53	0.338	0.241
b-a-3 R	7.65	0.204	0.46	0.562	38.12	0.297	2.653	0.279	26.24	0.144	0	0	0.033	76.66	0.412	0.281
b-a-4 C	9.19	0.322	0.051	0.017	49.42	0.321	1.062	0.269	37.5	0.009	0.027	0.191	0.047	98.45	0.367	0.272
b-b-6 C	8.705	0.188	0.045	0.016	48.23	0.343	0.976	0.252	38.77	0	0.017	0.199	0.074	97.82	0.354	0.298
b-c-3 C	7.478	0.125	0	0.017	47.89	0.294	1.484	0.301	41.52	0.017	0.01	0	0.047	99.43	0.304	0.296
b-c-3 R	6.751	0.494	4.391	6.886	42.12	0.281	1.299	0.275	35.45	0.017	0.014	0	0.032	98.25	0.344	0.381
b-c-6 C	10.34	0.309	0.003	0.046	49.21	0.325	1.142	0.319	36.85	0.081	0.021	0	0.046	98.98	0.416	0.326
b-c-6 R	9.526	0.584	8.297	9.7	37.52	0.24	1.01	0.284	25.97	0.256	0.035	0	0.029	93.6	0.561	0.511
b-c-7 C	7.67	0.176	0.005	0.013	49.23	0.288	1.123	0.247	40.65	0.029	0.021	0	0.066	99.67	0.306	0.267
b-c-7 R	7.493	0.237	3.625	2.173	46.54	0.293	1.028	0.252	37.45	0.462	0.014	0	0.039	99.87	0.321	0.27
b-d-1 C	7.896	0.206	0	0.022	49.05	0.34	1.156	0.282	40.67	0.122	0.02	0	0.055	100.06	0.319	0.291
b-d-1 R	8.7	0.169	1.607	2.782	44.64	0.283	1.069	0.309	38.15	0.051	0.025	0	0.039	98.1	0.393	0.405
b-d-3 C	10.23	0.309	0	0.028	51.2	0.31	1.794	0.233	35.16	0.12	0.023	0	0.095	99.65	0.402	0.251
b-d-3 R	9.765	0.267	0.027	0.04	50.28	0.281	1.785	0.224	34.7	0.134	0.015	0	0.101	97.72	0.391	0.241
b-d-4 C	7.38	0.116	0.002	0.017	47.24	0.356	0.947	0.319	40.63	0.012	0.024	0	0.028	97.29	0.306	0.297
b-d-4 R	8.155	0.11	0.064	0.134	43.13	0.312	0.812	0.401	37.25	0.029	0.013	0	0.044	90.66	0.369	0.366
b-d-6 C	8.425	0.171	0	0.005	48.95	0.306	1.077	0.254	40.05	0	0.022	0	0.075	99.63	0.336	0.289
b-d-6 R	7.542	0.283	6.481	6.671	44.55	0.262	0.924	0.318	31.42	0.074	0.026	0	0.044	98.89	0.348	0.216
b-e-3 C	7.562	0.124	0	0.011	49.54	0.299	1	0.278	39.05	0.007	0.007	0	0.044	98.2	0.301	0.222
b-e-3 R	8.7	0.194	0.415	0.45	44.01	0.264	0.885	0.399	33.15	0.058	0.059	0	0.034	88.87	0.393	0.307
b-e-4 C	10.45	0.404	0.032	0.032	49.45	0.341	1.751	0.204	35.37	0	0.033	0.401	0.087	98.58	0.416	0.286
b-e-5 C	7.602	0.194	0.032	0.007	48	0.305	0.974	0.275	40.68	0	0.014	0.267	0.063	98.41	0.308	0.283
b-e-6 C	7.746	0.107	0.033	0.019	48.25	0.31	1.229	0.286	40.41	0.052	0.025	0.287	0.031	98.82	0.315	0.286

APPENDIX B: Compositions of Chromite grains

Table B1: Kimberlite A, C = core analysis, R = rim analysis All Fe given as FeO

Sample	MgO	Al_2O_3	SiO_2	CaO	TiO_2	V_2O_3	Cr_2O_3	MnO	FeO	Na_2O	K_2O	Nb_2O_5	NiO	Total	Mg-no	Cr-no	Fe^{3+}/Fe^{tot}
c-b-3 C	12.45	11.08	0.006	0	0.043	0.215	56.79	0.29	17.5	0	0.023	0	0.062	98.59	0.621	0.775	0.238
c-b-3 R	13.17	10.1	0	0.008	0.195	0.207	57.62	0.276	17.19	0.005	0.02	0	0.058	98.96	0.651	0.793	0.279
c-b-4 C	10.99	8.046	0	0.01	0.533	0.166	57.62	0.328	21.03	0	0.022	0	0.086	98.98	0.549	0.828	0.249
c-b-4 R	5.771	2.328	0.034	0.014	0.41	0.159	58.77	0.301	12.78	0.002	0.003	0	0.045	80.72	0.446	0.944	0
c-b-5 C	7.498	5.48	0	0	1.04	0.157	54.65	0.361	29.53	0	0.001	0	0.065	98.98	0.376	0.87	0.272
c-b-5 R	8.315	5.529	0.042	0.001	1.139	0.163	51.73	0.378	29.61	0	0.015	0	0.079	97.15	0.418	0.863	0.33
c-b-6 C	12.18	9.372	0.004	0	1.014	0.294	59.99	0.404	14.48	0	0.03	0	0.072	97.98	0.612	0.811	0.051
c-b-6 R	11.46	9.587	0.023	0.016	0.982	0.309	60.17	0.294	14.67	0	0.015	0	0.081	97.73	0.582	0.808	0
c-c-5 C	11.54	11.25	0	0.014	0.934	0.291	52.76	0.318	21.72	0	0.016	0	0.105	99.1	0.565	0.759	0.285
c-c-5 R	10	4.454	0.097	0.016	1.193	0.205	58.71	0.397	23.67	0.012	0.019	0	0.087	99.01	0.502	0.898	0.269
c-c-6 C	9.222	2.836	0	0	1.864	0.241	59.79	0.405	25.16	0	0.015	0	0.09	99.76	0.459	0.934	0.248
c-c-6 R	9.597	2.829	0	0.021	1.896	0.224	58.82	0.398	25.43	0	0.011	0	0.106	99.47	0.476	0.933	0.278
c-c-7 R	9.726	1.175	0.015	0	2.634	0.239	58.44	0.364	26.02	0	0.021	0	0.125	98.98	0.477	0.971	0.289
c-c-7 C	9.703	1.227	0.021	0.006	2.606	0.247	57.92	0.377	26.06	0.004	0.016	0	0.137	98.44	0.479	0.969	0.299
c-d-1 C	9.952	4.445	0	0	1.745	0.207	58.27	0.346	23.86	0	0.026	0	0.105	99.09	0.493	0.898	0.252
c-d-1 R	10.22	4.827	0.026	0.003	2.193	0.215	55.8	0.393	24.82	0.006	0.016	0	0.104	98.7	0.499	0.886	0.281
c-d-2 C	13.45	14.82	0	0	0.116	0.232	52.32	0.297	16.91	0	0.017	0	0.068	98.37	0.656	0.703	0.269
c-d-2 R	14.16	15.46	0.012	0	0.132	0.224	50.12	0.271	16.76	0	0.012	0	0.062	97.36	0.689	0.685	0.332
c-d-3 C	9.648	1.852	0.003	0.002	2.274	0.2	57.88	0.438	26.67	0	0.014	0	0.142	99.25	0.474	0.954	0.305
c-d-3 R	9.645	1.462	0.13	0	2.604	0.212	56.12	0.357	26.35	0.036	0.01	0	0.141	97.19	0.478	0.963	0.31
c-d-4 C	13.25	8.774	0.038	0.004	0.116	0.23	60.58	0.298	15.97	0.013	0.026	0.003	0.091	99.48	0.675	0.822	0.302
c-d-4 C	13.13	8.547	0.072	0.015	0.127	0.235	59.67	0.286	16.04	0	0.02	0	0.078	98.31	0.677	0.824	0.315
c-d-5 C	12.59	7.721	0.032	0.009	1.435	0.295	57.21	0.288	18.18	0	0.025	0.018	0.116	98	0.685	0.832	0.449
c-d-5 C	12.65	8.048	0.077	0.005	1.46	0.31	55.9	0.326	18.16	0	0.016	0	0.11	97.15	0.631	0.823	0.286
c-d-7 C	12.61	12.2	0.056	0.007	1.05	0.339	52.4	0.26	19.05	0.02	0.022	0	0.104	98.26	0.703	0.742	0.517
c-e-2 C	8.955	2.017	0	0.002	3.124	0.269	55.29	0.384	27.28	0	0.013	0	0.134	97.6	0.441	0.948	0.28
c-e-2 C	9.424	2.058	0.04	0.017	3.074	0.269	54.39	0.377	28.37	0	0.022	0.03	0.131	98.35	0.418	0.947	0.193

Sample	MgO	Al_2O_3	SiO_2	CaO	TiO_2	V_2O_3	Cr_2O_3	MnO	FeO	Na_2O	K_2O	Nb_2O_5	NiO	Total	Mg-no	Cr-no	Fe^{3+}/Fe^{tot}
c-e-5 C	10.36	4.827	0.046	0.021	1.556	0.238	58.36	0.356	22.52	0.002	0.017	0.011	0.089	98.56	0.526	0.89	0.278
h-a-1 C	11.6	5.149	0.115	0.009	1.711	0.161	56.8	0.347	19.93	0	0.026	0.022	0.12	96.09	0.658	0.881	0.479
h-a-2 C	13.24	4.177	0.156	0	1.192	0.139	61.36	0.289	15.77	0.006	0.019	0	0.1	96.51	0.689	0.908	0.338
h-a-3 C	13.96	10.87	0.306	0.002	0.86	0.196	54.23	0.244	15.86	0.01	0.018	0.036	0.092	96.76	0.409	0.77	-1.443
h-a-4 C	11.88	10.25	0.572	0.024	0.858	0.161	49.5	0.316	22.23	0.048	0.015	0	0.078	96.14	0.535	0.764	0.183
h-b-1 C	15.14	17.16	0.067	0.004	0.101	0.164	50.85	0.238	16.27	0	0.022	0.009	0.085	100.2	0.764	0.665	0.501
h-b-3 C	9.426	4.644	0.096	0.003	1.612	0.209	58.81	0.418	19.51	0	0.018	0	0.09	94.96	0.525	0.895	0.232
h-b-4 C	12.61	7.763	0.056	0.009	0.108	0.226	59.17	0.293	17.55	0	0.034	0	0.099	98.01	0.618	0.836	0.219
h-b-4 C	12.69	7.659	0.147	0.004	0.116	0.229	57.36	0.262	17.24	0.004	0.024	0.05	0.09	95.96	0.627	0.834	0.229
h-b-5 C	12.81	11.28	0.048	0.003	0.093	0.198	55.35	0.271	17.89	0.007	0.02	0	0.057	98.17	0.586	0.773	0.14
h-b-5 C	12.62	10.98	0.041	0.004	0.071	0.202	55.65	0.293	18.32	0	0.012	0.014	0.071	98.37	0.644	0.767	0.308
h-b-6 C	10.94	10.53	0.05	0	0.562	0.193	50.82	0.359	24.4	0	0.019	0	0.085	98.14	0.496	0.764	0.204
h-b-6 C	10.62	10.61	0.111	0.019	0.478	0.213	49.72	0.305	23.11	0	0.025	0	0.089	95.47	0.504	0.759	0.207
h-b-6 R	9.234	1.315	0.108	0.028	3.065	0.387	55.46	0.361	25.1	0.024	0.021	0.009	0.127	95.38	0.478	0.966	0.304
h-c-2 C	13.38	15.35	0.118	0.002	0.022	0.157	50.71	0.279	16.07	0.022	0.016	0	0.049	96.29	0.761	0.701	0.494
h-c-2 C	15.05	14.32	0.166	0.002	0.044	0.154	49.94	0.244	16.16	0	0.025	0.01	0.063	96.29	0.739	0.689	0.489
h-c-2 R	13.7	15.47	0.034	0.005	0.036	0.151	51.28	0.234	16.53	0	0.025	0	0.081	97.66	0.658	0.69	0.243
h-c-5 C	9.275	3.483	0.047	0.003	1.838	0.225	58.81	0.363	22.87	0	0.033	0	0.084	97.19	0.474	0.919	0.211
h-c-5 C	9.527	3.632	0.059	0.01	1.874	0.235	57.99	0.368	23.6	0	0.021	0	0.098	97.56	0.483	0.912	0.243
h-c-5 C	9.302	3.698	0.106	0.001	1.833	0.211	56.99	0.332	22.93	0.016	0.019	0	0.091	95.7	0.485	0.915	0.254
h-c-6 C	7.825	2.618	0.117	0.025	2.265	0.231	52.26	0.364	29.36	0	0.023	0.011	0.118	95.34	0.36	0.93	0.171
h-c-6 C	7.793	2.616	0.089	0.016	2.336	0.258	53.36	0.428	29.93	0.026	0.011	0	0.105	97.12	0.392	0.932	0.306
h-d-5 C	10.94	5.642	0.029	0.005	0.601	0.189	58.44	0.333	21.57	0	0.01	0.008	0.075	97.97	0.535	0.874	0.228

Table B2: Kimberlite B, C = core analysis, R = rim analysis All Fe given as FeO

Sample	MgO	Al_2O_3	SiO_2	CaO	TiO_2	V_2O_3	Cr_2O_3	MnO	FeO	Na_2O	K_2O	Nb_2O_5	NiO	Total	Mg-no	Cr-no	Fe^{3+}/Fe^{tot}
a-f-1 C	16.96	37.92	0	0.013	0.022	0.119	21.78	0.17	17.66	0	0.023	0	0.278	95.1	0.749	0.278	0.439
a-f-1 R	18.06	32.89	1.681	0.034	0.24	0.109	21.58	0.158	15.64	0	0.027	0	0.28	90.84	0.789	0.306	0.462
b-f-3 C	12.2	12.21	0	0	0.431	0.175	55.25	0.255	17.94	0.011	0.029	0	0.063	98.74	0.599	0.752	0.197
b-f-3 R	13.79	12.02	0.371	0.007	0.398	0.184	53.92	0.261	17.5	0	0.026	0	0.082	98.7	0.661	0.751	0.292
b-f-4 C	16.66	39.18	0.011	0	0.022	0.121	20.05	0.154	17.53	0	0.009	0	0.303	94.21	0.739	0.256	0.415
b-f-4 R	17.24	39.78	0	0	0.028	0.12	20.1	0.175	17.54	0.001	0.017	0	0.298	95.46	0.753	0.253	0.439
b-g-2 C	13.59	16.96	0.002	0.007	0.027	0.24	51.03	0.277	15.56	0	0.029	0	0.071	97.94	0.664	0.669	0.22
b-g-2 R	13.54	17.04	0.019	0	0.049	0.217	51.32	0.279	15.65	0	0.022	0	0.068	98.36	0.657	0.669	0.202
c-f-1 C	5.156	0.444	0	0	2.337	0.283	58.21	0.363	16.8	0	0.006	0	0.056	83.76	0.354	0.989	0
c-f-1 R	6.909	0.549	0.579	0.42	2.308	0.293	53.92	0.341	17.08	0.057	0.036	0	0.069	82.7	0.424	0.985	0.021
c-f-2 C	13.5	17.03	0	0	0.02	0.226	51.24	0.264	15.48	0	0.001	0	0.068	97.96	0.657	0.669	0.196
c-f-2 R	14.29	16.86	0.266	0.007	0.125	0.214	51.26	0.26	15.62	0	0.039	0	0.056	99.13	0.678	0.671	0.234
c-f-3 C	9.48	2.017	0.004	0.004	2.34	0.299	58.09	0.415	24.81	0	0.016	0	0.117	97.73	0.478	0.951	0.274
c-f-3 R	9.128	1.156	0	0	2.27	0.311	59.87	0.459	24.32	0.023	0.017	0	0.127	97.83	0.467	0.972	0.254
c-f-4 C	13.55	7.274	0.042	0.002	0.357	0.2	60.71	0.265	15.81	0	0.021	0	0.079	98.34	0.675	0.848	0.275
c-f-4 R	13.42	7.308	0.041	0	0.289	0.181	61.09	0.231	15.52	0.005	0.014	0	0.089	98.21	0.67	0.849	0.251

APPENDIX C: Compositional Profiles

Table C1: Chromite grain from Kimberlite A, c-d-5 prof1 = core prof12 = rim

Mineral	Sample	MgO	Al_2O_3	SiO_2	CaO	TiO_2	V_2O_3	Cr_2O_3	MnO	FeO	Na_2O	K_2O	Nb_2O_5	NiO	Total
Chr	c_d_5 prof1	12.51	7.945	0.067	0	1.482	0.281	55.89	0.264	18.06	0.006	0.025	0	0.114	96.71
Chr	c_d_5 prof2	12.55	7.959	0.092	0.011	1.44	0.295	55.9	0.271	18.01	0	0.012	0.014	0.107	96.75
Chr	c_d_5 prof3	12.45	8.016	0.071	0	1.483	0.288	55.68	0.314	18.39	0	0.014	0	0.115	96.92
Chr	c_d_5 prof4	12.43	8.121	0.087	0	1.523	0.314	55.61	0.278	18.57	0	0.022	0	0.112	97.15
Chr	c_d_5 prof5	12.28	8.217	0.062	0.017	1.486	0.297	55.68	0.275	18.6	0	0.029	0	0.107	97.15
Chr	c_d_5 prof6	12.11	8.141	0.071	0.012	1.568	0.3	55.55	0.278	18.77	0	0.024	0	0.105	97.04
Chr	c_d_5 prof7	11.69	6.838	0.067	0	1.956	0.278	55.67	0.307	19.78	0.009	0.024	0	0.117	96.81
Chr	c_d_5 prof8	11.83	6.128	0.067	0.022	2.835	0.268	54.09	0.283	21.25	0.009	0.025	0	0.135	96.98
Chr	c_d_5 prof9	11.5	6.31	0.068	0	2.445	0.264	54.88	0.302	20.76	0.006	0.026	0	0.103	96.72
Chr	c_d_5 prof10	11.86	6.806	0.078	0	3.739	0.328	51.66	0.302	21.97	0.003	0.019	0.005	0.137	97.01
Chr	c_d_5 prof11	11.17	5.467	0.092	0.013	2.693	0.256	55.88	0.291	20.79	0.006	0.029	0	0.111	96.86
Chr	c_d_5 prof12	10.77	3.838	0.092	0	2.496	0.231	58.28	0.264	20.56	0	0.02	0	0.122	96.75

Table C2: Ilmenite grain from Kimberlite B with titanite reaction product, b-a-4 prof1 = ilmenite core prof14 = titanite core

Mineral	Sample	MgO	Al_2O_3	SiO_2	CaO	TiO_2	V_2O_3	Cr_2O_3	MnO	FeO	Na_2O	K_2O	Nb_2O_5	NiO	Total
Ilm	b_a_4 prof1	9.385	0.299	0.076	0.025	49.49	0.318	1.047	0.291	37.01	0	0.013	0.215	0.076	98.24
Ilm	b_a_4 prof2	9.403	0.351	0.075	0.025	49.56	0.335	1.047	0.301	36.68	0.029	0.036	0.13	0.07	98.04
Ilm	b_a_4 prof3	9.558	0.292	0.054	0.051	49.57	0.34	1.101	0.253	36.72	0.024	0.016	0.117	0.057	98.16
Ilm	b_a_4 prof4	9.703	0.336	0.054	0.061	49.72	0.33	1.078	0.276	36.62	0.036	0.023	0.149	0.058	98.46
Ilm	b_a_4 prof5	9.826	0.31	0.057	0.13	48.82	0.339	1.091	0.307	36.32	0.006	0.027	0.191	0.06	97.49
Ilm	b_a_4 prof6	10.02	0.32	0.06	0.282	49.36	0.333	1.071	0.321	36.42	0.059	0.018	0.159	0.071	98.51
Ilm	b_a_4 prof7	10.24	0.315	0.134	1.519	47.66	0.313	1.012	0.295	36.51	0.022	0.024	0.24	0.075	98.37
Titan	b_a_4 prof8	0.048	0.008	29.69	29.11	26.82	0.147	0.401	0.028	8.87	0.098	0.026	0.113	0	95.36
Titan	b_a_4 prof9	0.083	0.019	29.7	28.82	27.47	0.143	0.46	0	7.807	0.053	0.026	0.053	0	94.64
Titan	b_a_4 prof10	0.065	0.048	29.7	28.95	27.83	0.144	0.469	0	7.186	0.082	0.024	0.055	0	94.54
Titan	b_a_4 prof11	0	0.107	29.77	29.43	30.7	0.127	0.348	0.014	6.269	0.032	0.016	0.133	0.005	96.94
Titan	b_a_4 prof12	0.039	0.261	29.91	30.03	37.31	0.132	0.182	0.006	1.786	0	0.022	0.183	0.004	99.86
Titan	b_a_4 prof13	0.003	0.19	30.14	30.06	37.95	0.123	0.194	0	1.197	0	0.013	0.11	0	99.98
Titan	b_a_4 prof14	0.038	0.087	29.56	29.17	29.05	0.13	0.255	0.02	6.86	0.068	0.021	0.126	0	95.37

Table C3: Ilmenite grain from Kimberlite A, a-c-6 prof1 = ilmenite core prof14 = transition to leucoxene zone prof32 = transiton out of leucoxene zone prof34 = titanium magnetite zone

Mineral	Sample	MgO	Al_2O_3	SiO_2	CaO	TiO_2	V_2O_3	Cr_2O_3	MnO	FeO	Na_2O	K_2O	Nb_2O_5	NiO	Total
Ilm	a_c_6 prof1	15.82	0.104	0.003	0.045	55.19	0.298	2.577	0.533	23.9	0.006	0.025	0.624	0.095	99.23
Ilm	a_c_6 prof2	15.78	0.096	0.013	0.043	54.9	0.289	2.56	0.45	24.02	0	0.016	0.664	0.106	98.95
Ilm	a_c_6 prof3	15.85	0.098	0.005	0.038	54.63	0.295	2.566	0.489	23.99	0.029	0.02	0.654	0.082	98.77
Ilm	a_c_6 prof4	15.89	0.082	0.031	0.035	53.86	0.309	2.543	0.473	23.98	0.028	0.023	0.738	0.082	98.1
Ilm	a_c_6 prof5	15.89	0.117	0.023	0.051	55.19	0.292	2.532	0.449	23.92	0.041	0.028	0.675	0.117	99.36
Ilm	a_c_6 prof6	15.84	0.109	0.023	0.051	54.71	0.29	2.609	0.483	24.02	0.018	0.024	0.666	0.076	98.92
Ilm	a_c_6 prof7	15.9	0.136	0.012	0.038	54.96	0.309	2.704	0.524	23.8	0.024	0.016	0.673	0.095	99.22
Ilm	a_c_6 prof8	15.91	0.156	0.005	0.059	55.2	0.316	2.862	0.554	23.41	0.012	0.019	0.673	0.092	99.28
Ilm	a_c_6 prof9	14.24	0.133	1.029	0.07	51.08	0.304	2.671	0.508	25.85	0.033	0.029	0.619	0.092	96.69
Ilm	a_c_6 prof10	16.11	0.139	0.037	0.053	54.89	0.318	3.183	0.508	23.21	0.001	0.021	0.697	0.084	99.27
Ilm	a_c_6 prof11	16.2	0.134	0.037	0.051	55.25	0.321	3.278	0.535	22.96	0.029	0.018	0.607	0.064	99.49
Ilm	a_c_6 prof12	16.62	0.104	0.042	0.046	56.21	0.295	2.592	0.532	22.01	0.034	0.026	0.634	0.092	99.24
Ilm	a_c_6 prof13	16.96	0.054	0.046	0.058	57.08	0.284	1.967	0.599	21.73	0.031	0.031	0.714	0.081	99.63
Leuc	a_c_6 prof14	4.063	0.076	0.063	0.019	67.1	0.408	5.894	0.137	6.558	0	0.011	11.79	0.017	96.15
Leuc	a_c_6 prof15	1.604	0.087	0.075	0.02	71.96	0.468	6.864	0.057	2.463	0	0.014	12.94	0.007	96.56
Leuc	a_c_6 prof16	2.106	0.063	0.089	0.012	72.15	0.492	6.526	0.058	3.011	0	0.027	11.75	0.014	96.29
Leuc	a_c_6 prof17	4.847	0.068	0.054	0.016	69.25	0.488	6.356	0.159	5.479	0	0.013	11.75	0.027	98.51
Leuc	a_c_6 prof18	1.819	0.059	0.061	0.015	71.78	0.519	6.635	0.075	3.027	0	0.024	12.22	0.006	96.27
Leuc	a_c_6 prof19	1.404	0.064	0.07	0	71.28	0.485	6.528	0.049	3.247	0	0.03	12.06	0	95.21
Leuc	a_c_6 prof20	2.348	0.076	0.094	0.013	71.78	0.498	6.28	0.108	3.56	0	0.021	11.92	0.007	96.71
Leuc	a_c_6 prof21	3.578	0.054	0.061	0.011	70.06	0.517	6.233	0.111	4.452	0	0.027	11.63	0.017	96.78
Leuc	a_c_6 prof22	1.976	0.08	0.042	0.017	72.21	0.495	6.563	0.104	3.032	0	0.029	11.98	0.013	96.54
Leuc	a_c_6 prof23	0.22	0.062	0.072	0.002	74.91	0.511	7.227	0.028	0.738	0	0.018	12.63	0.01	96.43
Leuc	a_c_6 prof24	0.069	0.05	0.075	0.019	75.82	0.488	7.089	0.015	0.593	0	0.031	12.45	0.009	96.71
Leuc	a_c_6 prof25	0.073	0.058	0.067	0.017	75.47	0.494	7.112	0.012	0.582	0	0.029	12.52	0.005	96.45
Leuc	a_c_6 prof26	0.129	0.043	0.084	0.02	75.39	0.478	7.154	0	0.639	0	0.017	12.55	0	96.5
Leuc	a_c_6 prof27	0.235	0.049	0.062	0.025	75.31	0.478	7.025	0	0.649	0	0.023	12.14	0	96.01
Leuc	a_c_6 prof28	3.461	0.037	0.05	0.036	74.25	0.45	5.622	0.091	3.812	0	0.03	10.29	0.022	98.18
Leuc	a_c_6 prof29	0.122	0.034	0.05	0.037	75.96	0.431	6.51	0.013	0.794	0	0.023	12.68	0	96.65

Mineral	Sample	MgO	Al_2O_3	SiO_2	CaO	TiO_2	V_2O_3	Cr_2O_3	MnO	FeO	Na_2O	K_2O	Nb_2O_5	NiO	Total
Leuc	a_c_6 prof30	2.667	0.014	0.033	0.362	77.06	0.398	2.994	0.149	5.663	0	0.02	6.291	0.023	95.67
Leuc	a_c_6 prof31	7.165	0.052	0.072	0.102	73.15	0.352	2.047	0.953	8.539	0.029	0.033	4.697	0.021	97.24
Ilm	a_c_6 prof32	17.9	0.062	0.048	0.142	59.35	0.271	0.826	2.545	16.95	0.08	0.018	1.157	0.055	99.44
Ilm	a_c_6 prof33	18.23	0.122	0.026	0.254	57.25	0.255	1.492	3.047	18.48	0.028	0.02	0.123	0.065	99.41
Ti-Mag	a_c_6 prof34	14.35	4.827	0.06	0.397	19	0.206	4.465	0.792	52.83	0	0.016	0.018	0.15	97.17